BENCHMARK CASES FOR ADVANCED DESIGN OF STRUCTURAL STEEL CONNECTIONS

Wald F., Šabatka L., Bajer M., Barnat J.,
Gödrich L., Holomek J., Kabeláč J., Kočka M.,
Kolaja D., Král P., Kurejková M., Vild M.

Czech Technical University in Prague
Brno University of Technology

This publication introduces Benchmark Cases for Validation and Verification procedures of structural steel joints. The hierarchy of the System response quantity is prepared for welded and bolted connections as well as for column bases. Each Benchmark Case starts with task description and includes results of prediction by analytical model according to EN 1993-1-5, references to experiments, validated model and numerical experiments, results of prediction by design Finite Element Analyses described in terms of global behaviour and verification of resistance. Reader may also check his calculation against Benchmark cases prepared for particular joints.

Finite Element Analyses is the next step in design of steel joints and connections. It allows predicting generally loaded joints with complex geometry with the same efficiency and accuracy as traditionally designed connections based on the best engineering practice. Implementation of the FEA models for structural steel detailing is a qualitative step forward similar to what we see in other areas of engineering.

Česká technika – nakladatelství ČVUT
September 2016
ISBN 978-80-01-05826-8

ISBN 978-80-01-05826-8

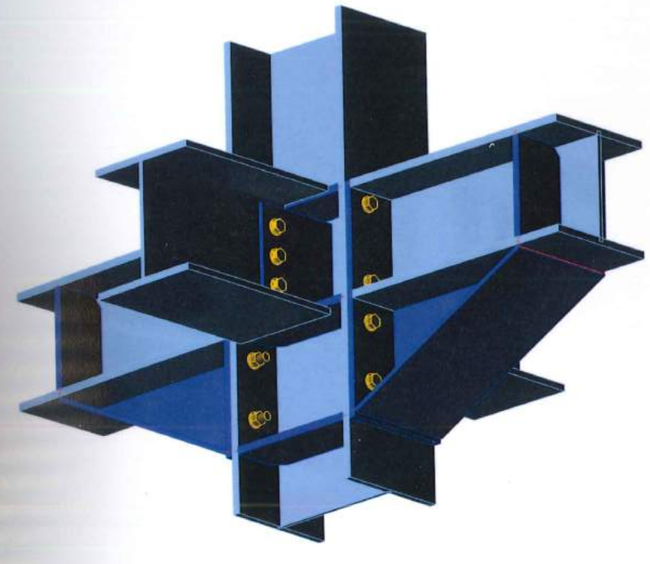

BENCHMARK CASES FOR ADVANCED DESIGN OF STRUCTURAL STEEL CONNECTIONS

František Wald et al.

Prof František Wald

Professor and Head of the Department of Steel and Timber Structures at Czech Technical University in Prague. During his rich professional career, he participated in ten European projects in connection design and several other projects focused on component method, column bases, steel and concrete connections, fire design, and the advanced finite element analysis. He has been working in ECCS TC 10 Structural joints and in Project team for preparation of EN199-3-8 version 2020.

Prof Wald is in charge of European Erasmus Mundus Master Course SUSCOS_M Sustainable Constructions under natural hazards and catastrophic events. He also works in CEN Working Group for EN1991-1-2 and EN1993-1-3 and chaired the COST TU0904 Action Integrated fire engineering and response.

Benchmark cases for advanced design of structural steel connections

Wald F., Šabatka L., Bajer M.,
Barnat J., Gödrich L., Holomek J., Kabeláč J.,
Kočka M., Kolaja D., Král P., Kurejková M., Vild M.

Benchmark cases for advanced design of structural steel connections
Wald F., Šabatka L., Bajer M.,
Barnat J., Gödrich L., Holomek J., Kabeláč J., Kočka M., Kolaja D., Král P., Kurejková M., Vild M.
Česká technika - nakladatelství ČVUT
September 2016
ISBN 978-80-01-05826-8

List of contents

Symbols

The symbols are introduced in relevant chapters. The terminology and symbols follows the rules applied in EN1993-1-8:2006. The major general variables are described further.

Connection

Connection is called location at which two or more elements meet. For design purposes it represents the location where are transferred the relevant internal forces and moments.

Initial stiffness

The secant rotational stiffness at the initial part of the moment rotational curve at 2/3 of the joint bending resistance.

Joint

Joint represents zone where two or more members are interconnected. A beam-to-column joint consists usually of a column web panel and either one connection (single sided joint configuration) or two connections (double sided joint configuration).

Node

Node is defined as point within which the axes of two or more inter-connected members intersect.

Rotational capacity

The angle through which the joint can rotate for a given resistance level without failing.

Rotational stiffness

The moment required to produce unit rotation in a joint.

Symbols

The following symbols are used:

a is the length of base plate;

a_w is the effective throat thickness of fillet weld;

b is the width of base plate;

b_b is the width of the beam;

b_c is the width of the column;

b_i is the overall out-of-plane width of RHS member i ($i = 0, 1, 2$ or 3);

b_{eff} is the effective width for a brace member to chord connection;

$b_{e,ov}$ is the effective width for an overlapping brace to overlapped brace connection;

$b_{e,p}$ is the effective width for punching shear;

b_p is the width of a plate;

c is the effective width of the flexible base plate;

d is the nominal bolt diameter, the diameter of the pin or the diameter of the fastener;

d_0 is the hole diameter for a bolt, a rivet or a pin;

d_c is the clear depth of the column web;

d_i is the overall diameter of CHS member i ($i = 0, 1, 2$ or 3);

d_m is the mean of the across points and across flats dimensions of the bolt head or the nut, whichever is smaller;

d_w is the depth of the web of an I or H section chord member;

e is the eccentricity of a joint;

e_1 is the end distance from the centre of a fastener hole to the adjacent end of any part, measured in the direction of load transfer;

e_2 is the edge distance from the centre of a fastener hole to the adjacent edge of any part, measured at right angles to the direction of load transfer;

e_3 is the distance from the axis of a slotted hole to the adjacent end or edge of any part;

e_4 is the distance from the centre of the end radius of a slotted hole to the adjacent end or edge of any part;

f_{cd} is the design value of compressive cylinder strength of concrete $f_{cd} = f_{ck} / \gamma_c$;

f_{ck} is the characteristic value of concrete compressive cylinder strength;

f_u is the material ultimate strength;

f_{ub} is the ultimate strength of the bolt;

f_y is the material yield stress;

f_{yb} is the yield stress of the bolt;

g is the gap between the brace members in a K or N joint (negative values of g represent an overlap q); the gap g is measured along the length of the connecting face of the chord, between the toes of the adjacent brace members;

h_b is the depth of the beam;

h_c is the depth of the column;

h_i is the overall in-plane depth of the cross-section of member i ($i = 0, 1, 2$ or 3);

i is an integer subscript used to designate a member of a joint, $i = 0$ denoting a chord and $i = 1$, 2 or 3 the brace members. In joints with two brace members, $i = 1$ normally denotes the compression brace and $i = 2$ the tension brace;

k_{eq} is the equivalent stiffness coefficient;

k_i is the stiffness coefficient of component i;

ℓ_{eff} is the effective length (of fillet weld or T stub);

n is the number of the friction surfaces or the number of fastener holes on the shear face;

p_1 is the spacing between centres of fasteners in a line in the direction of load transfer;

$p_{1,0}$ is the spacing between centres of fasteners in an outer line in the direction of load transfer;

$p_{1,i}$ is the spacing between centres of fasteners in an inner line in the direction of load transfer;

p_2 is the spacing measured perpendicular to the load transfer direction between adjacent lines of fasteners;

r is the root radius of an I or H section or the corner radius of a rectangular hollow section;

s_s is the length of stiff bearing;

t_a is the thickness of the angle cleat;

t_f is the flange thickness of an I or H section;

t_i is the wall thickness of member i ($i = 0, 1, 2$ or 3);

t_p is the thickness of the end plate or base plate;

t_w is the thickness of the web or bracket;

z is the lever arm;

A is the gross cross-section area of bolt;

A_i is the cross-sectional area of member i ($i = 0, 1, 2$ or 3);

A_{vc} is the shear area of the column;

A_s is the tensile stress area of the bolt or of the anchor bolt;

$A_{v,eff}$ is the effective shear area;

$B_{p,Rd}$ is the design punching shear resistance of the bolt head and the nut;

E is the Young's modulus of steel;

$F_{t,Ed}$ is the design tensile force per bolt for the ultimate limit state;

$F_{t,Rd}$ is the design tension resistance per bolt;

$F_{T,Rd}$ is the tension resistance of an equivalent T-stub flange;

$F_{v,Rd}$ is the design shear resistance per bolt;

$F_{b,Rd}$ is the design bearing resistance per bolt;

$F_{v,Ed}$ is the design shear force per bolt for the ultimate limit state;

L is the system length of a member;

$M_{ip,i,Rd}$ is the design value of the resistance of the joint, expressed in terms of the in-plane internal moment in member i ($i = 0, 1, 2$ or 3);

$M_{ip,i,Ed}$ is the design value of the in-plane internal moment in member i ($i = 0, 1, 2$ or 3);

$M_{j,Rd}$ is the design moment resistance of a joint;

$M_{pl,Rd}$ is the design plastic moment resistance of a cross section;

$N_{i,Rd}$ is the design value of the resistance of the joint, expressed in terms of the internal axial force in member i ($i = 0, 1, 2$ or 3);

$N_{i,Ed}$ is the design value of the internal axial force in member i ($i = 0, 1, 2$ or 3);

$N_{j,Rd}$ is the axial design resistance of the joint;

S_j is the rotational stiffness of a joint;

$S_{j,ini}$ is the initial rotational stiffness of a joint;

$V_{wp,Rd}$ is the plastic shear resistance of a column web panel;

$W_{et,i}$ is the elastic section modulus of member i ($i = 0, 1, 2$ or 3);

$W_{pt,i}$ is the plastic section modulus of member i ($i = 0, 1, 2$ or 3);

α is the reduction factor of bearing resistance;

α_b is the factor for bearing resistance;

α_{cr} is the critical buckling factor;

$\alpha_{ult,k}$ is the load amplifier;

β_{Lw} is the reduction factor for long welds;

ε is the material yield strain;

ϕ is the rotation of a joint;

ϕ_{Cd} is the design rotation capacity of a joint;

θ_i is the included angle between brace member i and the chord ($i = 1, 2$ or 3);

φ is the angle between the planes in a multiplanar joint.

n is the stiffness reduction factor;

λ_{ov} is the overlap ratio, expressed as a percentage ($\lambda_{ov} = (q/p) \times 100\%$);

λ_p is the plate slenderness;

ρ is the reduction buckling factor;

$\sigma_{0,Ed}$ is the maximum compressive stress in the chord at a joint;

$\sigma_{p,Ed}$ is the value of $\sigma_{0,Ed}$ excluding the stress due to the components parallel to the chord axis of the axial forces in the braces at that joint;

$\sigma_\perp$ is the normal stress perpendicular to the throat section;

$\tau_\perp$ is the shear stress (in the plane of the throat section) perpendicular to the axis of the weld;

$\tau_\parallel$ is the shear stress (in the plane of the throat section) parallel to the axis of the weld;

1 INTRODUCTION

Four decades ago Finite Element Analysis (FEA) of structural connection was treated by some researchers as a non-scientific matter. Two decades later it was already a widely accepted addition or even necessarily extension of experimental and theoretical work. Today computational analysis, in particular computational mechanics and fluid dynamics, is commonly used as an indispensable design tool and a catalyst of many relevant research fields. The recommendation for design by advanced modelling in structural steel is already hidden but ready to be used in Chapter 5 and Annex C of EN 1993-1-5:2005. Development of modern general-purpose software and decreasing cost of computational resources facilitate this trend. As the computational tools become more readily available and easier to use, even to relatively inexperienced engineers, more scepticism and scrutiny should to be employed when judging one's computational analysis. The FEA of structural connection is the coming step in structural steel design.

The only way to prove correctness of simulated results is through a methodical verification and validation (V&V) process. Without V&V the finite element analysis is meaningless and cannot be used for making any decisions. To help with this process is prepared the presented monography.

The authors divided the work as follows. Chapter 1 and 2 was prepared by F. Wald, Chapter 3 by L. Šabatka, D. Kolaja, J. Holomek, J. Kabeláč, M. Kurejková, L. Gödrich and M. Vild, Chapter 4 by M. Kurejková, Chapter 5 by L. Gödrich, Chapter 6 by M. Kurejková, Chapter 7 by P. Král and M. Kočka, Chapter 8 by M. Bajer, J. Barnat, J. Holomek and M. Vild, Chapter 9 by L. Gödrich and M. Kurejková, Chapter 10 by M. Kurejková, L. Gödrich and M. Vild and Chapter 11 by M. Kurejková and L. Gödrich. The review of the text was prepared by A. Uhlíř, M. Strejček and J. Šabatka.

The work was developed under the R&D project MERLION supported by Technology Agency of the Czech Republic, project No. TA02010159.

In Prague, 30 June 2016
František Wald

2 CONNECTION DESIGN

2.1 Design models

The structural steel connections are designed by experimental, curve fitting, analytical and numerical models. The tests with connections are simple and economical solution for prediction of its behaviour. Based on tests were prepared by interpolation and even extrapolation designed tables for standardised connections. In the nineties of the last century were collected and published databases of test, see e.g. (Chen and Abdalla, 1995). Described over three thousand tests is a valuable resource for learning about the behavior of typical joints, although some even important data is missing. Curve fitting models are known from 1930. Mathematical formulas expressing the influence of geometrical and material parameters are reproducing the behaviour of similar connections well, but are not appointing the major parameters for design and in particular the resistance. Today is applied in modelling of connections in seismic design. The analytical modelling of components of connections are well developed for connectors, bolts, welds, anchor bolts etc. Analytical model of connections needs good engineering assumption of internal forces and proper selection of components, which affects the resistance and stiffness.

The complexity of finite element analyses FEA was deeply studied in last twenty years. Later were commonly accepted the procedures to reach proper results in scientific oriented finite element models FEM and the strong limits for application of design FE models. Based on numerical experiments validated on experiments were developed behaviour of the well described and published components loaded by elevated temperature, as tying forces, moment normal interaction and torsion and of the new less described components, as backing channel. The fast development of the computer assisted design of steel and composite structures in field of complex structures, as plated structures in bridges, excavators and wind towers, glass structures and cold formed structures, clarified the design procedures in accuracy of models and its application in civil engineering.

2.2 Component method

The latest version of analytical models for connections of steel and steel and concrete structures predicts not only the most important design resistance but also the initial stiffness and the deformation capacity, which allows design of ductile structures. This model prepared for selected types of configuration in known as Component method (CM). CM builds up on standard procedures evaluating the internal forces in selected geometries of connections and their checking. Zoetemeijer (1985) was the first who equipped for the end plate connections the model for resistance with prediction of stiffness and deformation capacity. The formulation and calculation of the elastic stiffness was improved in the work of Steenhius (1994). For most beam to column joint configuration was under European network COST C1 prepared description of components behaviour by Jaspart (Jaspart, 2002) and by for column bases Wald et al (2008). Method is currently implemented in the current European structural standard for steel and

composite connections, see EN1993-1-8:2006 and EN1994-1-1:2010 and applied in majority of software for structural steel used in Europe. The component model was generalised by da Silva (2008). Currently is model applied for design of joints at elevated temperatures during fire, see e.g. (Block et al, 2013), for 3D modelling of connections in space structures, for joints in timber structures, for prediction of behaviour under cyclic loading during earthquake etc.

The procedure starts with decomposition of a joint to components followed by their description in terms of normal/shear force deformation behaviour. After that, components are grouped to examine joint moment-rotational behaviour and classification/representation in a spring/shear model and application in global analyses. Advantage of the component model is integration of current experimental and analytical knowledge of connections components behaviour, bolts, welds, end plates, flanges, anchor bolts and base plates. This provides very accurate prediction of behaviour in elastic and ultimate level of loading. Verification of the model is possible using simplified calculation. Disadvantage of component model is that experimental evaluation of internal forces distribution is done only for limited number of joint configurations. Also in temporary scientific papers, description of typical components is either not present or has low validity and description of background materials.

Compare to well accept methods for determination of the initial stiffness and resistance of many types' structural joints, there are no generally accepted standardised procedures for the determination of the rotation capacity. The deemed to satisfy criteria are selected to help the engineers in EN1993-1-8:2006. The estimation of the rotation capacity is important in many applications namely in connections exposed to seismic, see (Grecea et al, 2004). The deformation capacity of components has been studied from end of last century, see (Foley and Vinnakota, 1995). (Faella et al, 2000) carried out tests on T-stubs and derived for the deformation capacity the analytical expressions. Kuhlmann and Kuhnemund (2000) performed tests on the column web subjected to transverse compression at different levels of compression axial force in the column. Da Silva et al (2002) predicted deformation capacity at different levels of axial force in the connected beam. Based on the test results combined with FE analysis deformation capacities are established for the basic components by analytical models by Beg at al (2004). In the work are represented components by non-linear springs, and appropriately combined in order to determine the rotation capacity of the joint for the end-plate connections, with an extended or flush end-plate, and welded connections. For these connections, the most important components that may significantly contribute to the rotation capacity column were recognised as the web in compression, column web in tension, column web in shear, column flange in bending, and end-plate in bending. Components related to the column web are relevant only when there are no stiffeners in the column that resist compression, tension or shear forces. The presence of a stiffener eliminates the corresponding component, and its contribution to the rotation capacity of the joint can be therefore neglected. End-plates and column flanges are important only for end-plate connections, where the components act as a T-stub, where also the deformation capacity of the bolts in tension is included. The questions and limits of deformation capacity of connections of high strength steel was studied in (Girao et al, 2004). In all

works was the connector's behaviour combined with FEA analyses of plates to check the steel limiting strain, which was first prepared by Sherbourne and Bahaari (1994) and (1996).

Models of hollow section connections based on knowledge form nineties are described in Ch. 7 of EN1993-1-8:2006 by curve fitting procedures. The latest version brings the world standard IIW XV-1439-13 ISO/FDIS 14346 (2012). The transfer to higher level of analytical modelling by component method was finished by mechanical transferring of reduction factors to the effective widths and the predefined lever arms, see (Jaspart and Weinand 2015).

The CM´s is not developed for hand calculation. The analyses of all components in connection and its assembly is focus to preparation of design tables or tools.

2.3 Finite element models

Finite element analyses (FEA) for connections are used from 70s of last century as research-oriented procedure. Their ability to express real behaviour of connections is making it a valid alternative to testing standard and expensive source of knowledge of connection's behaviour. Material model for FEM uses true strain stress-strain diagram, which is calculated from experimental results of coupon tests taking into account the contraction of the sample during the inelastic stage of testing. Today computational analysis, in particular computational mechanics and fluid dynamics, is commonly used as an indispensable design tool and a catalyst of many relevant research fields. The recommendation for design by advanced modelling in structural steel is ready to be used in Chapter 5 and Annex C of EN 1993-1-5:2005. The design strain is recommended to be limited to 5%, see cl. C.8(1) EN 1993-1-5:2005. Implementation of safety into advanced design models under ultimate limit state design is summarised in cl. C.9(2) EN1993-1-5:2005. Standard procedure with partial safety factors for material/connections may be applied. More advanced and accurate solution, which takes into consideration the accuracy of model and material separately, gives more accurate and economical solution of structural connections.

The complexity of FE modelling of the structural steel connections was deeply studied since eighties, see (Krishnamurthy, 1978). Later were commonly accepted the procedures to reach proper results in scientific oriented FE models and the strong limits for application of design FE models, see (Bursi and Jaspart, 1997) and (Virdi K. S. et al, 1999).

2.4 Validation and verification

In publications dealing with computational mechanics the authors express a need for Validation and verification (V&V) studies which could be used by code users and software developers, see (Kwasniewski, 2010). However, there are different opinions on how such reference material should be developed, how complex problems should be considered, theoretical or with practical meaning, and if benchmark questions should refer only to analytical and numerical solutions or should also include experimental data. These inquiries are related to the differences between validation and verification. In the formal procedure called Validation and Verification, validation compares the numerical solution

with the experimental data, whereas verification uses comparison of computational solutions with highly accurate (analytical or numerical) benchmark solutions. According to (AIAA Guide 1998), code verification can be conducted through tests of agreement between a computational solution and four types of benchmark solutions: analytical, highly accurate numerical solutions, and manufactured solutions (Oberkampf and Trucano, 2008). In contrast to numerical solutions used in the validation stage, the numerical solutions applied for verification can represent mathematical models with little physical importance. The verification on the analyst's side is based on the test of agreement with the known correct results, if such are available. Most of commercial codes, such as ANSYS, ABAQUS. see (SIMULIA, 2011), and MIDAS support lists of well-documented benchmark cases (tests). For example, ABAQUS in three manuals provides a wide variety of benchmark tests (including 93 NAFEMS benchmarks) from simple one-element tests to complex engineering problems and experiments (validation benchmarks). These example problems, containing input files, are advantageous for a user not only as material for verification but also as a great help in individual modelling, see (Wald et al, 2014). Nevertheless, there is still lack of benchmark studies for some specific research areas such as, for example, connection design.

The experimental data which can be used for validation should be treated separately and in a different way comparing to benchmark solutions applied for verification. The reasons for that are unavoidable errors and uncertainties associated with the result of experimental measurement. An error of a measurement (calculation) can be defined as the result of a measurement (calculation) minus the value of the measured (accurate solution), see (ISO, 1993). As the accurate solution is usually unknown (eventually for simplified cases) the user can only deal with estimates of errors. Uncertainty can be thought of as a parameter associated with the result of a measurement (solution) that characterizes the dispersion of the values that could reasonably be attributed to the measured.

Experimental validation in the structural connections design through comparison between numerical results and experimental data obtained using the beam tests with for simple connections loaded in shear and cruciform tests for moment resistant connections loaded by bending moments are especially difficult and has limitations which are not economical, connection tests compare to most simple ones, but are due to inevitable uncertainties characterising the specimen behaviour. The limitations of experimental validation increase the importance of verification which is supposed to deliver evidence that mathematical models are properly implemented and that the numerical solution is correct with respect to the mathematical model.

2.5 Benchmark cases

Even though examples of experimental studies and examples of calculations following the Structural Eurocodes procedures are also useful and can be helpful for other users, here the term benchmark studies refers to computer simulations (numerical analysis). A well-developed benchmark example should satisfy the following requirements. The problem considered should be relatively simple, easy to

understand. In authors' opinion for more complex problem less reliable solution can be provided. For complex problems, for example with actual material properties of steel or concrete, only numerical solutions can be obtained. Comparison among the numerical solutions obtained with the help of different software shows quite often unexpected discrepancy among the results as well. Even if the results are similar this should not be considered as a strong evidence of the solution's reliability. Two different numerical solutions can be only compared based on a solution sensitivity analysis.

Seeking for the simplicity we should accept that a considered case can show little of practical meaning. It is supposed to be used for verification of computational models not to solve an engineering problem. Critical is the material model taken into account. If the material models developed for actual structural materials are used, for example based on EC, with all required nonlinearities, only approximate solutions are possible and can substantially vary for different software. It is difficult to find a good balance between simplicity and a practical meaning of the chosen benchmark case. To solve this difficulty it is recommended to use in benchmark studies a hierarchical approach where a set of problems is considered, starting from simple cases with analytical solutions and then more complex problems, closer to the practice are investigated numerically. Such approach gives more confidence towards obtained solutions.

As a part of benchmark study the complete input data must be provided in the way easy to follow. All assumptions such as of material properties, boundary conditions, temperature distribution, loading conditions, large/small deformations and displacements must be clearly identified. For experimental examples all measurements and detailed description of the test procedure should be provided. For numerical benchmark examples mesh density study should also be conducted. It should be shown that provided results are within the range of asymptotic convergence. If possible the recommended solution should be given as the estimate of the asymptotic solution based on solutions for at least two succeeding mesh densities. For finite element calculations the complete procedures such as Grid Convergence Index (GCI), based on Richardson extrapolation, are recommended (Roache, 1998). During the development of benchmark studies it also should be considered to check alternative numerical models. e. g. using different codes or solid vs. shell finite elements (if possible). Such approach increases the validity of the solution.

2.6 Numerical experiments

Parametric study is a desired element of the experimental work and an indispensable element of the numerical analysis. The cost needed to perform multiple experiments related to structural connections is usually small but a probabilistic distribution of the system response is rarely available. However, in the case of simulated benchmark problems computational cost of running multiple instances of a simple numerical experiment with varying input parameters is competitive.

The variance of a system response depends on the variance in the input parameters but also on the range at which it is tested. Nonlinearity of the response has to be taken into account as well when

designing the benchmark tests. The numerical experiments should be performed out in the range where a reasonable variation in an input parameter causes a reasonable change in the system's response. Designing a benchmark test producing either a non-sensitive or overly sensitive response is undesirable. The sensitivity study for a system with multiple variable input parameters and multiple responses should be performed by regression analysis or variance based methods.

Actually selection of the System Response Quantity (SRQ), see (Kwasniewski, 2010), is important for both, verification and validation. However, in both cases it is subject to different limitations. In verification, SRQ means a quantity which describes the response of the structure and is selected for comparison with the value obtained from the benchmark solution. A user is less limited here as in the case of validation where the experimental data is always limited with the number of gauges and other instrumentation. The selection of the SRQ should reflect the main objective of the analysis and for structures in fires it usually refers to quantities describing heat transfer or mechanical response. For heat transfer problems temperatures obtained at the specific time instance at selected locations seems to be an optimal choice. For mechanical structural response usually we can choose between local and global (integral) quantities. Engineers are usually interested in stresses and internal forces, which are local quantities. They are subject to larger uncertainties especially in the case of validation. More appropriate are global quantities such as deflection which reflects deformation of the whole, or a large part of, structure and its boundary condition.

2.7 Experimental validation

As the experimental data is stochastic by nature and is always subject to some variation it should be actually defined by a probability distribution such. For complete comparison the numerical results should also be presented in analogous probabilistic manner using a probability distribution, generated by repeated calculations with some selected input data varying following prescribed distributions, so called probability simulations. Such extensive calculations can be conducted automatically with the help of specialised optimization packages (e.g. LS-OPT®, HyperStudy® or ModeFrontier®) which are more often included in nowadays commercial computational systems.

For many authors working on principles of validation and verification (Kwasniewski, 2010) the term calibration has negative meaning and describes a practice which should be avoided in numerical modelling. Calibration means here unjustified modification of the input data applied to a numerical model in order to shift the numerical results closer to the experimental data. An example of erroneous calibration is shown in Fig. 2.1, where at the begging it is assumed that the numerical model well reflects the experiment however, due to some uncertainties associated with the experiment the first numerical prediction, differs from the first experimental result. Frequently in such cases the discrepancy between the experiment and the numerical simulation is attributable to some unidentified by the analyst input parameter and not to a limitation of the software and then through hiding one error by introducing another, the calibration process itself is erroneous. Calibration, applied for example through variation

of material input data, shifts the result closer to the experimental response but at the same time changes the whole numerical model whose probability is now moved away from the experimental one. Due to the calibration, the new numerical model may easily show poorer predictive capability. This fact is principally revealed for modified input data, e.g. loading conditions.

There is a situation when the calibration process actually makes sense. If a full stochastic description of experimental data is known and probabilistic analysis was performed for the simulation and there is a difference between means of measured and simulated responses then calibration of physics models may be needed. The adjustment of the model introduces a change in the response that brings the entire spectrum of results closer to the experimental set of data. The calibration defined that way is much more complex process than just tweaking of the models and must be confirmed on different simulated events.

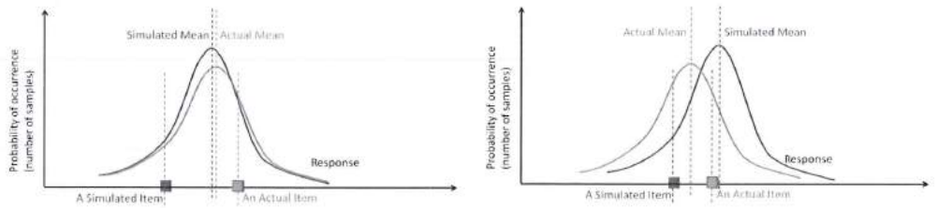

Fig. 2.1: Example of calibration meaning unjustified shifting the numerical results closer to the experimental data (Kwasniewski, 2010)

3 COMPONENT BASED FINITE ELEMENT METHOD

3.1 Material model

The most common material diagrams, which are used in finite element modelling of structural steel, are the ideal plastic or elastic model with strain hardening and the true stress-strain diagram, see Fig. 3.1.1. The true stress-strain diagram is calculated from the material properties of mild steels at ambient temperature obtained in tensile tests. The true stress and strain may be obtained as follows:

$$\sigma_{true} = \sigma\,(1 + \varepsilon) \qquad (3.1.1)$$

$$\varepsilon_{true} = \ln(1 + \varepsilon) \qquad (3.1.2)$$

where σ_{true} is true stress, ε_{true} true strain, σ nominal stress and ε nominal strain. The elastoplastic material with strain hardening is modelled according to EN1993-1-5:2005. The material behaviour is based on von Mises yield criterion. It is assumed to be elastic before reaching the yield strength f_y. The ultimate limit state criteria for regions not susceptible to buckling is reaching of a limiting value of the principal membrane strain. The value of 5 % is recommended.

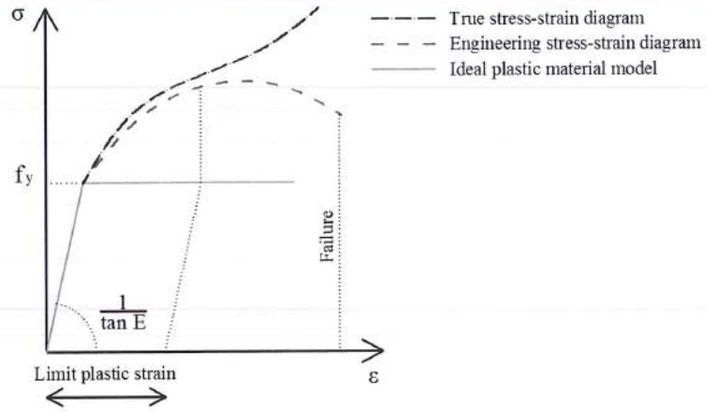

Fig. 3.1.1 Material diagrams of steel in numerical models

The limit value of plastic strain is often discussed. In fact that ultimate load has low sensitivity to the limit value of plastic strain when ideal plastic model is used. It is demonstrated on the following example of a beam to column joint. An open section beam IPE 180 is connected to an open section column HEB 300 and loaded by bending moment as shown in Fig. 3.1.2. The influence of the limit value of plastic strain on the resistance of the beam is shown in Fig. 3.1.3. The limit plastic strain is changing from 2 % to 8 %, but the change in moment resistance is less than 4 %.

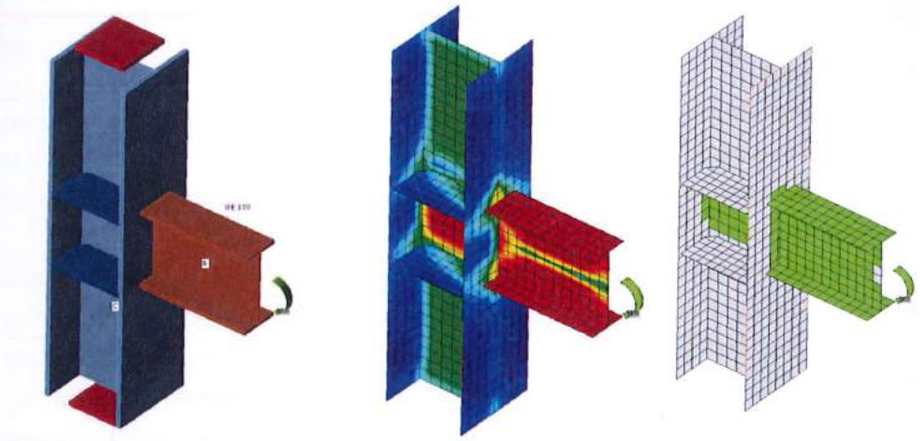

a) loads b) stresses c) strains

Fig. 3.1.2 Example of prediction of ultimate limit state of a beam to column joint

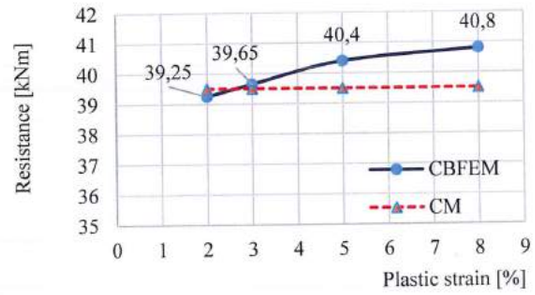

Fig. 3.1.3 Influence of the limit value of plastic strain on the moment resistance

3.2 Plate model and mesh convergence

3.2.1 Plate model

Shell elements are recommended for modelling of plates in design FEA of structural connection. 4-node quadrangle shell elements with nodes at its corners are applied. Six degrees of freedom are considered in every node: 3 translations (u_x, u_y, u_z) and 3 rotations (φ_x, φ_y, φ_z). Deformations of the element are divided into membrane and flexural components.

The formulation of the membrane behaviour is based on the work by Ibrahimbegovic (1990). Rotations perpendicular to the plane of the element are considered. Complete 3D formulation of the element is provided. The out-of-plane shear deformations are considered in the formulation of the flexural behaviour of element based on Mindlin hypothesis. The MITC4 elements are applied, see Dvorkin (1984). The shell is divided into five integration points along the height of the plate and plastic behaviour is analysed in each point. It is called Gaus - Lobatto integration. The nonlinear elastic-plastic stage of material is analysed in each layer based on the known strains.

3.2.2 Mesh convergence

There are some criteria of the mesh generation in the connection model. The connection check should be independent on the element size. Mesh generation on a separate plate is problem-free. The attention should be paid to complex geometries such as stiffened panels, T-stubs and base plates. The sensitivity analysis considering mesh discretisation should be performed for complicated geometries.

All plates of a beam cross-section have common size of elements. Size of generated finite elements is limited. Minimal element size is set to 10 mm and maximal element size to 50 mm. Meshes on flanges and webs are independent on each other. Default number of finite elements is set to 8 elements per cross-section height as shown in Fig. 3.2.1.

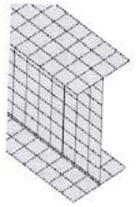

Fig. 3.2.1 Mesh on beam with constrains between web and flange plate

The mesh of end plates is separate and independent on other connection parts. Default finite element size is set to 16 elements per cross-section height as shown in Fig. 3.2.2.

Fig. 3.2.2 Mesh on end plate, with 7 elements on width

Following example of a beam to column joint shows the influence of mesh size on the moment resistance. An open section beam IPE 220 is connected to an open section column HEA200 and loaded by bending moment, as shown in Fig. 3.2.3. The critical component is column panel in shear. The number of finite elements along the cross-section height is changing from 4 to 40 and the results are compared, see Fig. 3.2.4. Dashed lines are representing 5%, 10% and 15% difference. It is recommended to subdivide the cross-section height into 8 elements.

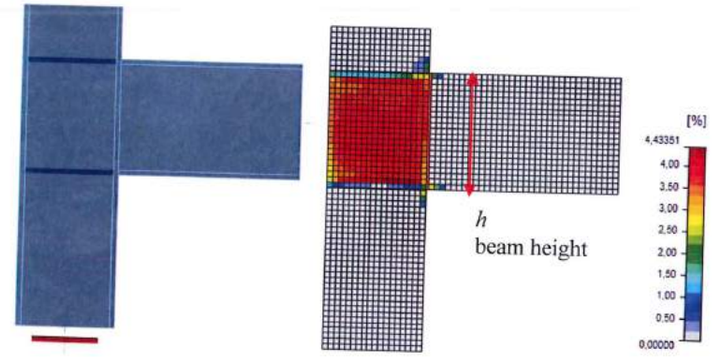

Fig. 3.2.3 Beam to column joint model and plastic strains at ultimate limit state

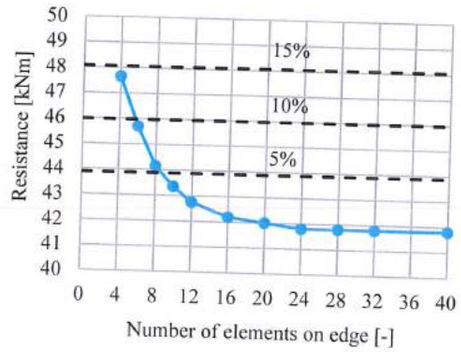

Fig. 3.2.4 Influence of number of elements on the moment resistance

Mesh sensitivity study of a slender compressed stiffener of column web panel is presented. The geometry of the example is taken from section 6.3. The number of elements along the width of the stiffener is changed from 4 to 20. The first buckling mode and the influence of number of elements on the buckling resistance and critical load are shown in Fig. 3.2.5. The difference of 5% and 10% are displayed. It is recommended to use 8 elements along the stiffener width.

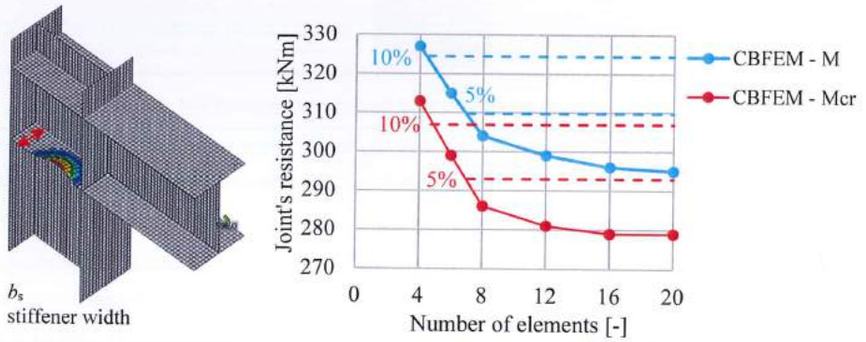

Fig. 3.2.5 First buckling mode and influence of number of elements along the stiffener on the moment resistance

Mesh sensitivity study of T-stub in tension is presented. The geometry of the T-stub is described in section 5.1. The half of the flange width is subdivided into 8 to 40 elements and the minimal element size is set to 1 mm. The influence of number of elements on the T-stub resistance is shown in Fig. 3.2.6. The dashed lines are representing the 5%, 10% and 15% difference. It is recommended to use 16 elements on the half of the flange width.

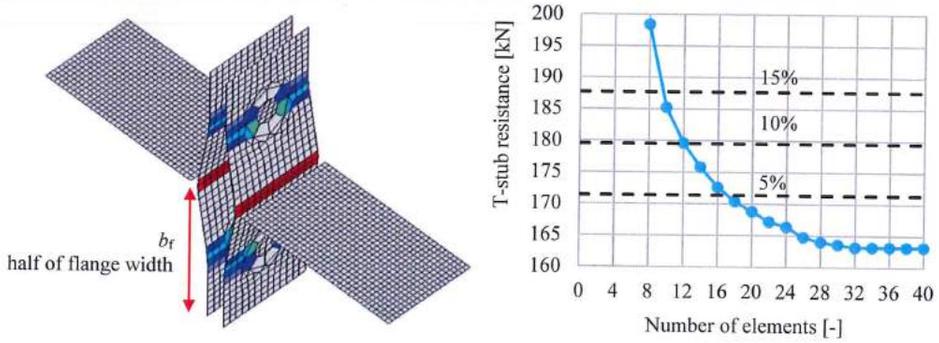

Fig. 3.2.6 Influence of number of elements on the T-stub resistance

3.3 Contacts

The standard penalty method is recommended for modelling of a contact between plates. If penetration of a node into an opposite contact surface is detected, penalty stiffness is added between the node and the opposite plate. The penalty stiffness is controlled by heuristic algorithm during nonlinear iteration to get better convergence. The solver automatically detects the point of penetration and solves the distribution of contact force between the penetrated node and nodes on the opposite plate. It allows to create the contact between different meshes as shown at Fig. 3.3.1. The advantage of the penalty method is the automatic assembly of the model. The contact between the plates has a major impact on the redistribution of forces in connection.

Fig. 3.3.1 Example of separation plates in contact between web and flanges of two overlapped Z sections purlins

3.4 Welds

There exist several options how to treat welds in numerical models. Large deformations makes the mechanical analysis more complex and it is possible to use different mesh descriptions, different kinetic and kinematic variables, and constitutive models. The different types of geometric 2D and 3D models and thereby finite elements with their applicability for different accuracy levels are generally used. Most often used material model is the common rate-independent plasticity model based on von Mises yield criterion. Two approaches which are used for welds are described.

3.4.1 Direct connection of plates

The first option of weld model between plates is direct merge of meshes as shown in Fig. 3.4.1. The load is transmitted through a force-deformation constrains based on Lagrangian formulation to opposite plate. The connection is called multi point constraint (MPC) and relates the finite element nodes of one plate edge to another. The finite element nodes are not connected directly. The advantage of this approach is the ability to connect meshes with different densities. The constraint allows to model midline surface of the connected plates with the offset, which respects the real weld configuration and throat thickness. The load distribution in weld is derived from the MPC, so the stresses are calculated in the throat section. This is important for the stress distribution in plate under the weld and for modelling of T-stubs.

This model does not respect the stiffness of the weld and the stress distribution is conservative. Stress peaks, which appear at the end of plate edges, in corners and rounding, govern the resistance along the whole length of the weld. To eliminate the effect three methods for evaluation of the weld can be chosen maximal stress (conservative)

- Average stress on weld
- Linear interpolation along weld

3.4.2 Plastic weld

To express the weld behaviour an improved weld model is applied. A special elastoplastic element is added between the plates. The element respects the weld throat thickness, position and orientation. The equivalent weld solid is inserted with the corresponding weld dimensions as shown in Fig. 3.4.2. The nonlinear material analysis is applied and elastoplastic behaviour in equivalent weld solid is determinate. Ideal plastic model is used and the plasticity state is controlled by stresses in the weld throat section. The plastic strain in weld is limited to 5% as in the plate. The stress peaks are redistributed along the longer part of the weld length.

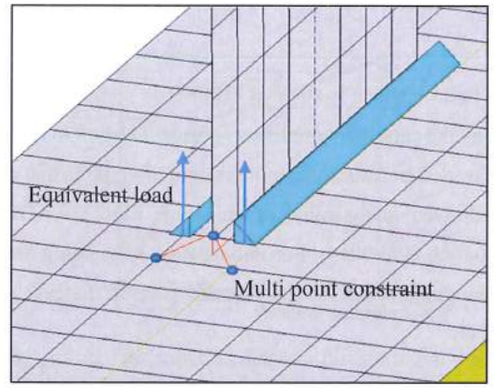

Fig. 3.4.1 Constraint between mesh nodes

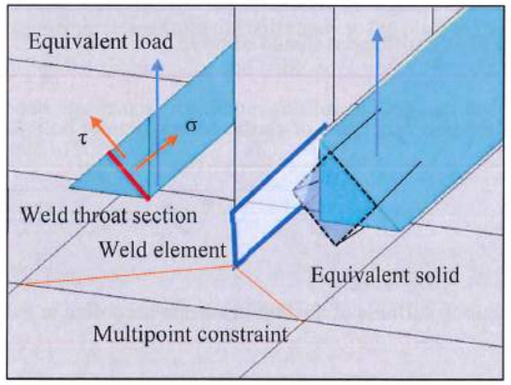

Fig. 3.4.2 Constraint between weld element and mesh nodes

3.5 Bolts

In the Component based finite element method (CBFEM) is component bolt with its behaviour in tension, shear and bearing by the dependent nonlinear springs. The bolt in tension is described by spring with its axial initial stiffness, design resistance, initialisation of yielding and deformation capacity. The axial initial stiffness is derived analytically in guideline VDI2230. The model corresponds to experimental data, see (Gödrich et al 2014). For initialisation of yielding and deformation capacity is assumed that plastic deformation occurs in the threated part of the bolt shank only. The force at beginning of yielding $F_{y,ini}$ is

$$F_{y,ini} = f_{y,b}\ A_t \tag{3.5.1}$$

where, $f_{y,b}$ is yield strength of bolts and A_t tensile area of the bolt. Relation (3.5.1) gives for materials with low ratio of the ultimate strength to yield strength higher values than design resistance $F_{t,Rd}$. To assure a positive value of plastic stiffness it should be taken

$$F_{y,ini} \leq F_{t,Rd} \tag{3.5.2}$$

Deformation capacity of the bolt δ_c consists of elastic deformation of bolt shank δ_{el} and plastic one of the threated part only δ_{pl}.

$$\delta_c = \delta_{el} + \delta_{pl} \tag{3.5.3}$$

$$\delta_{el} = \frac{F_{t,Rd}}{k_{ini}} \tag{3.5.4}$$

where k_{ini} is initial deformation stiffness of the bolt in tension according to guideline VDI2230, and

$$\delta_{pl} = \varepsilon_{pl}\ l_t \tag{3.5.5}$$

where, ε_{pl} is limiting plastic strain, given by value 5 %, and l_t is length of threated part. The tensile force is transmitted to the plates by interpolation links between the bolt shank and nodes in the plate. The transfer area corresponds to the mean value of the bolt shank and the circle inscribed in the hexagon of the bolt head.

The initial stiffness and design resistance of bolts in shear is in CBFEM modelled according to in cl. 3.6 and 6.3.2 in EN1993-1-8:2006. Linear behaviour up to failure is considered.

The spring representing bearing has bi-linear force deformation behaviour with initial stiffness and design resistance according to in cl. 3.6 and 6.3.2 in EN1993-1-8:2006. Deformation capacity is considered according to (Wald et al 2002) as

$$\delta_{pl} = 3\ \varepsilon_{el} \tag{3.5.6}$$

Initialization of yielding is expected, see Fig. 3.5.1, at

$$F_{ini} = 2/3\ F_{b,Rd} \tag{3.5.7}$$

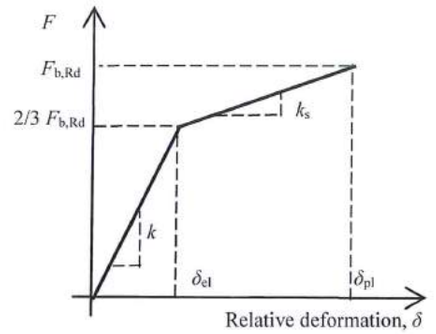

Fig. 3.5.1 Force deformation diagram for bearing of the plate

Interaction of axial and shear force in the bolt is considered according to Tab. 3.4 in EN1993-1-8:2006. Only the compression force is transferred from the bolt shank to the plate in the bolt hole. It is modelled by interpolation links between the shank nodes and holes edge nodes. The deformation stiffness of the shell element, which models the plates, distributes the forces between the bolts and simulates the adequate bearing of the plate.

3.6 Anchor bolt

3.6.1 Description

The anchor bolt is modelled with similar procedures as structural bolts. The bolt is on one side fixed to the concrete block. Its length L_b is taken according to EN1993-1-8:2006 as sum of washer thickness t_w, base plate thickness t_{bp}, grout thickness t_g and free length embedded in concrete, which is expected as $8d$, where d is bolt diameter. The stiffness in tension is calculated as $k = E\,A_s/L_b$. The load-deformation diagram of the anchor bolt is shown in Fig. 3.6.1. The values according to ISO 898:2009 are summarised in Tab. 3.6.1 and in formulas below.

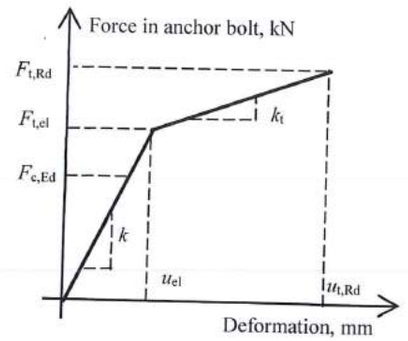

Fig. 3.6.1 Load–deformation diagram of the anchor bolt

$$F_{t,el} = \frac{F_{t,Rd}}{c_1 \cdot c_2 - c_1 + 1} \tag{3.6.1}$$

$$k_t = c_1 \cdot k;\; c_1 = \frac{R_m - R_e}{\left(\frac{1}{4}A - \frac{R_e}{E}\right)\cdot E} \tag{3.6.2}$$

$$u_l = \frac{F_{t,el}}{k} \tag{3.6.3}$$

$$u_{t,Rd} = c_2 \cdot u_l;\; c_2 = \frac{A \cdot E}{4 \cdot R_e} \tag{3.6.4}$$

Table 3.6.1 Anchor bolt parameters, based to ISO 898:2009

Grade	R_m	$R_e = R_{p02}$	A	E	c_1	c_2
	[MPa]	[MPa]	[%]	[MPa]	[-]	[-]
4.8	420	340	14	2,1E+05	0,011	21,6
5.6	500	300	20	2,1E+05	0,020	35,0
5.8	520	420	10	2,1E+05	0,021	12,5
6.8	600	480	8	2,1E+05	0,032	8,8
8.8	830	660	12	2,1E+05	0,030	9,5
10.9	1040	940	9	2,1E+05	0,026	5,0

The stiffness of the anchor bolt in shear is taken as the stiffness of the structural bolt in shear. The anchor bolt resistance is evaluated according to ETAG 001 Annex C or prEN1992-1-4.2015. Steel failure mode is determined according to cl. 6.2.6.12 in EN 1993-1-8.

3.7 Concrete block

3.7.1 Design model

In component based finite element method (CBFEM), it is convenient to simplify the concrete block as 2D contact elements. The connection between the concrete and the base plate resists in compression only. Compression is transferred via Winkler-Pasternak subsoil model, which represents deformations of the concrete block. Tension force between the base plate and concrete block is carried by anchor bolts. Shear force is transferred by friction between a base plate and a concrete block, by shear key, and by bending of anchor bolts and friction. The resistance of bolts in shear is assessed analytically. Friction and shear key are modelled as a full single point constraint in the plane of the base plate-concrete contact.

3.7.2 Resistance

The resistance of concrete in 3D compression is determined based on EN 1993-1-8:2006 by calculating the design bearing strength of concrete in the joint f_{jd} under the effective area A_{eff} of the base plate. The design bearing strength of the joint f_{jd} is evaluated according to Cl. 6.2.5 in EN 1993-1-8:2006 and Cl. 6.7 in EN 1992-1-1:2005. The grout quality and thickness is introduced by the joint coefficient β_{jd}. For grout quality equal or better than quality of the concrete block is expected $\beta_{jd} = 1{,}0$. The effective area A_{eff} under the base plate is estimated to be of the shape of the column cross-section increased by additional bearing width c

$$c = t\sqrt{\frac{f_y}{3\,f_j\,\gamma_{M0}}} \tag{3.7.1}$$

where t is the thickness of the base plate, f_y is the base plate yield strength, γ_c is the partial safety factor for concrete and γ_{M0} is the partial safety factor for steel.

The effective area is calculated by iteration until the difference between additional bearing widths of current and previous iteration $|c_i - c_{i-1}|$ is less than 1 mm.

The area where the concrete is in compression is taken from results of FEA. This area in compression A_{com} allows to determine the position of neutral axis. The intersection of the area in compression A_{com} and the effective area A_{eff} allows to assess the resistance for generally loaded column base of any column shape with any stiffeners. The average stress σ on the effective area A_{eff} is determined as the compression force divided by the effective area. Check of the component is in stresses $\sigma \leq f_{jd}$.

This procedure of assessing the resistance of the concrete in compression is independent on the mesh of the base plate as can be seen in Fig. 3.7.1 and 3.7.2. The geometry of the model used for comparison is described in detail in Chapter 8.1.3. Two cases were investigated: loading by pure compression 1200 kN, see Fig. 3.7.1, and loading by combination of compressive force 1200 kN and bending moment 90 kN, see Fig. 3.7.2.

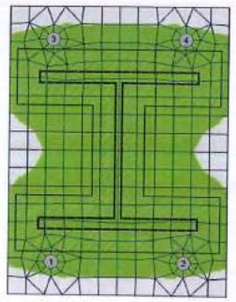

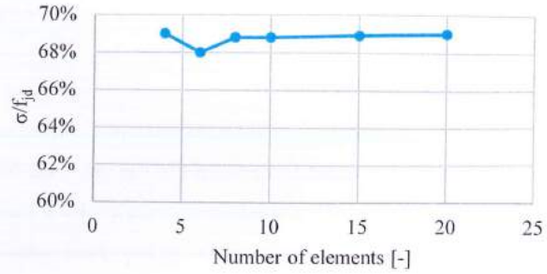

No. of elements	A_{eff} [m^2]	σ [MPa]	f_{jd} [MPa]
4	0,06	18,5	26,8
6	0,06	18,2	26,8
8	0,06	18,5	26,8
10	0,06	18,4	26,8
15	0,06	18,5	26,8
20	0,06	18,5	26,8

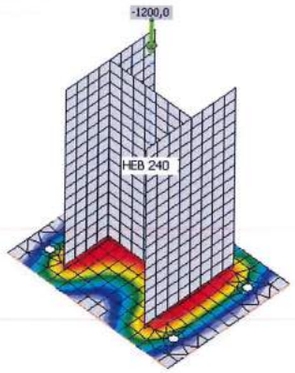

Fig. 3.7.1 Influence of number of elements on prediction
of resistance of concrete in compression in case of pure compression

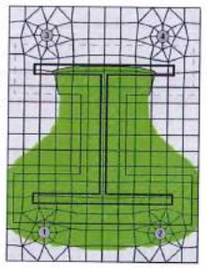

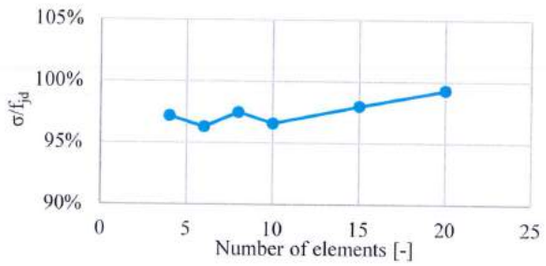

No. of elements	A_{eff} [m^2]	σ [MPa]	f_{jd} [MPa]
4	0,05	26,0	26,8
6	0,04	25,8	26,8
8	0,04	26,1	26,8
10	0,05	25,9	26,8
15	0,04	26,3	26,8
20	0,04	26,6	26,8

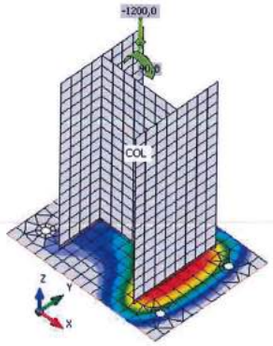

Fig. 3.7.2 Influence of number of elements on prediction
of resistance of concrete in compression in case of compression and bending

3.7.3 Deformation stiffness

The stiffness of the concrete block may be predicted for design of column bases as elastic hemisphere. A Winkler-Pasternak subsoil model is commonly used for a simplified calculation of foundations. The stiffness of subsoil is determined using modulus of elasticity of concrete and effective height of subsoil as

$$k = \frac{E_c}{(\alpha_1 + \upsilon)\cdot\sqrt{\frac{A_{eff}}{A_{ref}}}}\cdot\left(\frac{1}{\frac{h}{\alpha_2\cdot d}+\alpha_3}+\alpha_4\right) \qquad (3.7.2)$$

where, k is stiffness in compression, E_c is modulus of elasticity, n is Poisson coefficient of concrete foundation, A_{eff} is effective area, A_{ref} is reference area, d is base plate width, h is column base height, and α_i are coefficients. The following values for coefficient were used: A_{ref} =10 m^2; α_1 = 1,65; α_2 = 0,5; α_3 = 0,3; α_4 =1,0.

3.8 Local buckling of compressed plates

In research FEA models the slender plates in compression taking into account its plate geometrical imperfections, residual stresses and large deformation during analyses, see EN1993-1-5:2005. This should be precised according to the different plate/joint configuration. The FEA procedure naturally offers the prediction of the buckling load of the joint. The design procedure for class 4 cross-sections according to reduced stress method is described in Annex B of EN1993-1-5:2005. It allows predict the post buckling resistance of the joints. Critical buckling modes are determined by material linear and geometric nonlinear analysis. In the first step the minimum load amplifier for the design loads to reach the characteristic value of the resistance of the most critical point coefficient $\alpha_{ult,k}$ is obtained. Ultimate limit state is reached by 5 % plastic strain. The critical buckling factor α_{cr} is determined and stands for the load amplifier to reach the elastic critical load under complex stress field. Examples of critical buckling mode in steel joints are shown in Fig. 3.8.1.

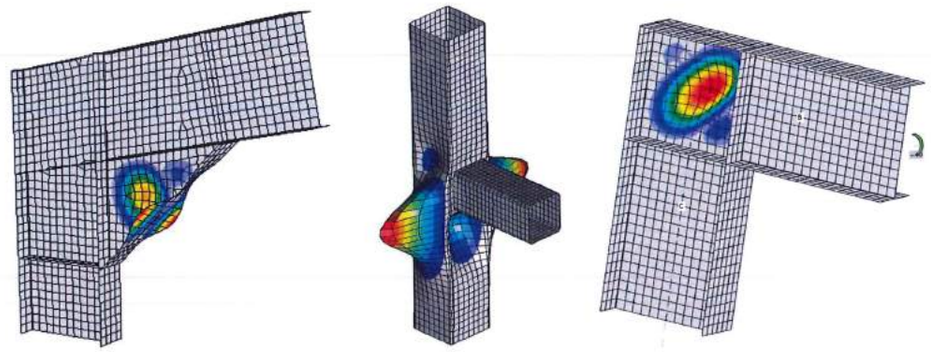

Fig. 3.8.1 Examples of first buckling mode in CBFEM models

The load amplifiers are related to the non-dimensional plate slenderness, which is determined as follows

$$\overline{\lambda} = \sqrt{\frac{\alpha_{ult}}{\alpha_{cr}}} \qquad (3.8.1)$$

Reduction buckling factor ρ is calculated according to EN 1993-1-5:2005 Annex B. Conservatively, the lowest value from longitudinal, transverse and shear stress is taken. Fig. 3.8.2 shows the relation between plate slenderness and reduction buckling factor.

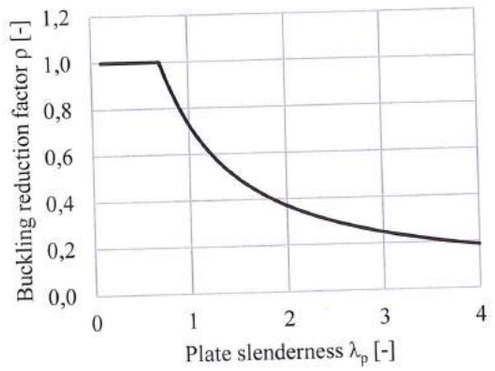

Fig. 3.8.2 Buckling reduction factor ρ according to EN 1993-1-5 Annex B

The verification of the plate is based on the von-Mises yield criterion and reduced stress method. Buckling resistance is assessed as

$$\frac{\alpha_{ult}\cdot\rho}{\gamma_{M1}} \geq 1 \qquad (3.8.2)$$

where γ_{M1} is partial safety factor.

3.9 Moment-rotation relation

The joint is generally three dimensional. The moment rotation curve for connection in joint is evaluated for each element, which is attached to the joint. The calculation of the moment rotation relation by the FEA model is different compare to the stress/strain analysis of joint. The moment rotation is analysed for connection of the connected member separately in the plains, where they are is loaded.

The modelling of the moment rotational curve may be documented on behaviour of a well-designed portal frame eaves moment bolted connection developed based on US best practice and applied in good European practice represented by British and German design books. The composition of the connection geometry of the bolted connection is demonstrated in Fig. 3.9.1. The rafter of cross section IPE 400 column is connected to column HEA 320 by the full depth end plate of thickness 25 mm by 12 bolts M24 8.8. The haunch 700 mm long is 300 mm high with flange 15x150 mm. The stiffeners are designed from P20. Material S355. The results of analyses show in Fig. 3.9.2 the development of plastic zones in connection by CBFEM analyses, from first yielding under the bolt in tension, through development of full plasticity in the column web panel in shear, till reaching the 5 % strain in panel. After reaching this strain the plastic zones propagate rapidly in the column web panel in shear and for small steps in bending moment the rotation of the joint rise significantly, see Fig. 3.9.3.

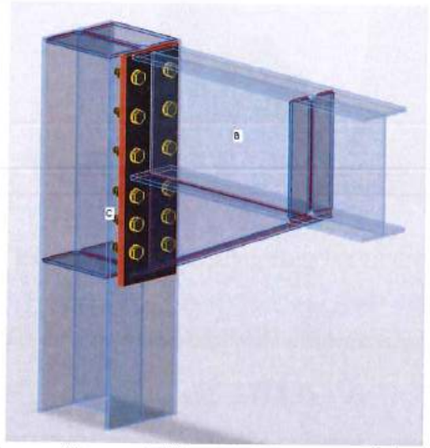

Fig. 3.9.1 Composition portal frame eaves moment bolted connection

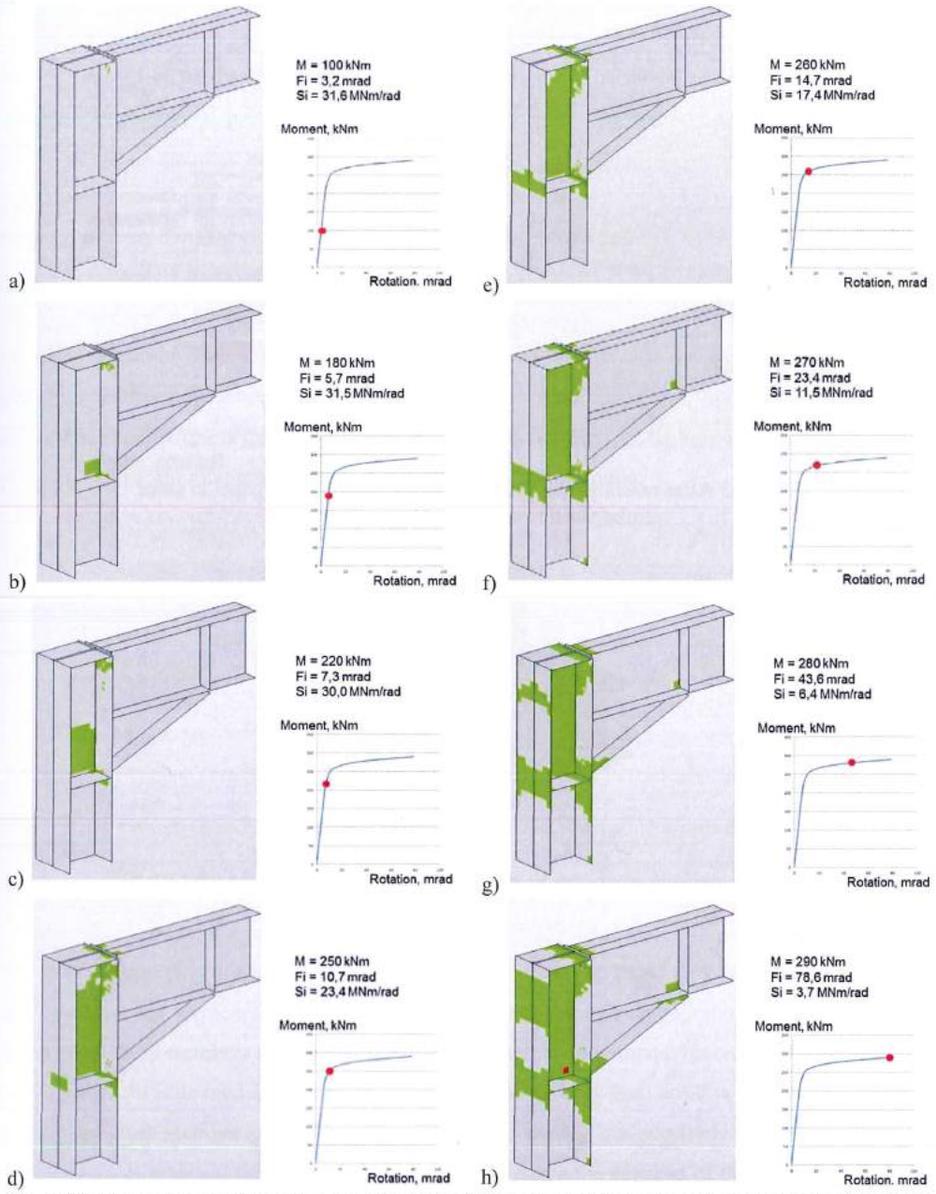

Fig. 3.9.2 Development of plastic zones in connection by CBFEM analyses, from first yielding under the tensile bolt a), through development of full plasticity in the column web panel loaded in shear e)-f), till reaching the 5 % strain in panel h)

As is commonly known in well-designed connections starts the plastification early, see Fig. 3.9.2a. The column web panel in shear bring the deformation capacity of connection and guide the nonlinear part of

behaviour, see Fig. 3.9.2e-f. Fig. 3.9.3 demonstrates the fast development of yielding in the column web panel after reaching the 5 % strain.

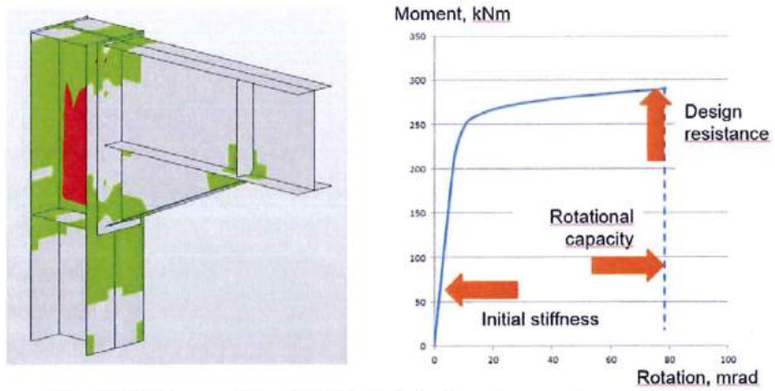

Fig. 3.9.3 After reaching the 5 % strain in the column web panel in shear the plastic zones propagate rapidly

3.10 Bending stiffness

The calculation of the bending/deformation stiffness by the FEA model is different compare to the stress/strain analysis of joint. The joint is three dimensional. The bending/deformation stiffness for connection of an element, which is attached to the joint, is influenced by the shear deformation in the joint and the connection deformation of the particular element in the selected plane of the element. For joints connecting more members are analysed the bending stiffness's of the connections of the connected members separately in the plains, where they are loaded.

For the evaluation of the bedding stiffness of a particular connection is assumed, that members are supported at the ends, and only the analysed member *i* has free end, see Fig. 3.10.1. The analysed member *i* is loaded by a bending moment in plane *yz* coming from the global analyses. To learn the secant rotational stiffness $S_{j,i,yz}$ for rotation $\phi_{i,yz}$ the bending moment $M_{j,Ed,i,yz}$ is applied in a selected plane *yz*. The secant rotational stiffness $S_{j,s,i,yz}$ is derived from formula:

$$S_{j,s,i,yz} = M_{j,Ed,i,yz} / \phi_{i,yz} \qquad (3.10.1)$$

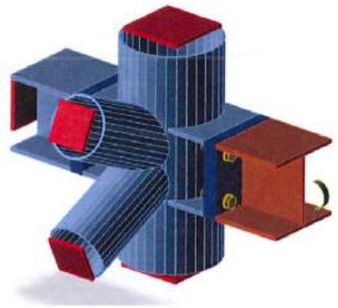

3.10.1 FEA model for analysis of stiffness of selected connected member

The total rotation $\phi_{j,i,yz}$ of the end section of analysed member *i* in plane *yz* is derived on a model with one free/observed element and the rest fixed elements. The calculated value is influenced by the deformation of all members in element. The effects of member deformation is removed analysing in the plane *yz* the substitute model of the node, which is composed only from one dimensional members with appropriate cross-sections as shown in Fig. 3.10.2. By loading this substitute 1D model by bending moment $M_{i,yz}$ is obtained the rotation $\phi_{j,ei,yz}$, which represents the stiffness of the particular connected members only. In the substitute 1D model the node is expected to be rigid. The rotation caused only by the construction of the connection is derived as:

$$\phi_{j,i,yz} = \phi_{j,ti,yz} - \phi_{j,ei,yz} \qquad (3.10.2)$$

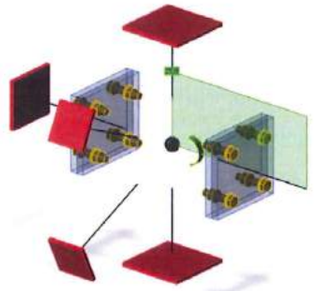

Fig. 3.10.2 The substitute 1D model to eliminate the bending flexibility if the connected elements

The secant stiffness's of connection $\phi_{j,i,yz}$ is derived during its loading. The initial stiffness $\phi_{j,ini}$ is defined as elastic stiffness and is expected to be linear till 2/3 $M_{j,Rd}$, see cl. 6.3.1 in EN1993-1-8:2006. The calculation of the initial bending stiffness by the FEA model is taken as a secant stiffness loaded till 2/3 $M_{j,Rd}$ from the acting bending moment till 2/3 $M_{2/3Rd,i,yz}$ and corresponding rotation in connection $\phi_{2/3Rd,i,yz}$ as:

$$S_{j,ini,i,zy} \cong S_{j,s,2/3Rd,i,zy} = M_{2/3Rd,i,yz} / \phi_{2/3Rd,i,yz} \qquad (3.10.3)$$

For the connection presented in Fig. 3.10.1 are the values of the bending resistance $M_{j,Rd,i,yz}$ and initial stiffness $\phi_{j,ini,i,yz}$ summarized in Fig. 3.10.3.

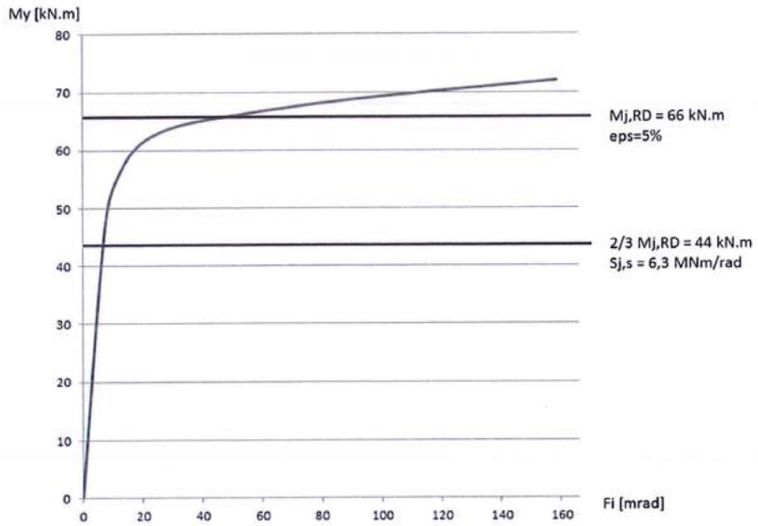

Fig. 3.10.3 Moment/rotation diagram of connection in joint for one connected member

The bending resistance $M_{j,Rd,i,yz}$ of connection is in CBFEM evaluated by strain 5 % in plates/sections or resistance of connectors, e.g. bolts. Fig. 3.10.4 shows the strain in the joint exposed to moments in the

plane of the strong axis of the connected open I section beam at Fig. 3.10.1 from M_y = 25 kNm to 72 kNm. The maximal reached strain ε_{max} from 0,2 % till 22,7 % is reached.

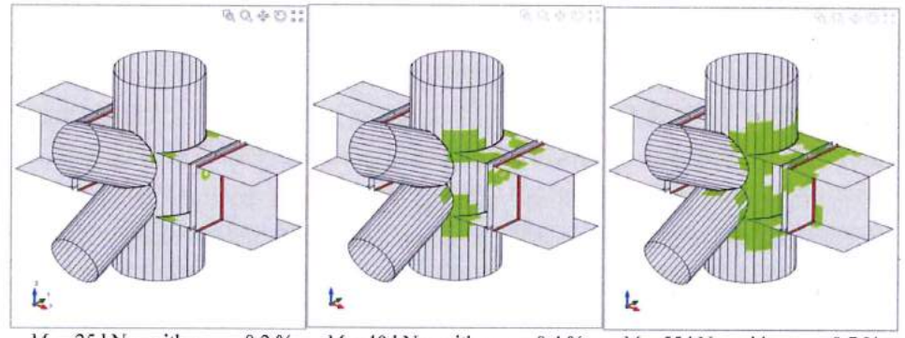

M_y = 25 kNm with ε_{max} = 0,2 % M_y =40 kNm with ε_{max} = 0,4 % M_y =55 kNm with ε_{max} = 0,7 %

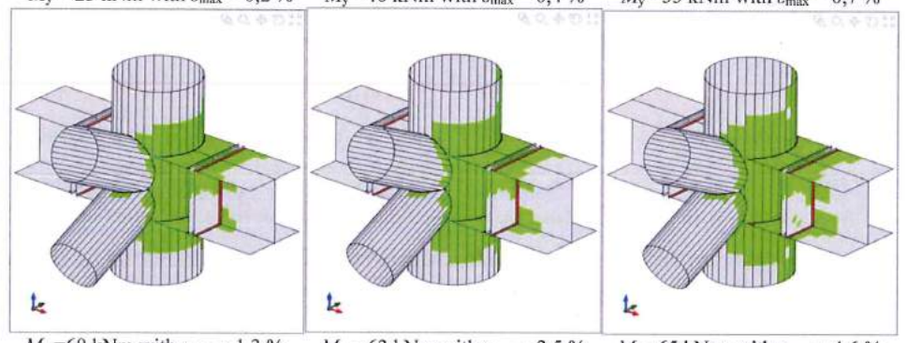

M_y =60 kNm with ε_{max} = 1,3 % M_y = 63 kNm with ε_{max} = 2,5 % M_y =65 kNm with ε_{max} = 4,6 %

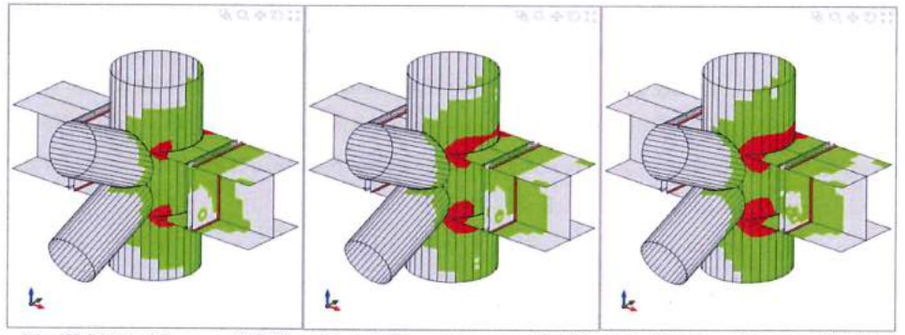

M_y =68 kNm with ε_{max} = 10,8 % M_y =70 kNm with ε_{max} = 16,4 % M_y =72 kNm with ε_{max} = 22,7 %

Fig. 3.10.4 The maximal strains ε_{max} in joint during its loading by bending moment M_y in the plane of the strong axis of the connected open I section beam

3.11 Deformation capacity

The deformation capacity/ductility δ_{Cd} belongs with resistance and stiffness to the three basic parameters describing the behaviour of connections. In moment resistant connections is achieved the ductility by a sufficient rotation capacity φ_{Cd}. The deformation/rotation capacity is calculated for each connection in the joint separatelly. The prediction of deformation capacity δ_{Cd} of connections is currently studied by component method (CM), but is not offered as standardised procedure. Compare to well accept methods for determination of the initial stiffness and resistance of many types' structural joints, there are no generally accepted standardised procedures for the determination of the rotation capacity. The deemed to satisfy criteria are selected to help the engineers in cl 6.4.2 of EN1993-1-8:2006.

A beam-to-column joint in which the design moment resistance of the joint $M_{j,Rd}$ is governed by the design resistance of the column web panel in shear, may be assumed to have adequate rotation capacity for plastic global analysis, provided that:

$$d/t_w \leq 69\,\varepsilon \qquad (3.11.1)$$

where d the column web panel width, t_w is the web thickness and $\varepsilon \leq \sqrt{235/f_y}$ is the steel yield strength ratio.

In cl 6.4.2(2) is limited the plastic distribution between the bolt rows, for joints with a bolted end-plate connection provided that the design moment resistance of the joint is governed by the design resistance of the column flange or the beam end-plate in bending or the thickness t of either the column flange or the beam end-plate or tension flange cleat satisfies:

$$t \leq 0{,}36\, d \sqrt{f_{ub}/f_y} \qquad (3.11.2)$$

where d and $f_{u.b}$ are the diameter and strength of the bolt and f_y is the yield strength of the relevant plate.

The rotation capacity φ_{Cd} of a welded beam-to-column connection may be assumed to be not less that the value given by the following expression provided that its column web is stiffened in compression but unstiffened in tension, and its design moment resistance is not governed by the design shear resistance of the column web panel, see 6.4.2(1):

$$\varphi_{Cd} = 0{,}025\, h_c / h_b \ldots \qquad (3.11.3)$$

where h_b is the depth of the beam and h_c is the depth of the column. An unstiffened welded beam-to-column joint designed in conformity with the provisions of this section, may be assumed to have a rotation capacity φ_{Cd} of at least 0,015 radians.

The estimation of the rotation capacity is important in connections exposed to seismic, see (Gioncu and Mazzolani, 2002) and (Grecea 2004), and extreme loading, see (Sherbourne AN, Bahaari, 1994 and 1996). The deformation capacity of components has been studied from end of last century (Foley and Vinnakota, 1995). Faella et al (2000) carried out tests on T-stubs and derived for the deformation capacity the analytical expressions. Kuhlmann and Kuhnemund (2000) performed tests on the column web subjected to transverse compression at different levels of compression axial force in the

column. Da Silva et al (2002) predicted deformation capacity at different levels of axial force in the connected beam. Based on the test results combined with FE analysis deformation capacities are established for the basic components by analytical models by Beg et al (2004). In the work are represented components by non-linear springs, and appropriately combined in order to determine the rotation capacity of the joint for the end-plate connections, with an extended or flush end-plate, and welded connections. For these connections, the most important components that may significantly contribute to the rotation capacity column were recognised as the web in compression, column web in tension, column web in shear, column flange in bending, and end-plate in bending. Components related to the column web are relevant only when there are no stiffeners in the column that resist compression, tension or shear forces. The presence of a stiffener eliminates the corresponding component, and its contribution to the rotation capacity of the joint can be therefore neglected. End-plates and column flanges are important only for end-plate connections, where the components act as a T-stub, where also the deformation capacity of the bolts in tension is included. The questions and limits of deformation capacity of connections of high strength steel was studied by Girao at al (2004).

4 WELDED CONNECTION

4.1 Fillet weld in lap joint

4.1.1 Description

The object of this chapter is verification of component based finite element method (CBFEM) of a fillet weld in a lap joint with component method (CM). Two plates are connected to each other in three configurations, i.e. with a transverse weld, with a longitudinal weld and combination of the transverse and longitudinal welds. The length and throat thickness of the weld are the changing parameters in the study. The study covers long welds, which resistance is reduced due to stress concentration. The joint is loaded by normal force.

4.1.2 Analytical model

The fillet weld is the only component examined in the study. The welds are designed to be the weakest component in the joint. The weld is designed according to EN1993-1-8:2006. The design resistance of the fillet weld is determined using the Directional method given in section 4.5.3.2 EN1993-1-8:2006. The available calculation methods for checking the strength of fillet welds are based upon the simplifying assumption that stresses are uniformly distributed within the throat section of a fillet weld. A uniform distribution of stress is assumed on the throat section of the weld, leading to the normal stresses and shear stresses shown in Fig. 4.1.1, as follows:

$\sigma_\perp$ is the normal stress perpendicular to the throat section;

$\sigma_\parallel$ is the normal stress parallel to the axis of the weld on its cross section;

$\tau_\perp$ is the shear stress (in the plane of the throat section) perpendicular to the axis of the weld;

$\tau_\parallel$ is the shear stress (in the plane of the throat section) parallel to the axis of the weld.

The normal stress $\sigma_\parallel$ parallel to the axis is not considered when verifying the design resistance of the weld.

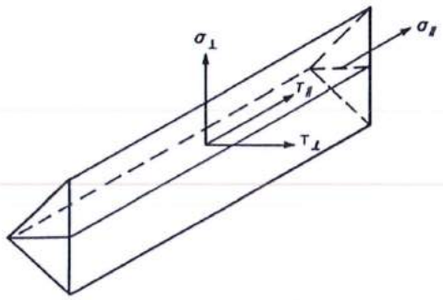

Fig. 4.1.1 Stresses on the throat section of a fillet weld

The design resistance of the fillet weld will be sufficient if the following are both satisfied:

$$\sqrt{\sigma_\perp^2 + 3\left(\tau_\perp^2 + \tau_\parallel^2\right)} \le \frac{f_u}{\beta_w \gamma_{M2}} \qquad (4.1.1)$$

$$\sigma_\perp \le \frac{0{,}9 f_u}{\gamma_{M2}} \qquad (4.1.2)$$

In lap joints longer than *150 a* the reduction factor β_{Lw1} is given by:

$$\beta_{Lw,1} = 1{,}2 - \frac{0{,}2 L_j}{150a} \quad \text{but} \quad \beta_{Lw,1} \le 1{,}0 \qquad (4.1.3)$$

Overview of the considered examples and the material properties are given in the Tab. 4.1.1. The weld configurations T is for transverse, P for parallel weld, and TP for combination of both are studied, in Fig. 4.1.2 see geometry. The sensitivity for two parameters: weld length and effective throat thickness were investigated.

Tab. 4.1.1 Overview of examples

Example	Material					Weld a		Plate 1		Plate 2	
	f_y	f_u	E	γ_{M0}	γ_{M2}	a_a	L_a	b_1	t_1	b_2	t_2
	[MPa]	[MPa]	[GPa]	[-]	[-]	[mm]	[mm]	[mm]	[mm]	[mm]	[mm]
T100	235	360	210	1	1,25	3	100	100	10	320	10
T110	235	360	210	1	1,25	3	110	110	10	320	10
T120	235	360	210	1	1,25	3	120	120	10	320	10
T130	235	360	210	1	1,25	3	130	130	10	320	10
T140	235	360	210	1	1,25	3	140	140	10	320	10
T150	235	360	210	1	1,25	3	150	150	10	320	10
T200	235	360	210	1	1,25	3	200	200	10	320	10
T250	235	360	210	1	1,25	3	250	250	10	320	10
T300	235	360	210	1	1,25	3	300	300	10	320	10

T3	235	360	210	1	1,25	3	120	120	20	200	20
T4	235	360	210	1	1,25	4	120	120	20	200	20
T5	235	360	210	1	1,25	5	120	120	20	200	20
T6	235	360	210	1	1,25	6	120	120	20	200	20
T7	235	360	210	1	1,25	7	120	120	20	200	20
T8	235	360	210	1	1,25	8	120	120	20	200	20
T9	235	360	210	1	1,25	9	120	120	20	200	20
T10	235	360	210	1	1,25	10	120	120	20	200	20

Example	Material					Weld b		Plate 1		Plate 2	
	f_y	f_u	E	γ_{M0}	γ_{M2}	a_a	L_a	b_1	t_1	b_2	t_2
	[MPa]	[MPa]	[GPa]	[-]	[-]	[mm]	[mm]	[mm]	[mm]	[mm]	[mm]
P150	235	360	210	1	1,25	3	150	200	20	300	20
P200	235	360	210	1	1,25	3	200	200	20	300	20
P250	235	360	210	1	1,25	3	250	200	20	300	20
P300	235	360	210	1	1,25	3	300	200	20	300	20
P350	235	360	210	1	1,25	3	350	200	20	300	20
P400	235	360	210	1	1,25	3	400	200	20	300	20
P450	235	360	210	1	1,25	3	450	200	20	300	20
P500	235	360	210	1	1,25	3	500	200	20	300	20
P550	235	360	210	1	1,25	3	550	200	20	300	20
P600	235	360	210	1	1,25	3	600	200	20	300	20
P700	235	360	210	1	1,25	3	700	200	20	300	20
P800	235	360	210	1	1,25	3	800	200	20	300	20

P3	235	360	210	1	1,25	3	140	200	20	300	20
P4	235	360	210	1	1,25	4	140	200	20	300	20
P5	235	360	210	1	1,25	5	140	200	20	300	20
P6	235	360	210	1	1,25	6	140	200	20	300	20
P7	235	360	210	1	1,25	7	140	200	20	300	20
P8	235	360	210	1	1,25	8	140	200	20	300	20
P9	235	360	210	1	1,25	9	140	200	20	300	20
P10	235	360	210	1	1,25	10	140	200	20	300	20

Example	Material					Weld a		Weld b		Plate 1		Plate 2	
	f_y	f_u	E	γ_{M0}	γ_{M2}	a_a	L_a	a_b	L_b	b_1	t_1	b_2	t_2
	[MPa]	[MPa]	[GPa]	[-]	[-]	[mm]	[mm]	[mm]	[mm]	[mm]	[mm]	[mm]	[mm]
TPa100	235	360	210	1	1,25	3	100	3	100	100	20	400	20
TPa150	235	360	210	1	1,25	3	150	3	100	150	20	400	20
TPa200	235	360	210	1	1,25	3	200	3	100	200	20	400	20
TPa250	235	360	210	1	1,25	3	250	3	100	250	20	400	20
TPa300	235	360	210	1	1,25	3	300	3	100	300	20	400	20

TPa3	235	360	210	1	1,25	3	100	4	100	100	20	200	20
TPa4	235	360	210	1	1,25	4	100	4	100	100	20	200	20
TPa5	235	360	210	1	1,25	5	100	4	100	100	20	200	20
TPa6	235	360	210	1	1,25	6	100	4	100	100	20	200	20
TPa7	235	360	210	1	1,25	7	100	4	100	100	20	200	20

Example	Material					Weld a		Weld b		Plate 1		Plate 2	
	f_y	f_u	E	γ_{M0}	γ_{M2}	a_a	L_a	a_b	L_b	b_1	t_1	b_2	t_2
	[MPa]	[MPa]	[GPa]	[-]	[-]	[mm]	[mm]	[mm]	[mm]	[mm]	[mm]	[mm]	[mm]
TPb80	235	360	210	1	1,25	3	120	3	80	120	20	300	20
TPb100	235	360	210	1	1,25	3	120	3	100	120	20	300	20
TPb120	235	360	210	1	1,25	3	120	3	120	120	20	300	20
TPb140	235	360	210	1	1,25	3	120	3	140	120	20	300	20
TPb160	235	360	210	1	1,25	3	120	3	160	120	20	300	20
TPb180	235	360	210	1	1,25	3	120	3	180	120	20	300	20
TPb200	235	360	210	1	1,25	3	120	3	200	120	20	300	20

TPb3	235	360	210	1	1,25	3	160	3	100	160	20	200	20
TPb4	235	360	210	1	1,25	3	160	4	100	160	20	200	20
TPb5	235	360	210	1	1,25	3	160	5	100	160	20	200	20
TPb6	235	360	210	1	1,25	3	160	6	100	160	20	200	20
TPb7	235	360	210	1	1,25	3	160	7	100	160	20	200	20
TPb8	235	360	210	1	1,25	3	160	8	100	160	20	200	20

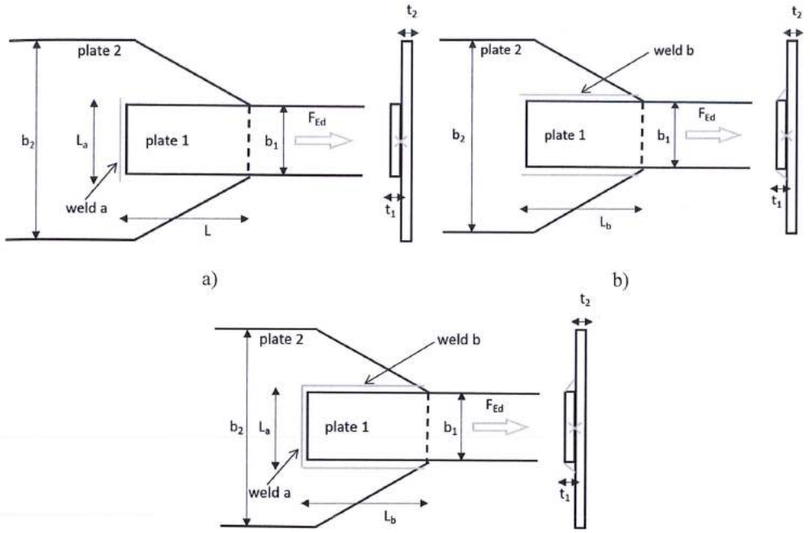

Fig, 4.1.2 Joint's geometry with dimensions

a) Transverse weld b) Parallel weld c) Combination of transverse with parallel weld

4.1.3 Numerical model

The weld component in CBFEM is described in Chapter 3.4. Nonlinear elastic-plastic material is used for welds in this study. The limiting plastic strain is reached in longer part of the weld and stress peaks are redistributed.

4.1.4 Verification of resistance

Design weld's resistance calculated by CBFEM is compared with the results of CM. Results are presented in Tab. 4.1.2. The study is performed for two parameters length of the weld and effective throat thickness in three weld configurations, e.g. for the transverse weld, for the parallel welds, and for combination of the transverse and parallel welds.

Tab. 4.1.2 Comparison of CBFEM and CM

Example	Design resistance		
	CM [kN]	CBFEM [kN]	Diff. [%]
T100	76	76	0
T110	84	84	0
T120	91	91	0
T130	99	99	0
T140	106	106	0
T150	114	114	0
T200	152	152	0
T250	190	191	1
T300	229	229	0
T3	91	93	2
T4	122	124	2
T5	152	155	2
T6	183	186	2
T7	213	217	2
T8	244	247	1
T9	274	278	1
T10	305	309	1

	Example	Design resistance		
		CM [kN]	CBFEM [kN]	Diff. [%]
Long weld	P150	187	183	-2
	P200	249	244	-2
	P250	311	305	-2
	P300	374	366	-2
	P350	436	427	-2
	P400	498	488	-2
	P450	561	548	-2
	P500	609	606	0
	P550	655	659	1
	P600	698	700	0
	P700	776	745	-4
	P800	842	788	-7
	P3	174	172	-1
	P4	232	230	-1
	P5	290	288	-1
	P6	349	344	-2
	P7	407	401	-2
	P8	465	460	-1
	P9	523	518	-1
	P10	581	574	-1

Example	Design resistance		
	CM [kN]	CBFEM [kN]	Diff. [%]
TPa100	201	200	0
TPa150	239	239	0
TPa200	277	278	0
TPa250	316	316	0
TPa300	354	355	0
TPa3	242	242	0
TPa4	267	268	0
TPa5	293	293	0
TPa6	319	317	-1
TPa7	344	330	-4

Example	Design resistance		
	CM [kN]	CBFEM [kN]	Diff. [%]
TPb80	191	190	-1
TPb100	216	215	0
TPb120	241	239	-1
TPb140	266	263	-1
TPb160	291	286	-2
TPb180	316	310	-2
TPb200	341	333	-2
TPb3	246	246	0
TPb4	288	288	0
TPb5	330	328	-1
TPb6	371	368	-1
TPb7	413	406	-2
TPb8	454	443	-3

Results of CBFEM and CM are compared and sensitivity study is presented. The influence of weld length and effective throat thickness on the design resistance of the transverse weld is shown

in Fig. 4.1.3. of the parallel weld in Fig. 4.1.4 and of the combination of both welds in Fig. 4.1.5. The sensitivity study shows good agreement for all weld configurations.

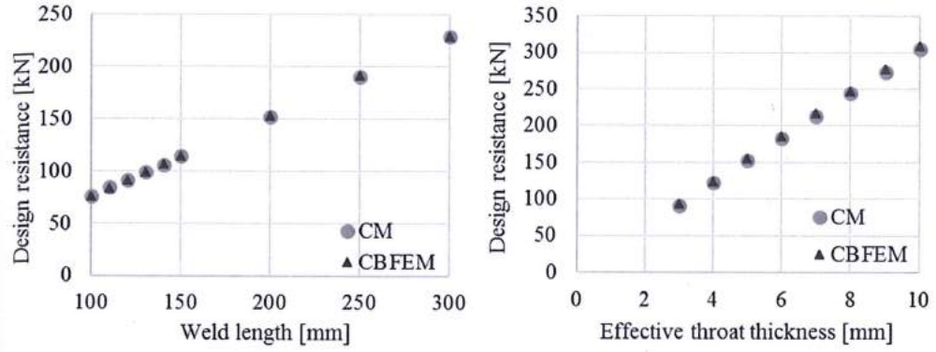

a) b)

Fig. 4.1.3 Parametric study of transverse weld a) Weld length b) Effective throat thickness

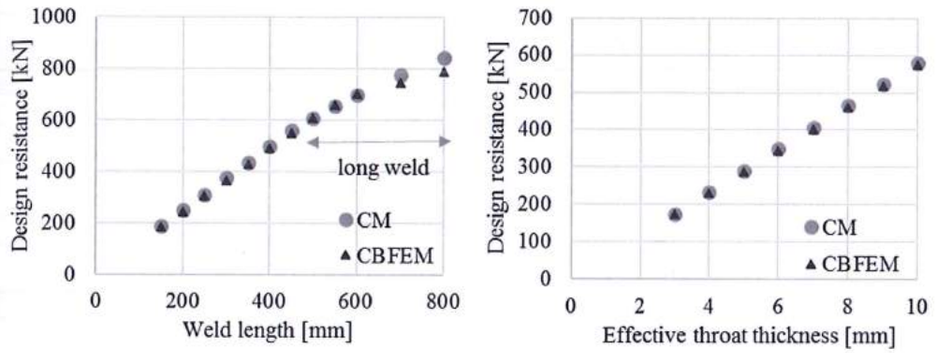

a) b)

Fig. 4.1.4 Parametric study of parallel weld a) Weld length b) Effective throat thickness

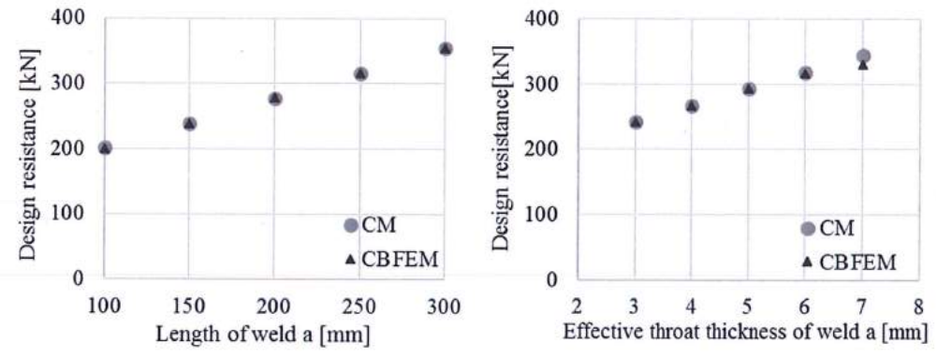

a) b)

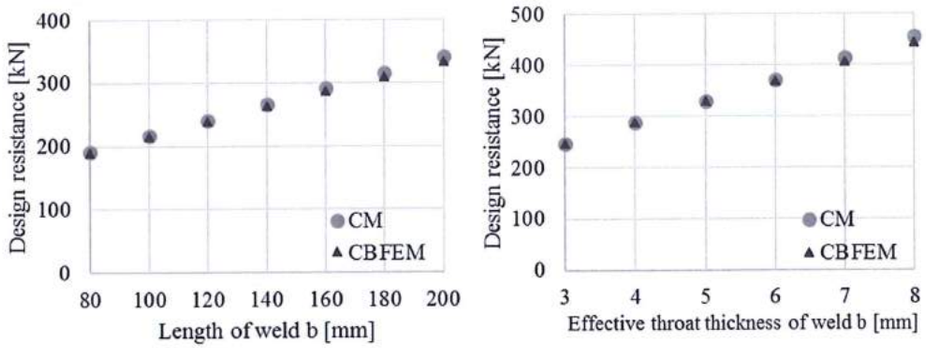

c) d)

Fig. 4.1.5 Parametric study of combination of transverse and parallel weld a) Length of weld *a* b) Effective throat thickness of weld *a* c) Length of weld *b* d) Effective throat thickness of weld *b*

To illustrate the accuracy of the CBFEM model the results of the sensitivity study are summarized in a diagram comparing CBFEM's and CM's design resistance, see Fig. 4.1.6. The results show that the difference of the two calculation methods is in all cases less than 10 %.

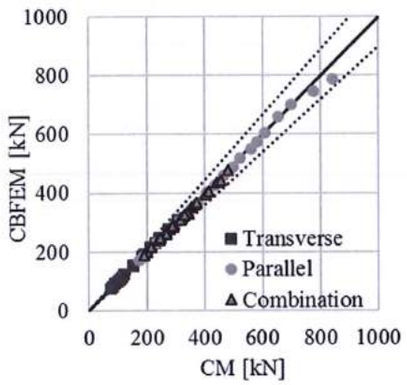

Fig. 4.1.6 Verification of CBFEM to CM

4.1.5 Benchmark example

Inputs

Plate 1

- Thickness t_1 = 20 mm
- Width b_1 = 200 mm
- Steel S235

Plate 2

- Thickness t_2 = 20 mm

- Width b_2 = 300 mm
- Offset e_z = -20 mm
- Steel S235

Weld, parallel fillet welds see Fig. 4.1.7.

- Throat thickness a_b = 3 mm
- Weld length L_b = 150 mm

Output

- Design resistance in tension F_{Rd} = 183 kN

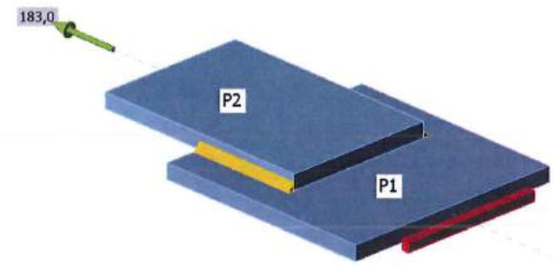

Fig. 4.1.7 Benchmark example for the welded lap joint with parallel fillet welds

4.2 Fillet weld in angle plate joint

4.2.1 Description

In this chapter is verified the model of the fillet weld in angle plate joint calculated by finite element method (CBFEM) on component method (CM). An angle is welded to a plate and loaded by normal force. The angle size and the length of the weld are studied in the sensitivity study.

4.2.2 Analytical model

The fillet weld is the only component examined in the study. The welds are designed according to Chapter 4 in EN1993-1-8:2006 to be the weakest component in the joint. The design resistance of the fillet weld is described in section 4.1. Overview of the considered examples and the material are given in the Tab. 4.2.1. The geometry of the joints with dimensions is shown in Fig. 4.2.1.

Tab. 4.2.1 Examples overview

Example	Material					Weld a		Weld b		Angle	Plate	
	f_y	f_u	E	γ_{M0}	γ_{M2}	a_a	L_a	a_b	L_b	section	b_p	t_p
	[MPa]	[MPa]	[GPa]	[-]	[-]	[mm]	[mm]	[mm]	[mm]	[-]	[mm]	[mm]
50xL80x10	235	360	210	1	1,25	3	50	3	50	80x10	240	10
100xL80x10	235	360	210	1	1,25	3	100	3	100	80x10	240	10
150xL80x10	235	360	210	1	1,25	3	150	3	150	80x10	240	10
200xL80x10	235	360	210	1	1,25	3	200	3	200	80x10	240	10
100xL160x16	235	360	210	1	1,25	5	100	3	100	160x16	400	16
170xL160x16	235	360	210	1	1,25	5	170	3	170	160x16	400	16
240xL160x16	235	360	210	1	1,25	5	240	3	240	160x16	400	16
310xL160x16	235	360	210	1	1,25	5	310	3	310	160x16	400	16
380xL160x16	235	360	210	1	1,25	5	380	3	380	160x16	400	16
450xL160x16	235	360	210	1	1,25	5	450	3	450	160x16	400	16

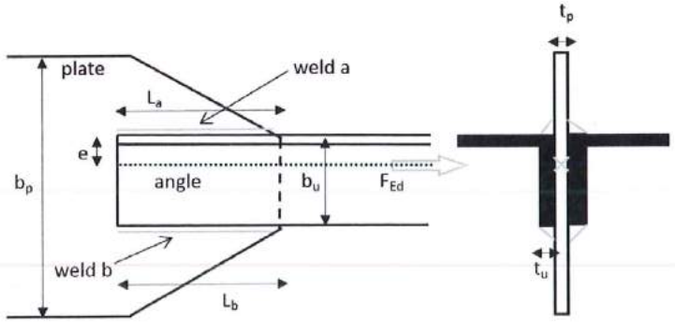

Fig. 4.2.1 Joint's geometry with dimensions

4.2.3 Numerical model

The model of the weld in CBFEM is described in section 3.4. The limit plastic strain is reached in the weld a and stress peaks are redistributed.

4.2.4 Verification of resistance

The weld's design resistances calculated by CBFEM are compared with the results of CM, the results see in Tab. 4.2.2. Two parameters are studied the length of the weld and the angle section.

Tab. 4.2.2 Comparison of CBFEM and CM

Example	Design resistance		
	CM	CBFEM	diff.
	[kN]	[kN]	[%]
50xL80x10	124	118	-5
100xL80x10	249	232	-7
150xL80x10	374	347	-8
200xL80x10	498	462	-8

Example	Design resistance		
	CM	CBFEM	diff.
	[kN]	[kN]	[%]
100xL160x16	332	324	-2
170xL160x16	565	551	-3
240xL160x16	798	770	-4
310xL160x16	1030	987	-4
380xL160x16	1263	1206	-5
450xL160x16	1496	1426	-5

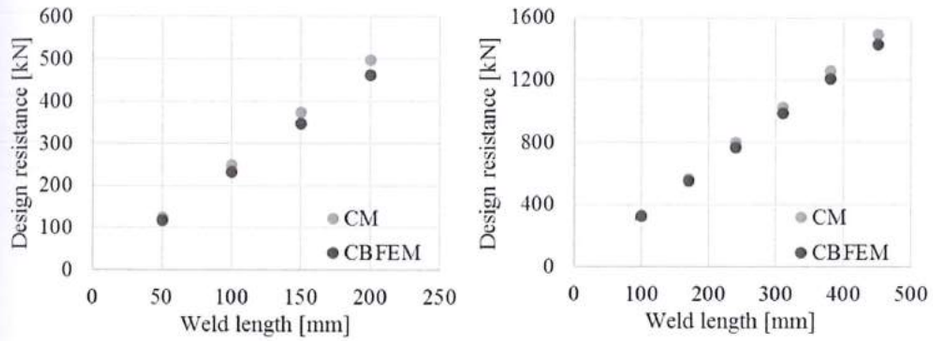

a) Angle cleat 80x10 b) Angle cleat 160x16

Fig. 4.2.2 Sensitivity study of weld length

Results of CBFEM and CM are compared and sensitivity study is presented. The influence of weld length on the design resistance of a welded angle joint is shown in Fig. 4.2.2. The study shows good agreement for all weld configurations. To illustrate the accuracy of the CBFEM model, results of the study are summarized in a diagram comparing CBFEM's and CM's design resistance, see Fig. 4.2.3. The results show that the difference of the two calculation methods is in all cases less than 10 %.

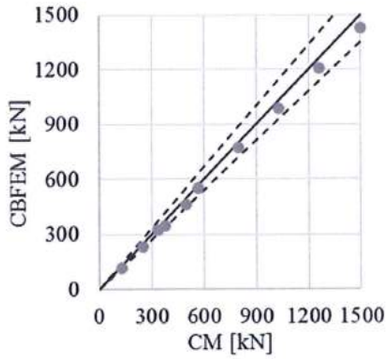

Fig. 4.2.3 Verification of CBFEM to CM

4.2.5 Benchmark example

Inputs

Angle

- Cross-section 2xL80x10
- Distance between angles 10 mm

Plate

- Thickness $t_p = 10$ mm
- Width $b_p = 240$ mm

Weld, parallel fillet welds see Fig. 4.2.4

- Throat thickness $a_w = 3$ mm
- Weld length $L_w = 200$ mm

Outputs

- Design resistance in tension $F_{Rd} = 462$ kN

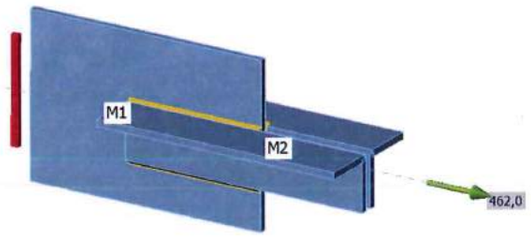

Fig. 4.2.4 Benchmark example of the welded angle plate joint with parallel fillet welds

4.3 Fillet weld in fin plate joint

4.3.1 Description

In this chapter is verified the component based finite element method (CBFEM) of a fillet weld in a fin plate joint with component method (CM). A fin plate is welded to open section column HEB. The height of the fin plate is changed from 150 to 300 mm. The plate/weld is loaded by normal and shear force and bending moment.

4.3.2 Analytical model

The fillet weld is the only component examined in the study. The welds are designed to be the weakest component in the joint according to Chapter 4 in EN1993-1-8:2006. The design resistance of the fillet weld is described in section 4.1. Overview of the considered examples and the material are given in the Tab. 4.3.1. Three load cases are considered, i.e. normal force N, shear force V and bending moment M. A geometry of the joint with dimensions is shown in Fig. 4.3.1.

Tab. 4.3.1 Examples overview

Example	Material					Weld	Fin plate			Column
	f_y	f_u	E	γ_{M0}	γ_{M2}	a_w	h_p	t_p	e	Section
	[MPa]	[MPa]	[GPa]	[-]	[-]	[mm]	[mm]	[mm]	[mm]	
N150	235	360	210	1	1,25	3	150	10	200	HEB400
N175	235	360	210	1	1,25	3	175	10	200	HEB400
N200	235	360	210	1	1,25	3	200	10	200	HEB400
N225	235	360	210	1	1,25	3	225	10	200	HEB400
N250	235	360	210	1	1,25	3	250	10	200	HEB400
N275	235	360	210	1	1,25	3	275	10	200	HEB400
N300	235	360	210	1	1,25	3	300	10	200	HEB400
V150	235	360	210	1	1,25	3	150	15	100	HEB200
V175	235	360	210	1	1,25	3	175	15	100	HEB200
V200	235	360	210	1	1,25	3	200	15	100	HEB200
V225	235	360	210	1	1,25	3	225	15	100	HEB200
V250	235	360	210	1	1,25	3	250	15	100	HEB200
V275	235	360	210	1	1,25	3	275	15	100	HEB200
V300	235	360	210	1	1,25	3	300	15	100	HEB200
M150	235	360	210	1	1,25	3	150	15	200	HEB200
M175	235	360	210	1	1,25	3	175	15	200	HEB200
M200	235	360	210	1	1,25	3	200	15	200	HEB200
M225	235	360	210	1	1,25	3	225	15	200	HEB200
M250	235	360	210	1	1,25	3	250	15	200	HEB200
M275	235	360	210	1	1,25	3	275	15	200	HEB200
M300	235	360	210	1	1,25	3	300	15	200	HEB200

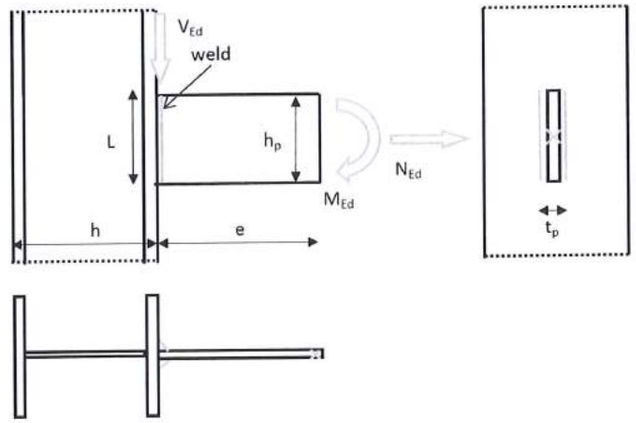

Fig. 4.3.1 Joint's geometry with dimensions

4.3.3 Numerical model

The weld in CBFEM model is described in section 3.4. The nonlinear elastic-plastic material is used for welds in this study. The limit plastic strain is reached in longer part of the weld and stress peaks are redistributed.

4.3.4 Verification of resistance

Design resistance calculated by CBFEM is compared with the results of CM. The weld's design resistances are compared as presented in Tab. 4.3.2. The study is performed for one parameter: length of the weld, i.e. height of the fin plate and three load cases: normal and shear force and bending moment. The shear force is applied in a weld plane to neglect the effect of an additional bending. The bending moment is applied at the end of the fin plate. The influence of the weld length on the design resistance of the fin plate joints loaded by the normal and shear force are shown in Fig. 4.3.2. The relation between the weld length and the bending moment resistance of the joint is shown in Fig. 4.3.3.

Tab. 4.3.2 Comparison of CBFEM and CM

Example	Design resistance			Example	Design resistance			Example	Design resistance		
	CM	CBFEM	diff.		CM	CBFEM	diff.		CM	CBFEM	diff.
	[kN]	[kN]	[%]		[kN]	[kN]	[%]		[kN]	[kN]	[%]
N150	229	227	-1	V150	187	184	-1	M150	8,5	8,4	-1
N175	267	264	-1	V175	218	216	-1	M175	11,6	11,5	-1
N200	305	301	-1	V200	249	247	-1	M200	15,2	15,0	-1
N225	343	338	-1	V225	280	278	-1	M225	19,3	19,0	-2
N250	381	375	-2	V250	310	309	0	M250	23,8	23,4	-2
N275	419	412	-2	V275	342	341	0	M275	28,8	28,4	-1
N300	457	449	-2	V300	374	372	-1	M300	34,3	33,8	-2

Results of CBFEM and CM are compared and sensitivity study is presented. The influence of weld length on the design resistance in a fin plate joint loaded by normal force is shown in Fig. 4.3.2, by shear force in Fig. 4.3.3 and by bending moment in Fig. 4.3.4. Study shows good agreement for all applied load cases.

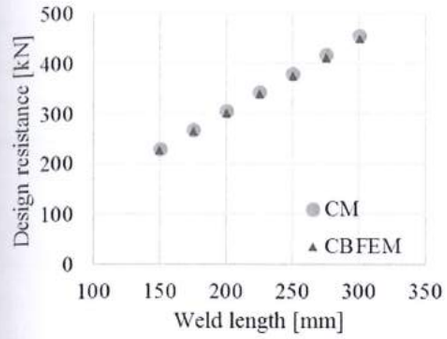

Fig. 4.3.2 Parametric study of fin plate joint loaded by normal force

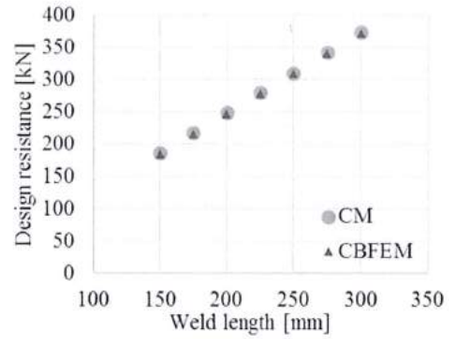

Fig. 4.3.3 Parametric study of fin plate joint loaded by shear force

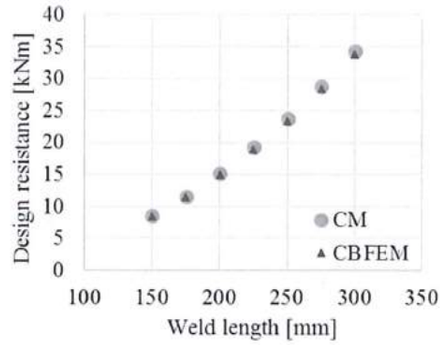

Fig. 4.3.4 Parametric study of fin plate joint loaded by bending moment

To illustrate the accuracy of the CBFEM model, results of the parametric studies are summarized in a diagram comparing the CBFEM's and CM's design resistances, see Fig. 4.3.5. The results show that the difference of the two calculation methods is in all cases less than 10 %.

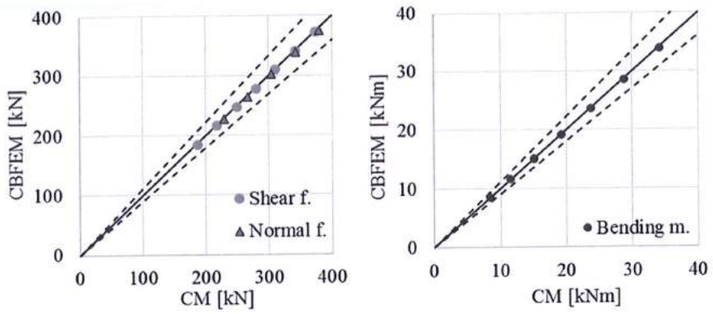

Fig. 4.3.5 Verification of CBFEM to CM

4.3.5 Benchmark example

Inputs

Column

- Steel S235
- HEB200

Fin plate

- Thickness t_p = 15 mm
- Height h_p = 175 mm

Weld, double fillet weld see Fig. 4.3.6

- Throat thickness a_w = 3 mm

Outputs

- Design resistance in poor bending M_{Rd} = 11,5 kNm

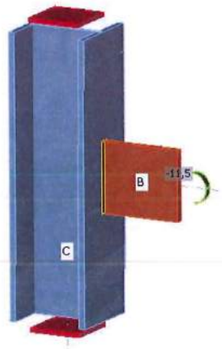

Fig. 4.3.6 Benchmark example for the welded fin plate joint

4.4 Fillet weld in beam to column joint

4.4.1 Description

The object of this chapter is verification of component based finite element method (CBFEM) for a fillet weld in a stiffened beam-to-column joint with component method (CM). An open section beam IPE is connected to open section column HEB400. The stiffeners are inside column opposite to beam flanges. The beam section is the changing parameter. Three load cases are considered, i.e. the beam is loaded in tension, shear and bending.

4.4.2 Analytical model

The fillet weld is the only component examined in the study. The welds are designed according to Chapter 4 in EN1993-1-8:2006 to be the weakest component in the joint. The design resistance of the fillet weld is described in section 4.1. Overview of the considered examples and the material are given in the Tab. 4.4.1. A geometry of the joint with dimensions is shown in Fig. 4.4.1.

Tab. 4.4.1 Examples overview

Example	Material					Weld	Beam		Column
	f_y	f_u	E	γ_{M0}	γ_{M2}	a_w	Section	e	Section
	[MPa]	[MPa]	[GPa]	[-]	[-]	[mm]		[mm]	
IPE160	235	360	210	1	1,25	3	IPE160	200	HEB400
IPE180	235	360	210	1	1,25	3	IPE180	200	HEB400
IPE200	235	360	210	1	1,25	3	IPE200	200	HEB400
IPE220	235	360	210	1	1,25	3	IPE220	200	HEB400
IPE240	235	360	210	1	1,25	3	IPE240	200	HEB400
IPE270	235	360	210	1	1,25	3	IPE270	200	HEB400
IPE300	235	360	210	1	1,25	3	IPE300	200	HEB400
IPE330	235	360	210	1	1,25	3	IPE330	200	HEB400
IPE360	235	360	210	1	1,25	3	IPE360	200	HEB400
IPE400	235	360	210	1	1,25	3	IPE400	200	HEB400

4.4.3 Numerical model

The weld in CBFEM model is described in section 3.4.

Nonlinear elastic-plastic material is used for welds in this study. The limit plastic strain is reached in longer part of the weld and stress peaks are redistributed.

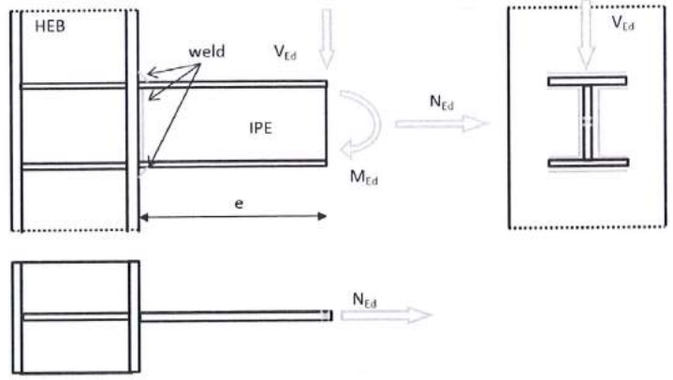

Fig. 4.4.1 Joint's geometry with dimensions

4.4.4 Verification of resistance

Design resistance calculated by CBFEM Idea RS software is compared with the results of CM. The weld's design resistances are compared, see Tab. 4.4.2. The study is performed for one parameter beam section and three load cases: normal force N_{Ed}, shear force V_{Ed} and bending moment M_{Ed}.

Tab. 4.4.2 Comparison of CBFEM and CM

Normal force N_{Ed}				Shear force V_{Ed}				Bending moment M_{Ed}			
Example	CM [kN]	CBFEM [kN]	Diff. [%]	Example	CM [kN]	CBFEM [kN]	Diff. [%]	Example	CM [kN]	CBFEM [kN]	Diff. [%]
IPE160	455	440	-3	IPE160	105	103	-2	IPE160	26	26	0
IPE180	511	509	0	IPE180	127	126	0	IPE180	33	33	0
IPE200	567	580	2	IPE200	151	150	-1	IPE200	40	41	2
IPE220	625	648	4	IPE220	175	175	0	IPE220	49	50	3
IPE240	684	703	3	IPE240	200	202	1	IPE240	59	60	2
IPE270	774	797	3	IPE270	239	244	2	IPE270	75	76	1
IPE300	863	886	3	IPE300	278	292	5	IPE300	93	94	1
IPE330	937	956	2	IPE330	315	336	6	IPE330	110	110	0
IPE360	1008	1026	2	IPE360	350	391	10	IPE360	129	128	-1
IPE400	1097	1116	2	IPE400	399	445	10	IPE400	155	153	-1

Results of CBFEM and CM are compared and a sensitivity study is presented. The influence of beam cross-section on the design resistance a welded beam-to-column joint loaded in tension is shown in Fig. 4.4.2, in shear in Fig. 4.4.3 and in bending in Fig. 4.4.4. The study shows good agreement for all applied load cases.

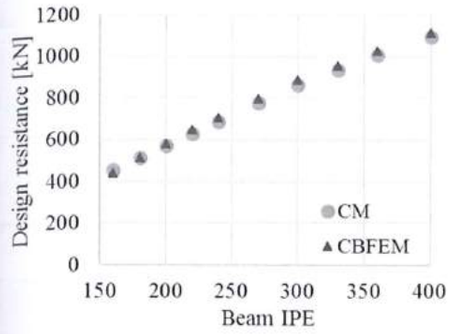

Fig. 4.4.2 Sensitivity study of beam-to-column joint loaded by normal force

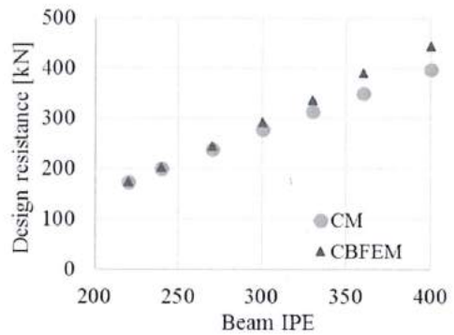

Fig. 4.4.3 Sensitivity study of beam-to-column joint loaded by shear force

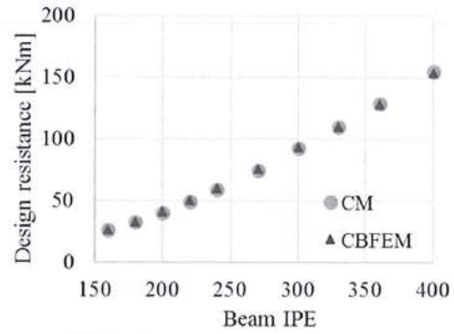

Fig. 4.4.4 Sensitivity study of beam-to-column joint loaded by bending moment

To illustrate the accuracy of the CBFEM model, results of the sensitivity study is summarized in a diagram comparing CBFEM's and CM's design resistances, see Fig. 4.4.5. The results show that the difference of the two calculation methods is in all cases less than 10%.

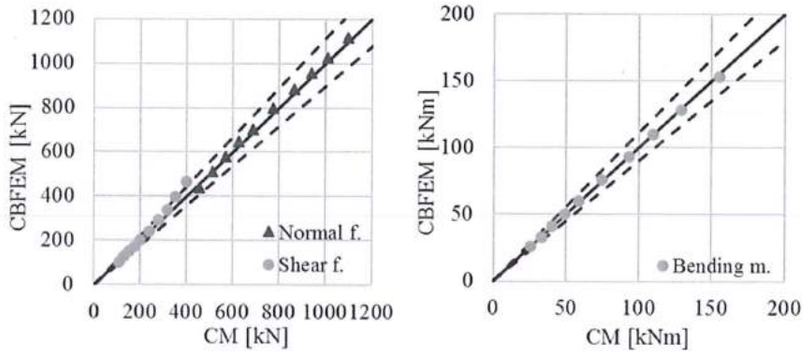

Fig. 4.4.5 Verification of CBFEM to CM

4.4.5 Benchmark example

Inputs

Column

- Steel S235
- HEB400

Beam

- Steel S235
- IPE270
- Length $L = 200$ mm
- Force eccentricity to weld $x = 400$ mm, see Fig. 4.4.6

Column stiffeners

- Thickness $t_s = 10$ mm
- Width $b_s = 140$ mm
- Related to beam flange, position upper and lower

Weld

- Throat thickness $a_w = 3$ mm

Outputs:

- Design resistance in shear $V_{Rd} = 244$ kN

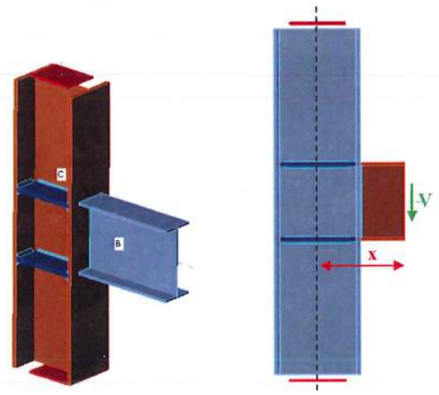

Fig. 4.4.6 Benchmark example of the welded beam to column joint with force eccentricity

4.5 Connection to unstiffened flanges

4.5.1. Description

In this chapter is verified the component based finite element method (CBFEM) of a fillet weld connecting a plate to an unstiffened column on the component method (CM). The steel plate is connected to the open and box section columns and loaded in tension.

4.5.2. Analytical model

The fillet weld is the only component examined in the study. The welds are designed according to Chapter 4 in EN1993-1-8:2006 to be the weakest component in the joint. The design resistance of the fillet weld is described in section 4.1. The force applied perpendicular to a flexible plate, which is welded to an unstiffened section, is limited. The stresses are concentrated in an effective width while the weld resistance around the unstiffened parts is neglected as shown in Fig. 4.5.1. For an unstiffened I or H section the effective width is obtained according to:

$$b_{eff} = t_w + 2s + 7kt_f \qquad (4.5.1)$$

$$k = \frac{t_f f_{y,f}}{t_p f_{y,p}} \qquad (4.5.2)$$

The dimension s is for a rolled section $s = r$ and for a welded section $s = \sqrt{2}\, a$. For a box or channel section the effective width should be obtained from:

$$b_{eff} = 2t_w + 5t_f \quad \text{but} \quad b_{eff} \leq 2t_w + 5kt_f \qquad (4.5.3)$$

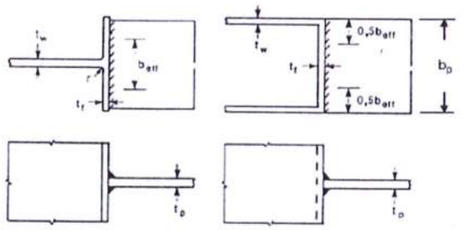

Fig. 4.5.1 Effective width of an unstiffened joint (Fig. 4.8 in EN1993-1-8:2006)

4.5.3. Numerical model

The model of weld in CBFEM is described in section 3.4. The limit plastic strain is reached in longer part of the weld and stress peaks are redistributed.

4.5.4. Verification of resistance

Design resistance calculated by CBFEM is compared with the results of CM. The weld's design resistance is compared only. Overview of the considered examples and the material are given in the Tab. 4.5.1. A geometry of the joint with dimensions is shown in Fig. 4.5.2.

Tab. 4.5.1 Examples overview

Column	Material					Weld	Plate	
Section	f_y	f_u	E	γ_{M0}	γ_{M2}	a_w	b_p	t_p
	[MPa]	[MPa]	[GPa]	[-]	[-]	[mm]	[mm]	[mm]
HEB160	235	360	210	1	1,25	3	160	15
HEB180	235	360	210	1	1,25	3	180	16
HEB200	235	360	210	1	1,25	3	200	17
HEB220	235	360	210	1	1,25	3	220	18
HEB240	235	360	210	1	1,25	3	240	19
HEB260	235	360	210	1	1,25	3	260	19

Column	Material					Weld	Flexible plate		Column		
	f_y	f_u	E	γ_{M0}	γ_{M2}	a_w	b_p	t_p	b_f	t_f	t_w
	[MPa]	[MPa]	[GPa]	[-]	[-]	[mm]	[mm]	[mm]	[mm]	[mm]	[mm]
K200/5	235	360	210	1	1,25	3	180	5	200	5	5
K200/6,3	235	360	210	1	1,25	3	180	6,3	200	6	6,3
K200/7	235	360	210	1	1,25	3	180	7	200	7	7
K200/8	235	360	210	1	1,25	3	180	8	200	8	8
K200/10	235	360	210	1	1,25	3	180	10	200	10	10

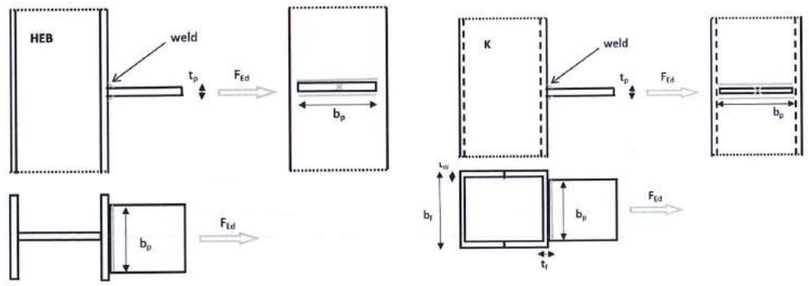

a) Flexible plate to open section b) Flexible plate to box section

Fig. 4.5.2 Joint's geometry and dimensions

The results are presented in Tab. 4.5.2. The study is performed for two parameters: flange width of the HEB section and web thickness of the box section. The flexible plate is loaded in tension. The influence

of the flange width of the HEB section on the design resistance of the joint is shown in Fig. 4.5.3. The relation between the web thickness of the box section on the design resistance of the joint is shown in Fig. 4.5.4.

Tab. 4.5.2 Comparison of CBFEM and CM

Example	Design resistance		
	CM	CBFEM	Diff.
	[kN]	[kN]	[%]
HEB160	178	157	-13
HEB180	189	174	-9
HEB200	210	190	-11
HEB220	221	206	-7
HEB240	242	222	-9
HEB260	260	235	-11

Example	Design resistance		
	CM	CBFEM	Diff.
	[kN]	[kN]	[%]
K200/5	53	49	-8
K200/6,3	64	59	-9
K200/7	74	67	-11
K200/8	85	79	-8
K200/10	106	95	-12

Results of CBFEM and CM are compared in a sensitivity study. The influence of the flange width of the HEB section on the design resistance of the joint is studied in Fig. 4.5.3. The influence of the web thickness of the box section on the design resistance of the joint is presented in Fig. 4.5.4. The parametric studies show very good agreement of the results for all weld configurations.

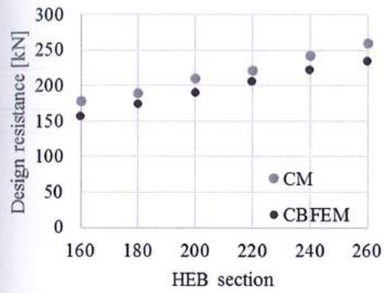

Fig. 4.5.3 Flange width of the HEB section

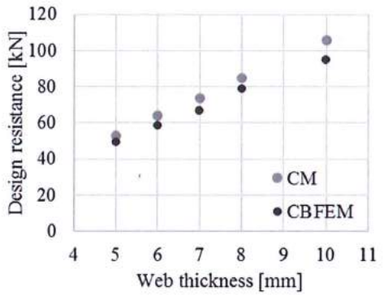

Fig. 4.5.4 Web thickness of the box section

Results of the sensitivity study are summarized in a diagram comparing CBFEM's and CM's design resistance, see Fig. 4.5.5, to illustrate the accuracy of the CBFEM model.

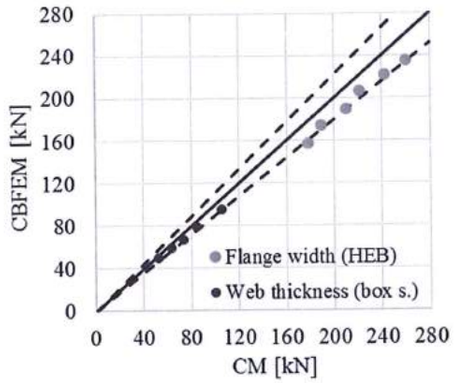

Fig. 4.5.5 Verification of CBFEM to CM

The influence of the plate thickness on the design resistance of the weld is shown in Fig. 4.5.6. The column cross section is HEB 180 with flange thickness of 14 mm. A weld connecting a plate thicker than the column flange has same resistance for CM and CBFEM. On the other side the weld connecting the plate to column flange of same or smaller thickness has in numerical models smaller design resistance by 20%. The plate thickness is not taken into account in numerical models with shell elements, which causes the difference.

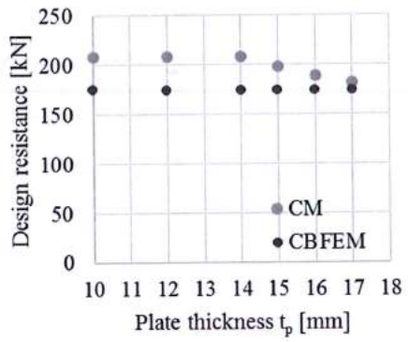

Fig. 4.5.6 Influence of plate thickness on the resistance of joint with unstiffened column HEB180

4.5.5. Benchmark example

Inputs

Column

- Steel S235
- RHS200/200/5

Flexible plate

- Steel S235

- Thickness $t_p = 5$ mm
- Width $b_p = 180$ mm

Weld, double fillet welds see Fig. 4.5.7

- Throat thickness $a_w = 3$ mm

Outputs

- Design resistance in tension $N_{Rd} = 49$ kN

Fig. 4.5.7 Benchmark example for the welded connection of plate to unstiffened column

5 BOLTED CONNECTION

5.1 T-stub in tension

5.1.1. Description

The objective of this chapter is verification of component based finite element method (CBFEM) of T-stubs connected with two bolts loaded in tension with component method (CM) and research FEM model (RM) created in Midas FEA software.

5.1.2. Analytical model

Welded T-stub and bolt in tension are components examined in the study. Both components are designed according to EN1993-1-8:2006. The welds are designed not to be the weakest component. Effective lengths for circular and noncircular failures are considered according to EN1993-1-8:2006 cl. 6.2.6. Only tension loads are considered. Three modes of collapse according to EN1993-1-8:2006 cl. 6.2.4.1 are considered 1. mode with full yielding of the flange, 2. mode with two yield lines by web and rupture of the bolts and 3. mode for rupture of the bolts, see Fig. 5.1.1. Bolts are designed according to cl. 3.6.1 in EN1993-1-8:2006. Design resistance considers punching shear resistance and rupture of the bolt.

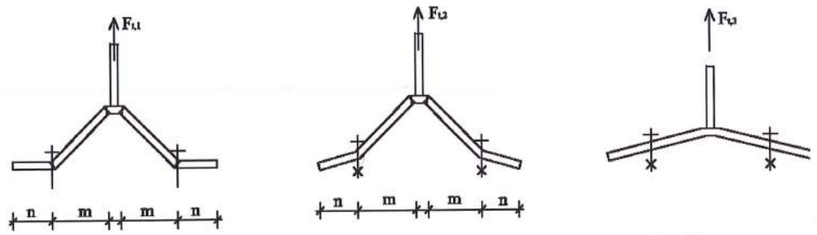

1. Mode 2. Mode 3. Mode

Fig. 5.1.1 Collapse modes of T-stub

5.1.3. Design numerical model

T-stub is modelled by 4-nodes shell elements as described in Chapter 3 and summarised further. Every node has 6 degrees of freedom. Deformations of the element consist of membrane and flexural contributions. Nonlinear elastic-plastic material status is investigated in each layer of integration point. Assessment is based on the maximum strain given according to EN1993-1-5:2005 by value of 5 %. Bolts are divided into three sub-components. The first is the bolt shank, which is modelled as a nonlinear spring and caries tension only. The second sub-component transmits tensile force into the flanges. The third sub-component solves shear transmission.

5.1.4. Research numerical model

In cases, where the CBFEM gives method higher resistance, initial stiffness or deformation capacity. Research FEM model (RM) from brick elements validated on experiments (Gödrich et al, 2013) is used to verify the CBFEM model. RM is created in Midas FEA software of hexahedral and octahedral solid elements, see Fig. 5.1.2 Mesh sensitive study was provided to reach proper results in adequate time. Numerical model of the bolts is based on the model by (Wu et al, 2012). The nominal diameter is considered in the shank and the effective core diameter is considered in the threaded part. Washers are coupled with the head and nut. Deformation caused by stripping of the threads in thread-nut contact area is modelled using interface elements. Interface elements are unable to transfer tensile stresses. Contact elements allowing the transmission of pressure and friction are used between washers and flanges of the T-stub. One quarter of the sample was modelled using the symmetry.

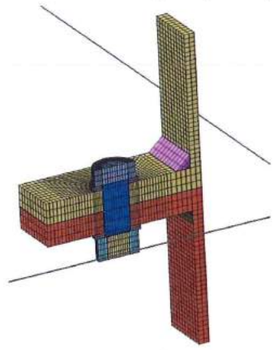

Fig. 5.1.2 Research FEM model

5.1.5. Range of validity

CBFEM was verified for the selected typical T-stub geometries. The minimal thickness of flange is 8 mm. Maximal distance of the bolts to bolt diameter is limited by $p/d_b \leq 20$. The distance of the bolt line to web is limited to $m/d_b \leq 5$. Overview of the considered samples with steel plates of S235 $f_y = 235$ MPa, $f_u = 360$ MPa, $E = E_{bolt} = 210$ GPa is shown in the Tab. 5.1.1 and in Fig. 5.1.3.

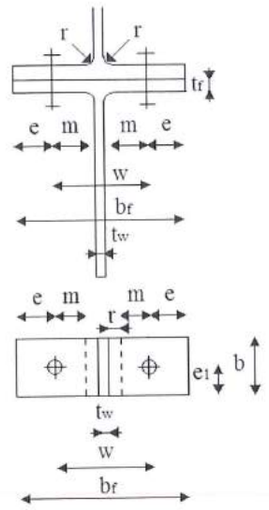

Fig. 5.1.3 Geometry of the T stubs

Tab. 5.1.1 Overview of the considered samples of T stubs

Sample	T-stub										Bolts	
	t_f	t_w	b_f	a_w	b	w	e_1	m	e	n	Diam.	Mat.
	[mm]	[mm]	[mm]	[mm]	[mm]	[mm]	[mm]	[mm]	[mm]	[mm]		
tf10	10	20	300	10	100	165	50	61,19	67,5	67,5	M24	8.8
tf12	12	20	300	10	100	165	50	61,19	67,5	67,5	M24	8.8
tf15	15	20	300	10	100	165	50	61,19	67,5	67,5	M24	8.8
tf20	20	20	300	10	100	165	50	61,19	67,5	67,5	M24	8.8
tf25	25	20	300	13,5	100	165	50	57,23	67,5	67,5	M24	8.8
tf30	30	20	300	13,5	100	165	50	57,23	67,5	67,5	M24	8.8
tf35	35	20	300	13,5	100	165	50	57,23	67,5	67,5	M24	8.8
tf40	40	20	300	13,5	100	165	50	57,23	67,5	67,5	M24	8.8
tf45	45	20	300	13,5	100	165	50	57,23	67,5	67,5	M24	8.8
tf50	50	20	300	13,5	100	165	50	57,23	67,5	67,5	M24	8.8
M16 8.8	25	20	300	10	100	165	50	61,19	67,5	67,5	M16	8.8
M20 8.8	25	20	300	10	100	165	50	61,19	67,5	67,5	M20	8.8
M24 8.8	25	20	300	10	100	165	50	61,19	67,5	67,5	M24	8.8
M27 8.8	25	20	300	10	100	165	50	61,19	67,5	67,5	M27	8.8
M24 4.8	25	20	300	10	100	165	50	61,19	67,5	67,5	M24	4.8
M24 5.8	25	20	300	10	100	165	50	61,19	67,5	67,5	M24	5.8
M24 6.8	25	20	300	10	100	165	50	61,19	67,5	67,5	M24	6.8
M24 10.9	25	20	300	10	100	165	50	61,19	67,5	67,5	M24	10.9

w110	20	20	300	7	100	110	50	37,08	95	46,35	M24	8.8
w150	20	20	300	7	100	150	50	57,08	75	71,35	M24	8.8
w200	20	20	300	7	100	200	50	82,08	50	50	M24	8.8
w240	20	20	300	7	100	240	50	102,1	30	30	M24	8.8
b100	20	20	300	7	100	110	50	37,08	95	46,35	M24	10.9
b250	20	20	300	7	250	110	125	37,08	95	46,35	M24	10.9
b300	20	20	300	7	300	110	150	37,08	95	46,35	M24	10.9
b400	20	20	300	7	400	110	200	37,08	95	46,35	M24	10.9

5.1.6. Global behaviour

Comparison of the global behaviour of the T-stub described by force-deformation diagrams for all design procedures was prepared. Attention was focused to the main characteristics: initial stiffness, design resistance and deformation capacity. Sample tf20 was chosen to present as reference, see Fig. 5.1.4 and Tab. 5.1.2. CM generally gives higher initial stiffness compared to CBFEM and RM. In all cases RM gives the highest design resistance as shown in chapter 6. Deformation capacity is compared also. Deformation capacity of T-stub was calculated according to (Beg et al, 2004). RM does not consider cracking of the material so the prediction of deformation capacity is limited.

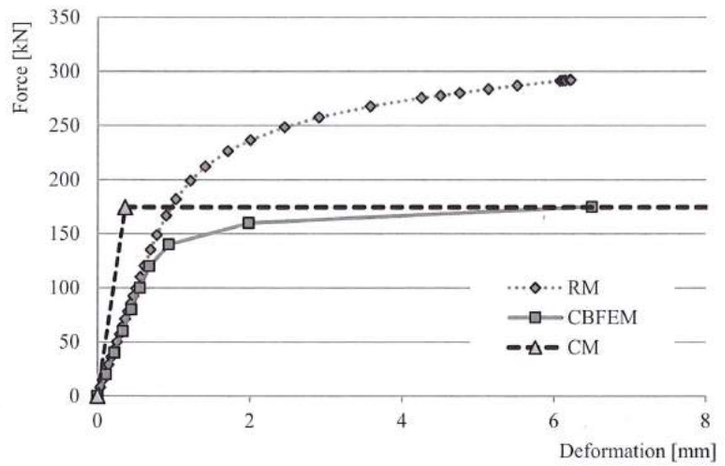

Fig. 5.1.4 Force-deformation diagram

Tab. 5.1.2 Global behaviour overview

		CM	CBFEM	RM	CM/CBFEM	RM/CBFEM
Initial stiffness	[kN/m]	484727	181818	197400	2,67	1,09
Design resistance	[kNm]	174	179,7	268,8	0,96	1,5
Deformation capacity	[mm]	24,5	6,5	-	3,77	-

5.1.7. Verification of resistance

Design resistances calculated by CBFEM were compared with the results of CM and RM in the next step. The comparison was focused on the deformation capacity and determination of the collapse mode too. All results are ordered in Tab. 5.1.3. The study was performed for five parameters: thickness of the flange, bolt size, bolt material, bolt space and T-stub width.

Tab. 5.1.3 Global behaviour overview

Sample	CM			CBFEM			RM		
	Design resistance	Collapse mode	Initial stiffness	Design resistance	Collapse mode	Initial stiffness	Design resistance	Collapse mode	Initial stiffness
	[kN]		[kN/mm]	[kN]		[kN/mm]	[kN]		[kN/mm]
Parameter: Thickness of the flange									
tf10	44	1	80,0	75	1	39,4	115	1	53,6
tf12	63	1	134,6	90	1	58,8	144	1	80,9
tf15	98	1	246,6	115	1	97,1	199,7	1	120,5
tf20	174	1	484,7	175	1	181,8	268,8	2	197,4
tf25	279	2	789,3	249	1	285,7	310,3	2	297,8
tf30	305	2	922,6	288	2	392,2	328,7	2	363
tf35	335	2	968,8	320	2	485,4	347,3	2	416,8
tf40	371	2	961,3	358	2	573,8	370,7	2	464,4
tf45	407	3	927,3	385	2	654,2	400	2	510,6
tf50	407	3	882,4	412	3	736,8	407	3	553,8
Parameter: bolt size									
M16 8.8	152	2	486,6	150	2	-	-	-	-
M20 8.8	205	2	612,7	200	2	-	-	-	-
M24 8.8	270	2	710,2	249	1	-	-	-	-
M27 8.8	278	1	782,4	260	1	-	-	-	-
Parameter: bolt material									
M24 4.8	164	2	710,2	163	2	-	-	-	-
M24 5.8	190	2	710,2	186	2	-	-	-	-
M24 6.8	217	2	693,6	210	2	-	-	-	-
M24 10.9	273	1	677,8	262	1	-	-	-	-
Parameter: bolt space									
w110	282	2	1129,7	273	1	465,1	344	2	432,5
w150	188	1	562,4	194	1	229,0	281	2	228,0
w200	129	1	237,8	144	1	111,9	222	2	112,7
w240	107	1	131,9	124	1	66,1	162,7	2	64,9
Parameter: T-stub width									
b100	314	1	1129,7	296	1	463,0	407	2	432,2
b250	423	2	1443,5	448	2	534,4	480,5	2	640,0
b300	433	2	1443,5	466	2	534,4	486	2	686,0
b400	433	2	1443,5	492	2	538,5	494	2	721,5

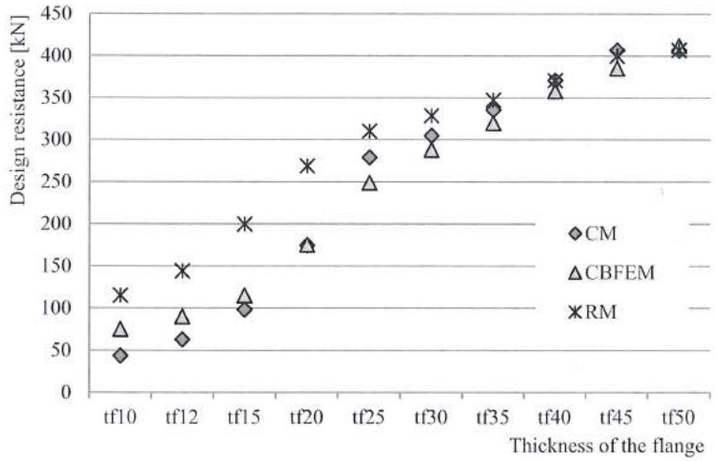

Fig. 5.1.5 Sensitivity study of flange thickness

The sensitivity study of thickness of the flange shows higher resistance according to CBFEM compared to CM for samples with flange thicknesses up to 20 mm. RM gives even higher resistance for these samples, see Fig. 5.1.5. Higher resistance of both numerical models is explained by neglecting of membrane effect in CM. In case of the bolt diameter, see Fig. 5.1.6 and bolt material, Fig. 5.1.7, respectively, correspond results of CBFEM and CM. Due to a good agreement of both methods, results of RM are not required.

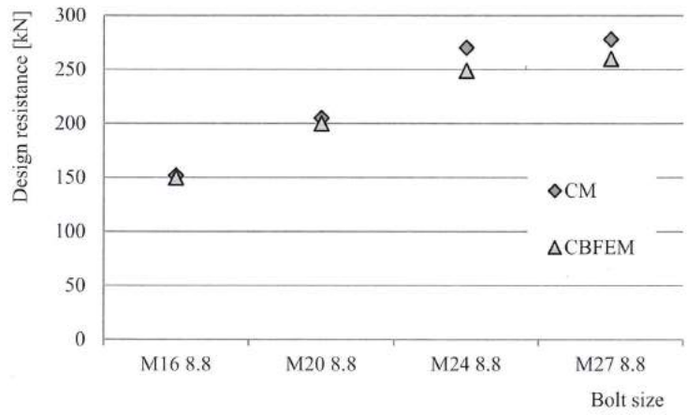

Fig. 5.1.6 Sensitivity study of the bolt size

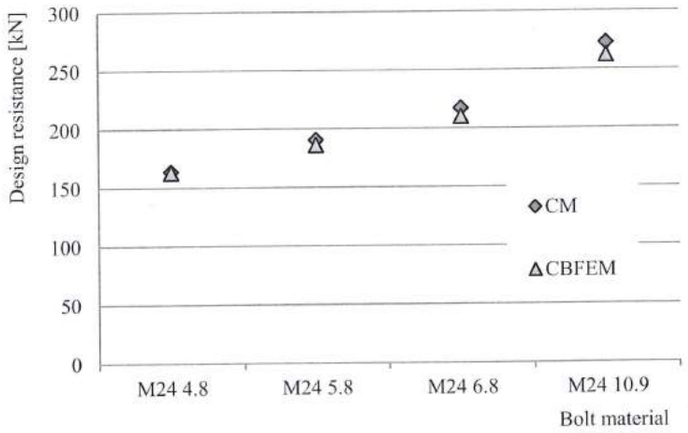

Fig. 5.1.7 Sensitivity study of the bolt material

In the case of the bolt distances results of CBFEM and CM show generally good agreement, see Fig. 5.1.8. With increase of bolt space, CBFEM gives slightly higher resistance compared to CM. For that reason, results of RM are showed also. RM gives the highest resistance in all cases.

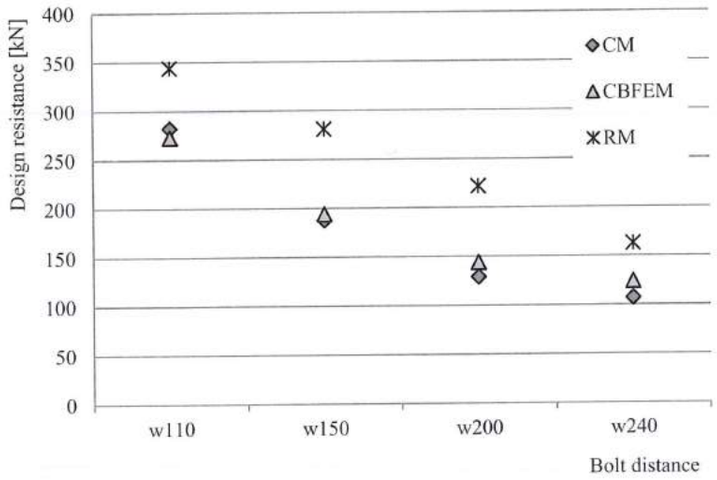

Fig. 5.1.8 Sensitivity study of the bolt distance

In study of T-stub width shows CBFEM higher resistance compared to CM with increase of width. Results of RM were prepared, which gives again the highest resistance in all cases, see Fig. 5.1.9.

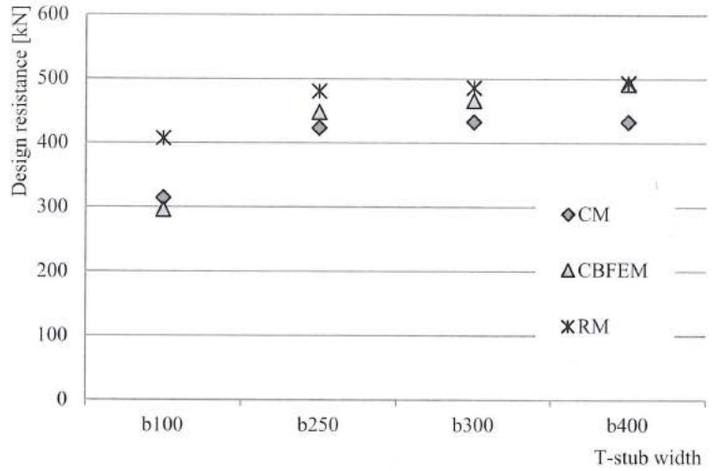

Fig. 5.1.9 Sensitivity study of T-stub width

To show the prediction of the CBFEM model, results of the studies were summarized in graph comparing resistances by CBFEM and component method, see Fig. 5.1.10. The results show that the difference of the two calculation methods is mostly up to 10 %. In cases with CBFEM/CM > 1,1 accuracy of CBFEM was verified by the results of RM which gives highest resistance in all selected cases.

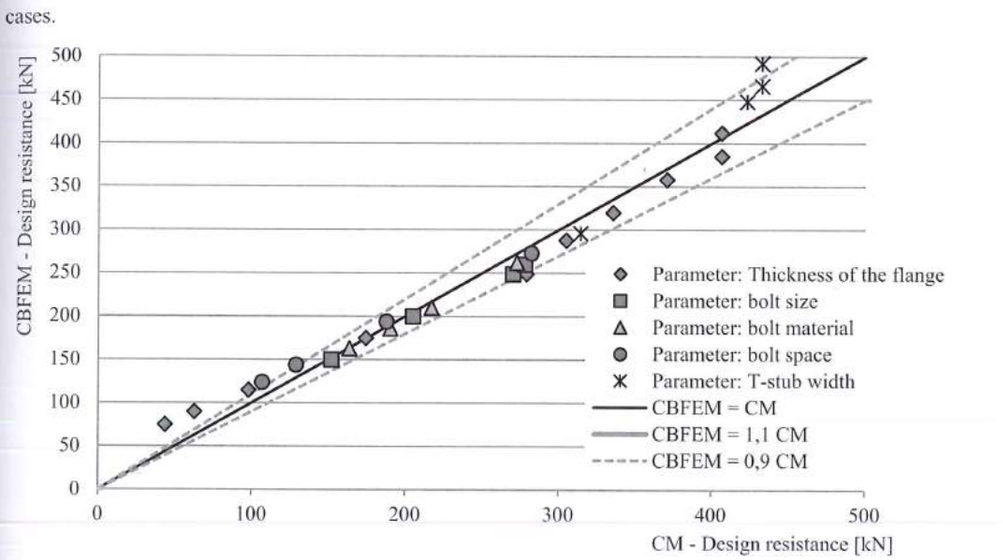

Fig. 5.1.10 Summary of verification of CBFEM to CM

5.1.8. Benchmark example

Inputs

T-stub

- Steel S235
- Flange thickness t_f = 20 mm
- Web thickness t_w = 20 mm
- Flange width b_f = 300 mm
- Length b = 100 mm
- Double fillet weld a_w = 10 mm

Bolts

- 2 x M24 8.8
- Distance of the bolts w = 165 mm

Outputs

- Design resistance in tension $F_{T,Rd}$ = 175 kN
- Collapse mode - full yielding of the flange with maximal strain 5 %
- Utilization of the bolts 88,4 %
- Utilization of the welds 49,1 %

5.2 Splices in shear

5.2.1. Description

This study is focused on the verification of component based finite element method (CBFEM) for the resistance of the symmetrical double splice bolted connection to analytical model (AM).

5.2.2. Analytical model

The bolt resistance in shear and the plate resistance in bearing are designed according to Tab. 3.4 chapter 3.6.1 in EN1993-1-8:2006. For long connection is considered reduction factor according to cl. 3.8. Design resistance of connected members with reductions for fastener holes is considered according to cl 3.10.

5.2.3. Verification of resistance

Design resistances calculated by CBFEM were compared with results of analytical model (AM). Results are summarised in Tab. 5.2.1. The parameters are bolt material, splice thickness, bolt diameter and bolt distances, see Figs. 5.2.1 to 5.2.4.

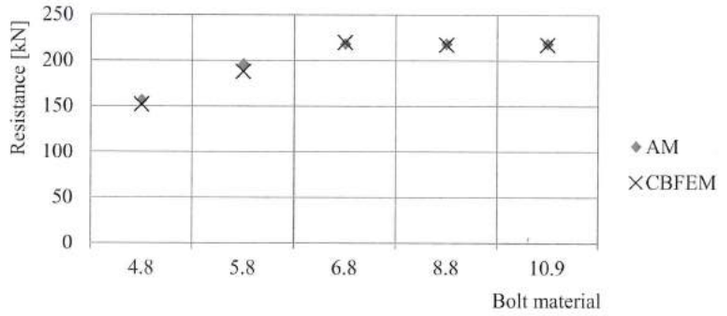

Fig. 5.2.1 Sensitivity study for the bolt material

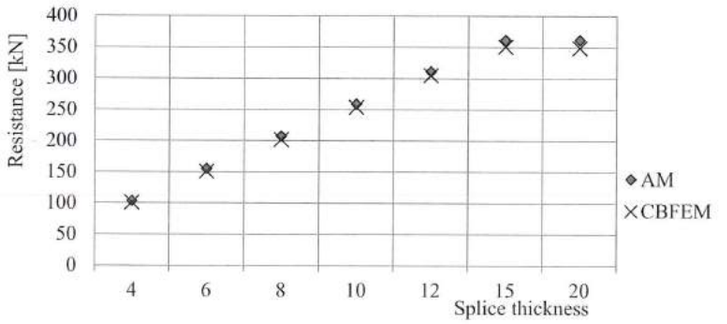

Fig. 5.2.2 Sensitivity study for the splice thickness

Tab. 5.2.1 Sensitivity study of resistance

Parameter		Analytical Model (AM)		CBFEM		AM/ CBFEM
		Resist. kN	Critical component	Resist. kN	Critical component	
Bolt material		Joint description: splice 150/10mm, bolts 2xM20 in distances p =70, e_1=50, plates 2x150/6mm, steel S235				
4.8		157	Bolt in shear	152	Bolt in shear	1,03
5.8		196	Bolt in shear	188	Bolt in shear	1,04
6.8		218	Bearing	220	Bearing	0,99
8.8		218	Bearing	218	Bearing	1,00
10.9		218	Bearing	218	Bearing	1,00
Splice thickness		Joint description: splice height 200mm, bolts 3xM16 8,8 in distances p = 55mm e_1 = 40mm, plates 2x200/10mm, steel S235				
4		104	Bearing	101	Bearing	1,03
6		156	Bearing	151	Bearing	1,03
8		208	Bearing	202	Bearing	1,03
10		259	Bearing	254	Bearing	1,02
12		311	Bearing	305	Bearing	1,02
15		362	Bolt in shear	351	Bolt in shear	1,03
20		362	Bolt in shear	349	Interaction of tension and shear in bolt	1,04
Diam.	Distances	Joint description: splice 120/10mm, bolts 2xMX 8,8, plates 2x120/6mm, steel S235				
M16	p = 55, e_1 = 40	171	Bearing	170	Bearing	1,00
M20	p = 70, e_1= 50	218	Bearing	217	Bearing	1,01
M24	p = 80, e_1 = 60	244	Splice in tension	237	Splice in tension	1,03
M27	p = 90, e_1 = 70	233	Splice in tension	233	Splice in tension	1,00
M30	p = 100, e_1 = 75	226	Splice in tension	228	Splice in tension	0,99
Bolt spacing		Joint description: Splice 200/6mm, bolts 3xM16 8,8, plates 2x200/3mm, steel S235				
p =40, e_1 = 25		104	Bearing	101	Bearing	1,03
p =55, e_1 = 40		156	Bearing	153	Bearing	1,02
p =70, e_1 = 55		207	Bearing	201	Bearing	1,03

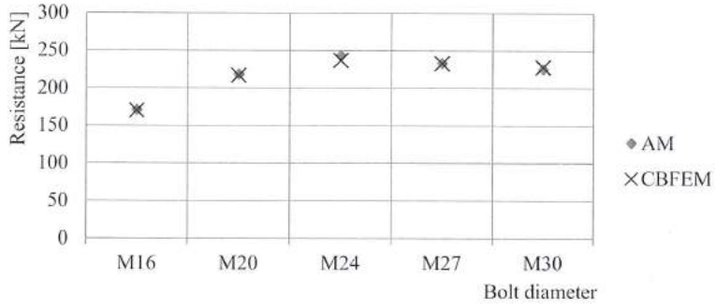

Fig. 5.2.3 Sensitivity study for the bolt diameter

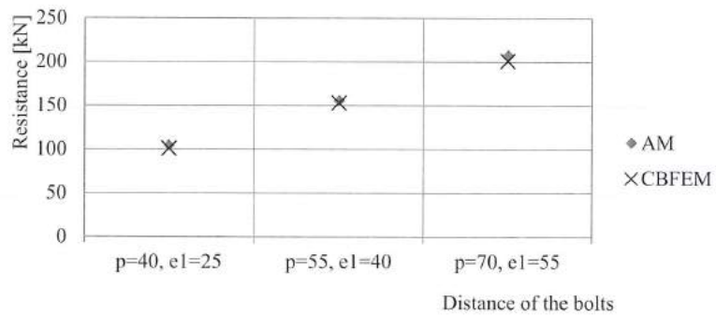

Fig. 5.2.4 Sensitivity study for the distance of bolts

The results of sensitivity studies are summarized in graph in Fig. 5.2.5. The results show that the differences of the two calculation methods are up to 5 %. Analytical model gives generally higher resistance.

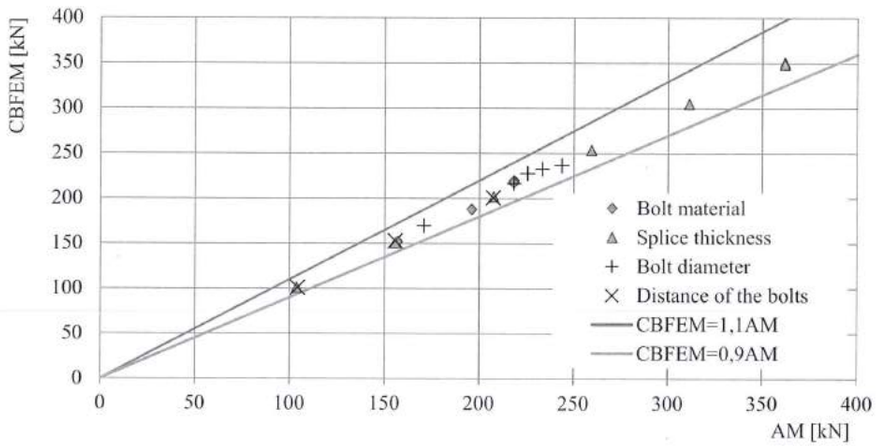

Fig. 5.2.5 Verification of CBFEM to AM for the symmetrical double splice connection

5.2.4. Benchmark example

Inputs

Connected member

- Steel S235
- Splice 200/10 mm

Connectors

Bolts

- 3 x M16 8.8
- Distances e_1=40mm, p=55mm

2 x splice

- Steel S235
- Plate 380x200x10

Outputs

- Design resistance F_{Rd} = 254 kN
- Critical is bearing of the connected splice

Fig. 5.2.6 Benchmark example of the bolted splices in shear

5.3 End plate minor axis connection

5.3.1 Description

In the Chapter is verified the Component based finite element method (CBFEM) model of the beam to column joint on Component method (CM). The extended end plate with three bolt rows is connected to column web and loaded by bending moment, see Fig. 5.3.1.

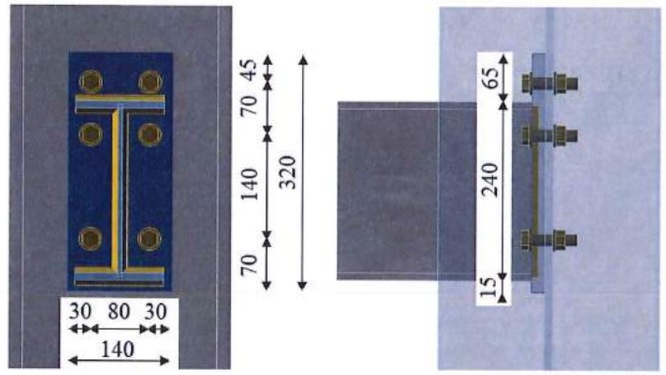

Fig. 5.3.1 Joint geometry

5.3.2 Analytical model

Three components, which are guiding the behaviour, are the end plate in bending, the beam flange in tension and in compression, and the column web in bending. The end plate and the beam flange in tension and in compression are designed according to EN 1993-1-8:2006. The behaviour of the column web in bending is predicted according to (Steenhuis et al., 1998). The results of experiments of the beam to column minor axis joints e.g. (Lima et al., 2009) shows the good prediction of this type of join loaded in plane of connected beam.

5.3.3 Numerical model

Assessment is based on the maximum strain given according to EN1993-1-5:2005 by value of 5 %. Detailed information about CBFEM model is summarised in Chapter 3.

5.3.4 Verification of resistance

The sensitivity study of the joint resistance was prepared for column cross sections. Joint geometry is shown in Fig. 5.3.1. In Tab. 5.3.1 and in Fig. 5.3.2 are summarised results of calculation in case of relatively enlarging of geometry of the end plate P18.

Tab. 5.3.1 Results of prediction of the of end plate minor axis connection for different rafters

Column HEB	200	220	240	260	280	300	320	340	360	400	450	500	550	600	650	700	800	900	1000
CM	40	35	35	31	31	32	33	34	36	38	38	39	40	42	44	48	49	52	54
CBFEM	35	32	33	30	32	32	33	34	35	40	38	39	39	40	41	44	44	47	48
CM/CBFEM	1,14	1,09	1,06	1,03	0,97	1,0	1,00	1,00	1,03	0,95	1,00	1,00	1,03	1,05	1,07	1,09	1,11	1,11	1,13

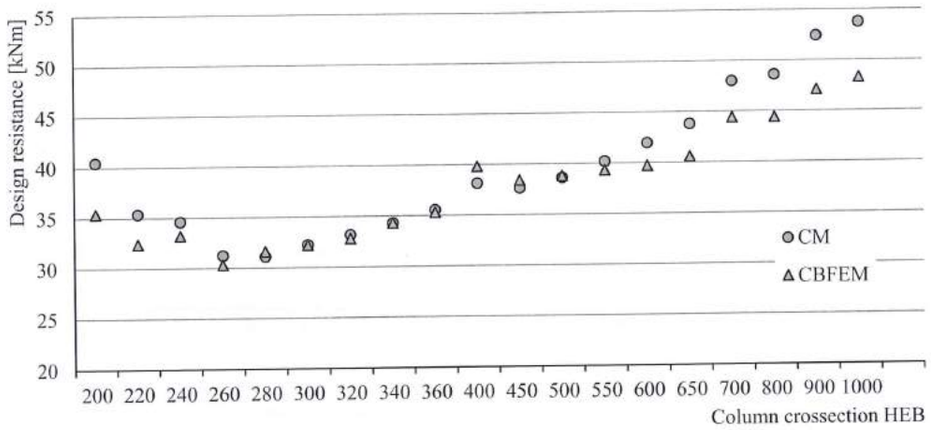

Fig. 5.3.2 Comparison resistance of end plate minor axis connection predicted by CBFEM and CM

5.3.5 Global behaviour

Global behaviour is presented on force-deformation curve. Beam IPE 240 is connected to column HEB 300 with six bolts M16 8.8. End plate geometry is shown in Fig. 5.3.1 and in Tab. 5.3.1. Comparison of both methods results is presented in Fig. 5.3.3 and in Tab.5.3.2. Both methods predict similar design resistance. CBFEM generally gives lower initial stiffness compared to CM.

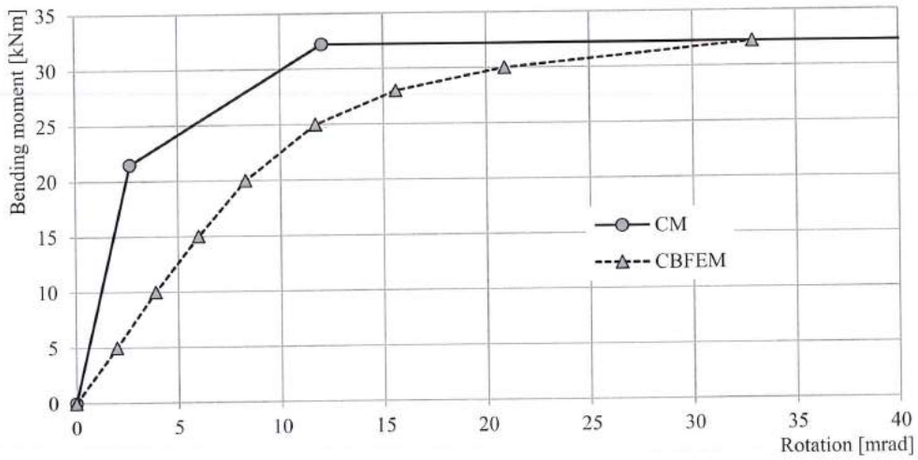

Fig. 5.3.3 Prediction of behaviour of end plate minor axis connection on moment rotational curve

Tab. 5.3.2 Main characteristics for global behaviour

		CM	CBFEM	CM/CBFEM
Initial stiffness	[kNm/rad]	8013	2564	3,13
Design resistance	[kNm]	32	32	1,00
Deformation capacity	[mrad]	-	33	-

Results of studies are summarized in graph comparing resistances by CBFEM and component method, see Fig. 5.3.4. The results show the difference of methods is up to 13 %. CBFEM predicts in all cases lower resistance compare to CM, which is based on simplification in (Steenhuis et al., 1998). Similar results may be observed in work by (Wang and Wang, 2012).

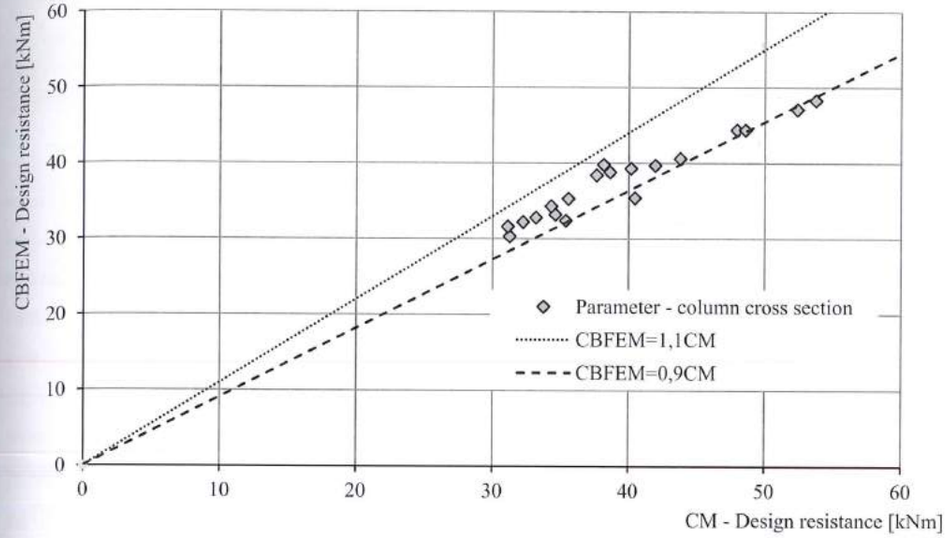

Fig. 5.3.4 Summary of verification of CBFEM to CM for the end plate minor axis connection

5.3.6 Benchmark example

The benchmark case is prepared for the end plate minor axis connection according to Fig. 5.3.1 with modified geometry as summarised below.

Inputs

- Steel S235
- Column HEB 300
- Beam IPE 240
- Bolts 6xM16 8.8
- Welds thickness 5 mm
- End-plate thickness t_p = 18 mm

Outputs

- Design resistance in bending M_{Rd} = 32,2 kNm
- Guiding component – column web in bending

5.4 Generally loaded end plate

5.4.1 Description

In this chapter is verified the component based finite element method (CBFEM) of the generally loaded end plate joint with component method (CM). The end plate joints of hollow section beams were loaded with combination of bending moments and shear forces to both axis.

5.4.2 Experimental investigation

Experimental investigation of three samples of end plate joints was performed. End plates were welded on two RHS 250x150x16 beams of different lengths 2000 mm and 1000 mm. The beams and plates were designed from S355, with measured values of $f_{y,m}$ = 410 MPa and $f_{u,m}$ = 582 MPa. The end plates P10 – 400 x 300 were connected by M20 8.8 bolts, with the vertical distances 35 – 230 – 100 - 35 mm and horizontal ones 30 – 240 – 30 mm. The beam with connection 500 mm from its centre was loaded in its centre through P20 by hydraulic jack, see Fig. 5.4.1. The configuration creates in the connection shear forces and bending moments. The results of the contact imprints on paper placed between the end plates is included on right side of the Fig, see (Wald et at 2016). The inclination of the specimens varied from 0°; 30° till 45°. The test set up with 0° inclination is documented at Fig. 5.4.2.

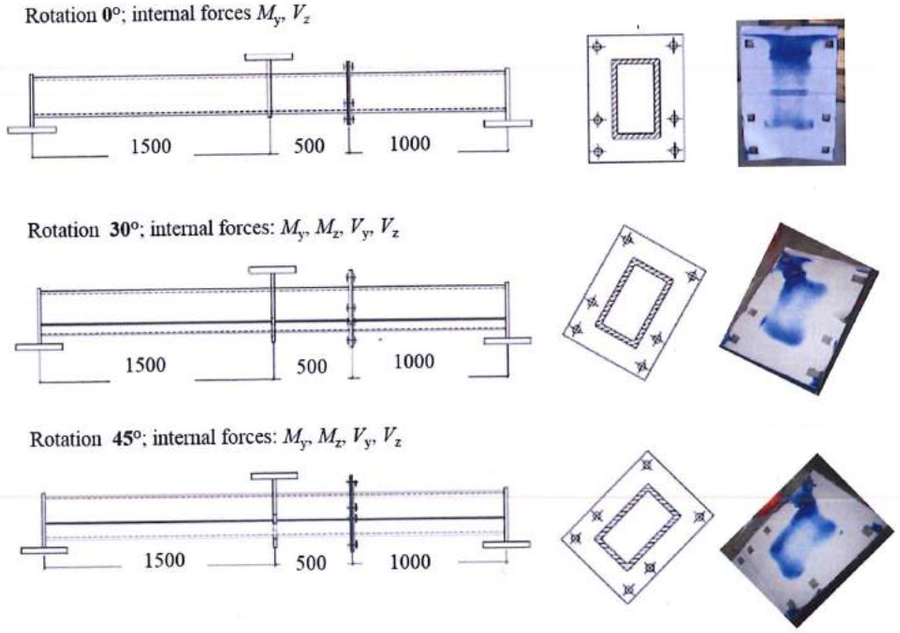

Fig. 5.4.1 Position of the beam splice joins on beam, inclination and contact imprints

Fig. 5.4.2 The test sample with 0° inclination

5.4.3 Analytical model

Connections were designed according to EN 1993-1-8:2006. Four components are guiding the behaviour the fillet welds, the beam flange in compression and in tension, the end plate in bending and the bolts in tension. Effective lengths for circular and noncircular failures are considered according to EN 1993-1-8:2006 cl. 6.2.6. Three modes of collapse according to EN 1993-1-8:2006 cl. 6.2.4.1 are considered. Bolts are designed according to cl. 3.6.1 in EN1993-1-8:2006. Design resistance considers punching shear resistance and rupture of the bolt. For component method is in EN1993-1-8:2006 recommended a linear interaction. The quadratic interaction curve according to (Neumann, 2014) is included in verification study.

5.4.4 Verification of resistance

Resistance calculated by CBFEM was compared with the results of CM and experimental results. The sensitivity study was focused on ratio of bending moments in strong and week axis, see Fig. 5.4.4. CM with linear interaction gives conservative values of resistance. CM with quadratic interaction gives the highest resistances, which are to experimental results still rather conservative. CBFEM gives similar results as CM with quadratic interaction.

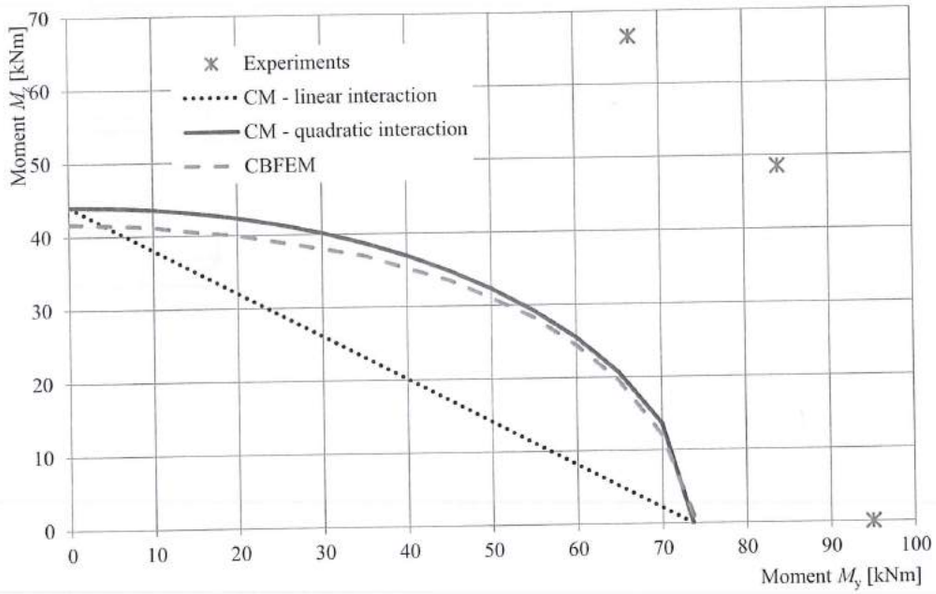

Fig. 5.4.4 Sensitivity study of the bending moment's ratio

5.4.5 Global behaviour

Comparison of the global behaviour described by moment-rotation diagram was prepared. Attention was focused to initial stiffness, resistance and deformation capacity. Sample 0° with strong axis bending moment was chosen to present as reference, see Fig. 5.4.5 and Tab. 5.4.1. CM y gives higher initial stiffness compared to CBFEM and experimental data. In all cases are resistances by CM and CBFEM similar. Experimentally measured resistance is higher.

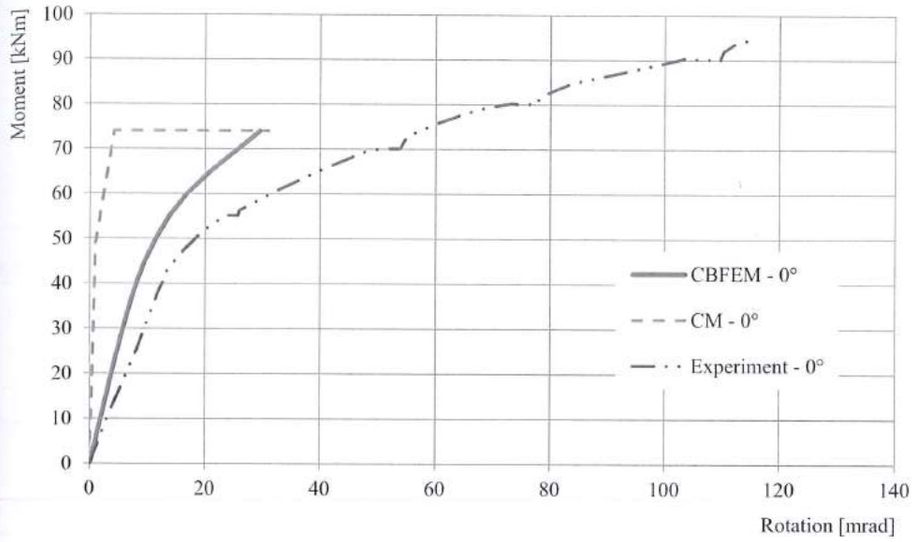

Fig. 5.4.5 Moment rotational diagram in case of 0° rotation

Tab. 5.4.1 Global behaviour overview

		CM	CBFEM	Experiment	CM/CBFEM	Exp./CBFEM
Initial stiffness	[kN/m]	53533	5400	3350	9,91	0,62
Design resistance	[kNm]	74	74	95	1,00	1,28
Deformation capacity	[mrad]	31	30	116	1,05	3,93

5.4.6 Benchmark example

Inputs

Beam

- Steel S355
- Cross section RHS 250x150x16

End plate

- Bolts 6 x M20 8.8
- Vertical distances of the bolts 35 – 230 – 100 - 35 mm
- Horizontal distances 30 – 240 – 30 mm
- End plate thickness 10 mm
- Fillet welds, thickness 8 mm

Outputs

- Resistance in bending $M_{y,Rd}$ = 74 kNm
- Vertical shear load V_{Ed} = 74 kN
- Critical component bolts in tension in second row

6 SLENDER PLATE IN COMPRESSION

6.1 Triangular haunch

6.1.1 Description

The object of this study is a verification of component based finite element method (CBFEM) a class 4 triangular haunch without a flange and a class 4 triangular haunch with a flange with reduced stiffness with research FEM model (RFEM) and design FEM model (DFEM).

6.1.2 Experimental investigation

Experimental results of six specimens of haunches with and without flanges are presented. Three specimens are without flanges and three specimens are supported by additional flanges. Unstiffened specimens differ in the web thickness t_w and the web width b_w. Reinforced specimens differ in the web thickness t_w, the flange thickness t_f and the flange width b_f. The dimensions of specimens are summarized in Tab. 6.1.1. The test set-up for the specimen without a flange is shown in Fig. 6.1.1 top and for the specimen with a flange in Fig. 6.1.1 bottom. The material characteristics of the steel plates are summed up in Tab. 6.1.2.

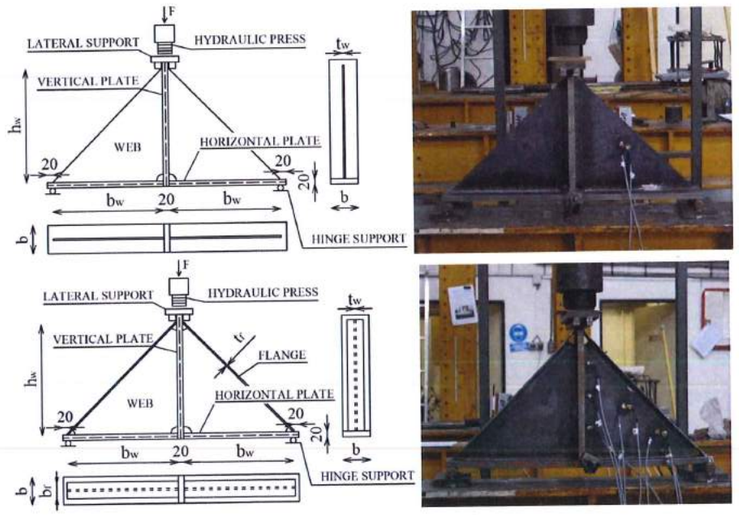

Fig. 6.1.1 Specimens geometry and test set-up

Tab. 6.1.1 Examples overview

Example	Triangular web			Flange	
	b_w	h_w	t_w	b_f	t_f
	[mm]	[mm]	[mm]	[mm]	[mm]
A	200	400	6	-	-
B	400	400	6	-	-
C	400	400	4	-	-
D	400	400	6	60	6
E	400	400	6	120	12
F	400	400	4	120	12

Tab. 6.1.2 Material characteristics used in numerical models

		Plate thickness [mm]			
Material characteristics		4	6	12	20
Young's Modulus	E [GPa]	163,0	158,7	159,8	160,0
Yield strength	f_y [MPa]	417,5	323,5	395,4	355,0
Ultimate tensile strength	f_u [MPa]	499,3	467,0	529,6	510,0

6.1.3 Research FEM model

Research FEM model (RFEM) is used to verify the DFEM model and is validated on the experiments. In the numerical model, 4-node quadrilateral shell elements with nodes at its corners are applied, with a maximum side length of 10 mm. Material and geometric nonlinear analysis with imperfections (GMNIA) is applied. Equivalent geometric imperfections are derived from the first buckling mode and the amplitude is set according to Annex C of EN1993-1-5:2005. Numerical models are shown in Fig. 6.1.2.

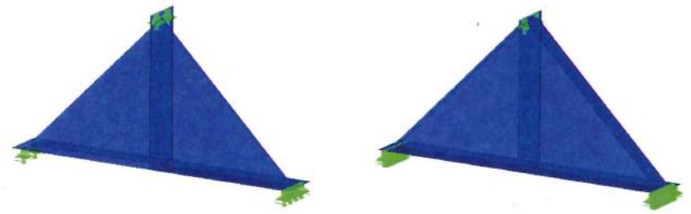

a) b)

Fig. 6.1.2 Research FEM model a) a haunch without a flange b) a haunch with a flange

An example of the comparison of RFEM and experimental test on the load-deflection behaviour is shown in Fig. 6.1.3a. The comparison of resistances measured in experiment and obtained from RFEM is shown in Fig. 6.1.3b. The resistance calculated in the numerical model is displayed on the horizontal axis. The resistance measured in the experimental study is displayed on the vertical axis. It can be seen that good agreement exists.

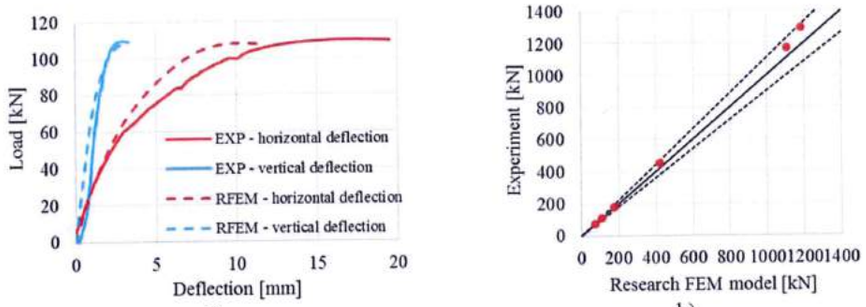

a) b)

Fig. 6.1.3 a) Load deflection curve of a haunch without a flange

b) Experiments' resistances compared against RFEMs'

The comparisons of the final deformation states between numerical simulations and experimental results are performed at the end of the tests. Fig. 6.1.4 presents the comparison of the deformation of specimens A, B and D after failure with RFEA. It can be found that good agreements between numerical models and experimental results of the haunches exist in the failure mode.

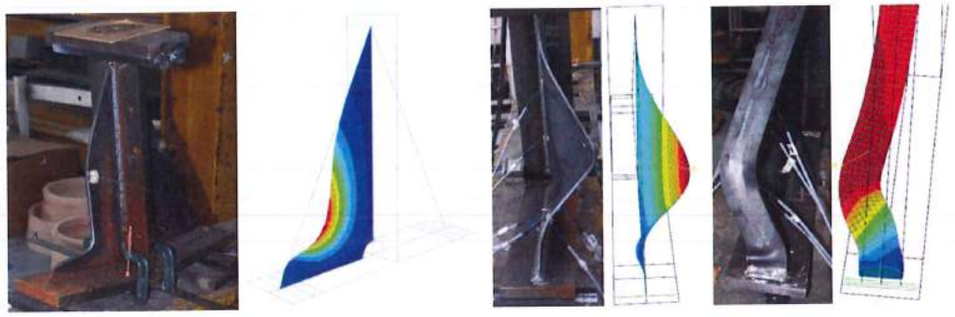

a) specimen A b) specimen B c) specimen D

Fig. 6.1.4 Experimental and numerical deflection of specimens A, B and D after failure

6.1.4 Design FEM model

Design procedure for class 4 cross-sections is described in section 3.8 local buckling.

The design procedure is verified on the comparison of DFEM and RFEM models. Both models are created in Dlubal RFEM software. The procedure is applied in CBFEM models, see (Kurejková et al, 2015). The resistance by 5% plastic strain is obtained in the first step and followed by buckling analysis. The critical component in the buckling analysis is studied and exhibit also the 5% plastic strain. The design resistance is interpolated until the condition $\rho \cdot \alpha_{ult,k} = 1$ is reached.

The first buckling mode of a haunch without a flange is shown in Fig. 6.1.4 a. The resistance is assessed according to formula (3.8.2) in section 3.8. The comparison of DFEM's and RFEM's resistances is shown in Fig. 6.1.4 b. The resistance calculated in the DFEM is displayed on the horizontal axis. The resistance calculated in RFEM is displayed on the vertical axis. It can be seen that good agreement exists and the procedure is verified.

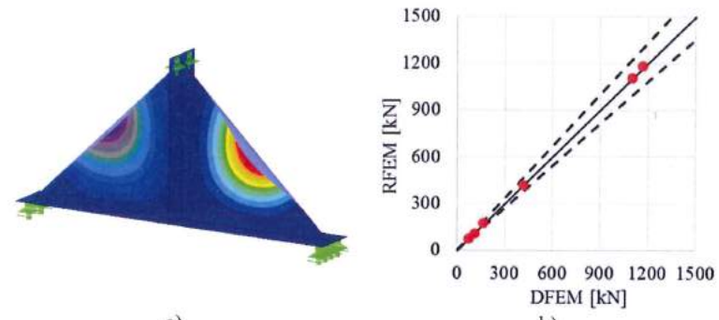

a) b)

Fig. 6.1.4 a) First buckling mode of DFEM model b) DFEMs' resistances compared against RFEMs'

6.1.5 Global behaviour and verification

Comparison of the global behaviour of a haunch without flange described by load-deflection diagrams in DFEM model is prepared. The deflection is measured in vertical direction in the middle of the specimen. Attention is focused to the main characteristics: design resistance and critical load. Two examples of a haunch without a flange are chosen to present as reference, see Fig. 6.1.5. The design procedure in DFEM models covers the post-buckling reserve, which is observed in Fig. 6.1.5 a. The critical load F_{cr} is smaller than the design resistance F_{DFEM}. The post-buckling reserve is observed in cases with very slender plates. Typical diagram is shown in Fig. 6.1.5 b, where the design resistance F_{DFEM} does not reach the critical load F_{cr}. The load $F_{ult,k}$ refers to resistance by 5 % of plastic strain.

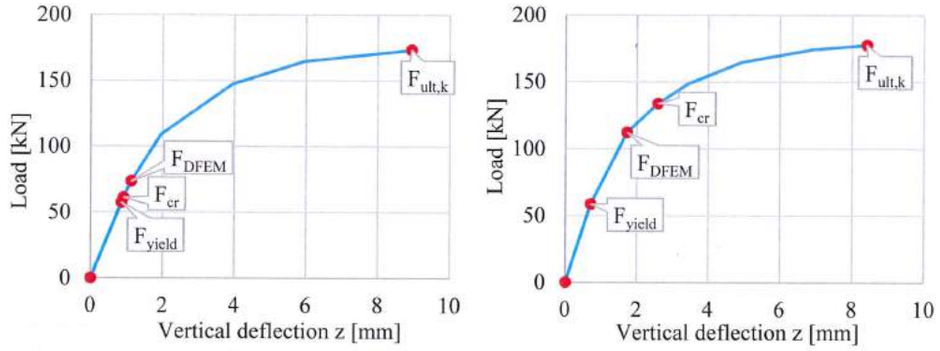

a) b)

Fig. 6.1.5 a) Load-deflection curve with post-buckling reserve

b) Load-deflection curve without post-buckling reserve

The design procedure in CBFEM models is described in section 3.8 local buckling. The buckling analysis is implemented in the software. The calculation of the design resistances is done manually according to design procedure. F_{CBFEM} is interpolated by the user until the formula (2) is equal to 1.

A beam-column joint with a haunch without a flange is studied. The thickness of beam and column webs are changing in the same way as a triangular haunch. The same cross section is used for beam and column. The geometry of the examples is described in Tab. 6.1.3. The joint is loaded by bending moment.

Tab. 6.1.3 Examples overview

Example	Material	Triangular haunch			Beam/column flange		Beam/column web	
		b_w	h_w	t_w	b_f	t_f	h_w	t_w
		[mm]	[mm]	[mm]	[mm]	[mm]	[mm]	[mm]
tw3	S355	400	400	3	120	10	300	3
tw4	S355	400	400	4	120	10	300	4
tw5	S355	400	400	5	120	10	300	5
tw6	S355	400	400	6	120	10	300	6

6.1.6 Verification of resistance

The design resistance calculated by CBFEM Idea RS software is compared with RFEM. The comparison is focused on the design resistance and critical load. The results are ordered in Tab. 6.1.4. The diagram in Fig. 6.1.6 c) shows the influence of the haunch thickness on the resistances and critical loads in the examined examples.

The results show very good agreement in critical load and design resistance. The post-buckling reserve is observed for beam web and triangular haunch thickness of 3 and 4 mm. The CBFEM model of the joint with a haunch thickness of 3 mm is shown in Fig. 6.1.6a. The first buckling mode of the joint is shown in Fig. 6.1.6b.

Tab. 6.1.4 Design resistance

Example	M_{cr}		α_{cr}	M		$\alpha_{ult,k}$	Difference
	RFEM	CBFEM	CBFEM	RFEM	CBFEM	CBFEM	M_{CBFEM}/M_{RFEM}
	[kNm]	[kNm]	[-]	[kNm]	[kNm]	[-]	[%]
tw3	22	26	0,70	41	37	2,62	10
tw4	50	62	0,97	60	64	1,94	6
tw5	89	114	1,21	85	94	1,57	10
tw6	142	144	1,25	120	115	1,50	4

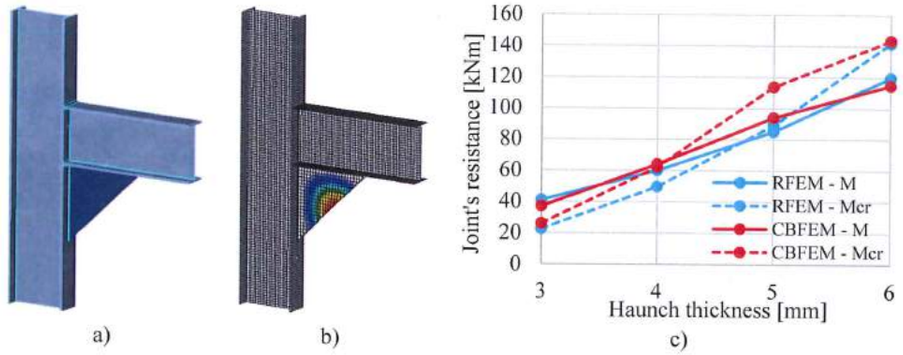

Fig. 6.1.6 a) CBFEM model b) First buckling mode
c) Influence of haunch thickness on resistances and critical loads

Verification studies confirmed the accuracy of the CBFEM model for prediction of a triangular haunch behaviour. Results of CBFEM are compared with the results of the RFEM. The design procedure is verified on the RFEM model, which is validated on experiments. All procedures predict similar global behaviour of the joint. The difference in design resistance is in all cases up to 10%.

6.1.7 Benchmark example

Inputs

Beam and column

- Steel S355
- Flange thickness t_f = 10 mm
- Flange width b_f = 120 mm
- Web thickness t_w = 3 mm
- Web height h_w = 300 mm

Triangular haunch

- Thickness t_w = 3 mm
- Width b_w = 400 mm
- Height h_w = 400 mm

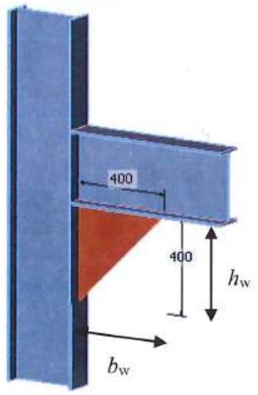

Fig. 6.1.7 Triangular haunch calculated in the benchmark example

Code setup

- Buckling analysis

Outputs

- Load by 5% plastic strain $M_{ult,k}$ = 97 kNm
- Design resistance M_{CBFEM} = 37 kNm
- Critical buckling factor (for M_{CBFEM} = 37 kNm) α_{cr} = 0,70
- Load factor by 5 % plastic strain $\alpha_{ult,k} = M_{ult,k} / M_{CBFEM}$ = 97 / 37 = 2,62

6.2 Column web panel in shear

6.2.1 Description

The objective of this study is a verification of component based finite element method (CBFEM) of a beam-column joint with a class 4 column web with research FEM model (RFEM) and component method (CM).

6.2.2 Analytical model

The component column web panel in shear is described in cl. 6.2.6.1 EN1993-1-8:2006. The design method is limited to column web slenderness $d / t_w \leq 69\,\varepsilon$. Webs with higher slenderness are designed according to EN1993-1-5:2005 cl. 5 and Annex A. The shear resistance is made of shear buckling resistance of the web panel and resistance of the frame made of the flanges and stiffeners surrounding the panel. The buckling resistance of the web panel is based on the shear critical stress

$$\tau_{cr} = k_\tau \sigma_E \qquad (6.2.1)$$

where σ_E is the Euler critical stress of the plate

$$\sigma_E = \frac{\pi^2 E}{12(1-\nu^2)}\left(\frac{t_w}{h_w}\right)^2 \qquad (6.2.2)$$

The buckling coefficient k_τ is obtained in EN 1993-1-5 Annex A.3.

The slenderness of the web panel is

$$\bar{\lambda}_w = 0{,}76\sqrt{\frac{f_{yw}}{\tau_{cr}}} \qquad (6.2.3)$$

The reduction factor χ_w may be obtained in EN 1993-1-5 cl. 5.3.

The shear buckling resistance of the web panel is

$$V_{bw,Rd} = \frac{\chi_w f_{yw} h_w t_w}{\sqrt{3}\gamma_{M1}} \qquad (6.2.4)$$

The resistance of the frame may be designed according to cl. 6.2.6.1 EN 1993-1-8:2006.

6.2.3 Research FEM model

Research FEM model (RFEM) is used to verify the CBFEM model. In the numerical model, 4-node quadrilateral shell elements with nodes at its corners are applied. Material and geometric nonlinear analysis with imperfections (GMNIA) is applied. Equivalent geometric imperfections are derived from the first buckling mode and the amplitude is set according to EN1993-1-5:2005 Annex C. A numerical model is shown in Fig. 6.2.1.

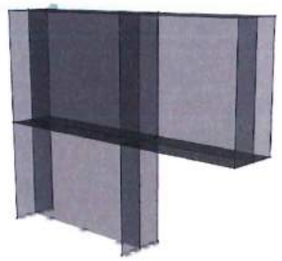

Fig. 6.2.1 Research FEM model of a beam-column joint with slender column panel

6.2.4 Design finite element model

The design procedure for slender plates is described in section 3.8. The buckling analysis is implemented in the software. The calculation of the design resistances is done according to design procedure. F_{CBFEM} is interpolated by the user until $\rho \cdot \alpha_{ult,k}/\gamma_{M1}$ is equal to 1.

A beam-column joint with a slender column web is studied. The height of the beam web is changing, thus the width of the column web panel is changing. The geometry of the examples is described in Tab. 6.2.1. The joint is loaded by bending moment.

Tab. 6.2.1 Examples overview

Example	Column flange		Column web		Beam	Material
	b_f	t_f	h_w	t_w	IPE	
	[mm]	[mm]	[mm]	[mm]		
IPE400	250	10	820	4	400	S235
IPE500	250	10	820	4	500	S235
IPE600	250	10	820	4	600	S235

6.2.5 Global behaviour and verification

The global behaviour of a beam-column joint with slender column web described by moment-rotation diagram in CBFEM model is shown in Fig. 6.2.2. Attention is focused to the main characteristics: design resistance and critical load. The diagram is completed with a point where yielding starts and resistance by 5 % plastic strain.

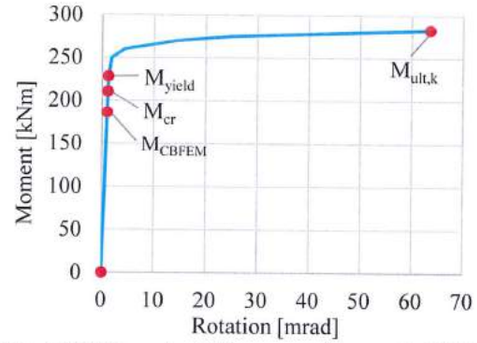

Fig. 6.2.2 Moment-rotation curve of example IPE600

6.2.6 Verification of resistance

The design resistance calculated by CBFEM is compared with RFEM and CM. The comparison is focused on the design resistance and critical load. The results are ordered in Tab. 6.2.2. The diagram in Fig. 6.2.3c shows the influence of the width of the column web on the resistances and critical loads in the examined examples.

Tab. 6.2.2 Design resistances and critical loads of RFEM, CBFEM and CM

Example	M_{cr}			α_{cr}	M			$\alpha_{ult,k}$	Difference	
	RFEM	CM	CBFEM	CBFEM	RFEM	CM	CBFEM	CBFEM	M_{CBFEM}/M_{RFEM}	M_{CBFEM}/M_{CM}
	[kNm]	[kNm]	[kNm]	[-]	[kNm]	[kNm]	[kNm]	[-]	[%]	[%]
IPE400	256	275	303	1,75	170	177	186	1	9	5
IPE500	216	234	236	1,31	177	194	180	1,29	2	8
IPE600	195	210	210	1,13	200	205	186	1,52	8	10

The results show good agreement in critical load and design resistance. The CBFEM model of the joint with a beam IPE600 is shown in Fig. 6.2.3a. The first buckling mode of the joint is shown in Fig. 6.2.3b.

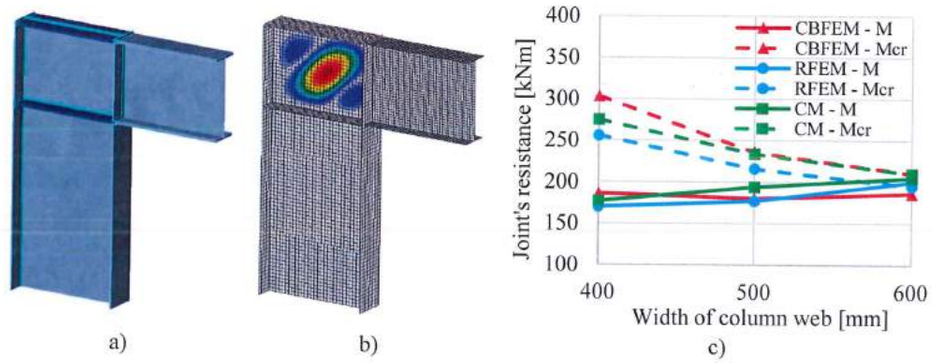

Fig. 6.2.3 a) CBFEM model b) First buckling mode
c) Influence of width of column web on resistances and critical loads

Verification studies confirmed the accuracy of the CBFEM model for prediction of a column web panel behaviour. Results of CBFEM are compared with the results of the RFEM and CM. The design procedure is verified on the RFEM model. Procedures predict similar global behaviour of the joint. The difference in design resistance is in all cases up to 10 %.

6.2.7 Benchmark example

Inputs

Beam

- Steel S235
- IPE600

Column

- Steel S235
- Flange thickness $t_f = 10$ mm
- Flange width $b_f = 250$ mm
- Web thickness $t_w = 4$ mm
- Web height $h_w = 820$ mm

Web stiffener

- Steel S235
- Stiffener thickness $t_w = 19$ mm
- Stiffener width $h_w = 250$ mm
- Stiffeners opposite to upper and lower flange

Outputs

- Load by 5 % plastic strain $M_{ult,k} = 283$ kNm
- Design resistance $M_{CBFEM} = 186$ kNm
- Critical buckling factor (for $M = 186$ kNm) $\alpha_{cr} = 1{,}13$
- Load factor by 5 % plastic strain $\alpha_{ult,k} = M_{ult,k} / M_{CBFEM} = 283/186 = 1{,}52$

6.3 Column web stiffener

6.3.1 Description

The objective of this study is a verification of component based finite element method (CBFEM) of a class 4 column web stiffener in a beam-to-column joint with research FEA model (RFEM) created in Dlubal RFEM software and component method (CM).

6.3.2 Research FEA model

Research FEA model (RFEM) is used to verify the CBFEM model. In the numerical model, 4-node quadrilateral shell elements with nodes at its corners are applied. Material and geometric nonlinear analysis with imperfections (GMNIA) is applied. Equivalent geometric imperfections are derived from the first buckling mode and the amplitude is set according to Annex C in EN1993-1-5:2005. A numerical model is shown in Fig. 6.3.1.

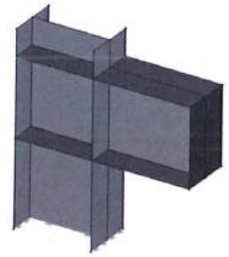

Fig. 6.3.1 Research FEA model of a beam-to-column joint with slender column web stiffener

6.3.3 CBFEM

The design procedure for slender plates is described in section 3.8. The buckling analysis is implemented in the software. The calculation of the design resistances is done according to design procedure. F_{CBFEM} is interpolated by the user until $\rho \cdot \alpha_{ult,k}/\gamma_{M1}$ is equal to 1. A beam-to-column joint with a slender column web stiffener is studied. Same cross-section is used for the beam and the column. The thickness of the column web stiffener is changing. The geometry of the examples is described in Tab. 6.3.1. The joint is loaded by bending moment.

Tab. 6.3.1 Examples overview

Example	Column/beam flange		Column/beam web		Stiffener	Material
	b_f	t_f	h_w	t_w	t_s	
	[mm]	[mm]	[mm]	[mm]	[mm]	
t3	400	20	600	12	3	S235
t4	400	20	600	12	4	S235
t5	400	20	600	12	5	S235
t6	400	20	600	12	6	S235

6.3.4 Global behaviour and verification

The global behaviour of a beam-to-column joint with a slender column web stiffener of thickness 3 mm described by moment-rotation diagram in CBFEM model is shown in Fig. 6.3.2. Attention is focused to the main characteristics: design resistance and critical load. The diagram is completed with a point where yielding starts and resistance by 5 % plastic strain.

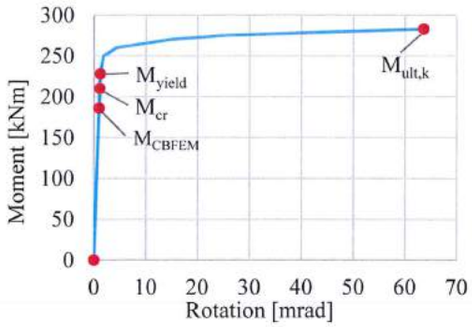

Fig. 6.3.2 Moment-rotation curve of example t3

6.3.5 Verification of resistance

The design resistance calculated by CBFEM Idea RS software is compared with RFEM. The comparison is focused on the design resistance and critical load. The results are ordered in Tab. 6.3.2. The diagram in Fig. 6.3.3 c) shows the influence of the thickness of the column web stiffener on the resistances and critical loads in the examined examples.

Tab. 6.3.2 Design resistances and critical loads of RFEM and CBFEM

Example	M_{cr}		α_{cr}	M_{Rd}		$\alpha_{ult,k}$	Diff.
	RFEM	CBFEM	CBFEM	RFEM	CBFEM	CBFEM	M_{CBFEM} / M_{RFEM}
	[kNm]	[kNm]	[-]	[kNm]	[kNm]	[-]	[%]
t3	260	286	0,94	290	304	1,96	5
t4	511	561	1,32	419	426	1,43	2
t5	874	950	1,73	532	549	1,13	3
t6	1346	1460	2,32	580	629	1,00	8

The results show very good agreement in critical load and design resistance. The CBFEM model of the joint with web stiffener thickness 3 mm is shown in Fig. 6.3.3a. The first buckling mode of the joint is shown in Fig. 6.3.3b.

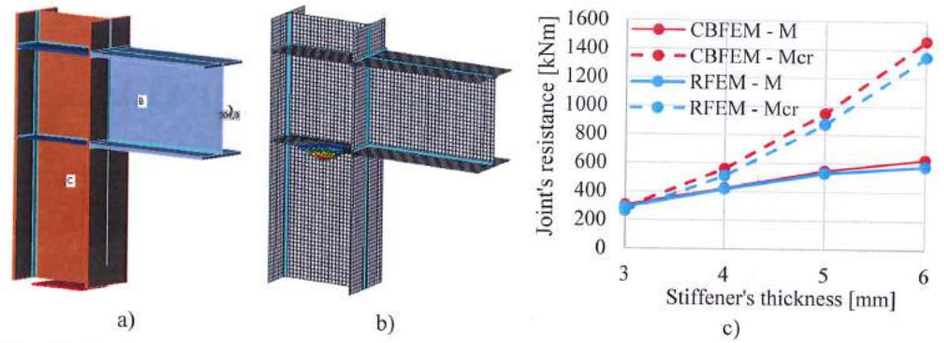

Fig. 6.3.3 a) CBFEM model b) First buckling mode c) Influence of stiffener's thickness on resistances and critical loads

Verification studies confirmed the accuracy of the CBFEM model for prediction of a column web stiffener behaviour. Results of CBFEM are compared with the results of the RFEM. All procedures predict similar global behaviour of the joint. The difference in design resistance is in all cases up to 10%.

6.3.6 Benchmark example

Inputs

Beam

- Steel S235
- Flange thickness $t_f = 20$ mm
- Flange width $b_f = 400$ mm
- Web thickness $t_w = 12$ mm
- Web height $h_w = 600$ mm

Column

- Steel S235
- Flange thickness $t_f = 20$ mm
- Flange width $b_f = 400$ mm
- Web thickness $t_w = 12$ mm
- Web height $h_w = 600$ mm

Upper column web stiffener

- Steel S235
- Stiffener thickness $t_w = 20$ mm
- Stiffener width $h_w = 400$ mm

Lower column web stiffener

- Steel S235
- Stiffener thickness $t_w = 3$ mm
- Stiffener width $h_w = 400$ mm

Outputs

- Load by 5% plastic strain $M_{ult,k} = 596$ kNm
- Design resistance $M_{CBFEM} = 304$ kNm
- Critical buckling factor (for $M = 304$ kNm) $\alpha_{cr} = 0{,}94$
- Load factor by 5 % plastic strain $\alpha_{ult,k} = M_{ult,k} / M_{CBFEM} = 596/304 = 1{,}96$

7 HOLLOW SECTION JOINT

7.1 Uniplanar gap K-joint between RHS braces and RHS chord

7.1.1 Description

The object of this study is a verification of component based finite element method (CBFEM) uniplanar gap K-joint of welded rectangular hollow sections in which RHS braces are welded directly onto the RHS chord without the use of reinforcing plates with the method of failure modes (FM). The gap K-joint is considered to be only axially loaded in this study.

7.1.2 Method of failure modes

In the case of axially loaded gap K-joint of welded rectangular hollow sections four failure modes can occur. These being chord plastification (chord face failure), local yielding of brace (brace failure), chord punching shear and chord shear. The chord plastification and local yielding of brace are two failure modes examined only in this study, see Fig. 7.1.1. The welds are considered not to be the weakest components in the joint and they are designed according to EN1993-1-8:2006.

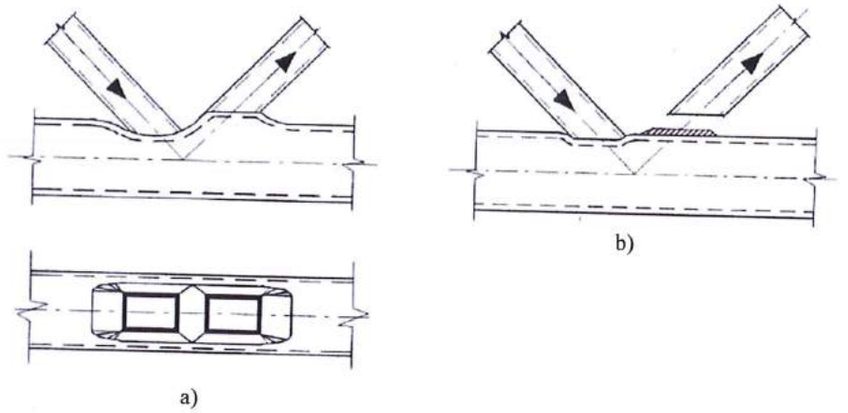

a) b)

Fig. 7.1.1 Examined failure modes, a) Chord plastification, b) Local yielding of brace

Chord plastification

The design resistance of the RHS chord face can be determined using the method given in section 7.5 of EN1993-1-8:2006. This method is also given in the International standard ISO/FDIS 14346 (CIDECT) and it is closely described in Wardenier et al. (2010). The design resistance of the axially loaded gap K-joint of welded rectangular hollow sections is

$$N_{i,Rd} = Q_u Q_f \frac{f_{y0} t_0^2}{\sin \theta_i} \qquad (7.1.1)$$

where Q_u is the function which depends on the joint geometry; Q_f is the chord stress function, f_{y0} is the yield stress of the chord; t_0 is the wall thickness of the RHS chord and θ_i is the included angle between the brace member i and the chord ($i = 1, 2$).

Local yielding of brace

The design resistance of the RHS brace in the joint can be determined using the method given in section 7.5 of EN 1993-1-8:2006 and in the International standard ISO/FDIS 14346 (CIDECT). The design resistance of the axially loaded gap K-joint of welded rectangular hollow sections is

$$N_{i,Rd} = f_{yi} t_i l_{b,eff} \qquad (7.1.2)$$

where f_{yi} is the yield stress of the brace member i ($i = 1, 2$); t_i is the wall thickness of the RHS brace member i; and $l_{b,eff}$ is the effective perimeter for local yielding of the brace.

Examined examples

Overview of the considered examples are given in the Tab. 7.1.1. A geometry of the gap K-joint with dimensions is shown in Fig. 7.1.2. In the selected cases failed the joints according to the method based on failure modes (FM) by the chord plastification and local yielding of brace only.

Tab. 7.1.1 Examples overview

Example	Chord	Braces	Eccentricity	Angles	Material		
	Section	Section	e	θ	f_y	f_u	E
			[mm]	[°]	[MPa]	[MPa]	[GPa]
a1	RHS 120x80x5	RHS 60x40x5	0	50	235	360	210
a2	RHS 120x80x5	RHS 60x40x5	0	50	275	430	210
a3	RHS 140x80x5	RHS 60x40x5	0	55	275	430	210
a4	RHS 140x80x5	RHS 60x40x5	0	55	355	490	210
a5	RHS 160x80x5	RHS 60x40x5	0	55	275	430	210
a6	RHS 160x80x5	RHS 60x40x5	0	55	355	490	210
a7	RHS 180x100x6.3	RHS 100x50x6.3	0	50	275	430	210
a8	RHS 180x100x6.3	RHS 100x50x6.3	0	50	355	490	210
a9	RHS 180x100x6.3	RHS 100x60x6.3	0	50	275	430	210
a10	RHS 180x100x6.3	RHS 100x60x6.3	0	50	355	490	210
b1	RHS 100x60x10	RHS 60x40x4	0	45	235	360	210
b2	RHS 100x60x10	RHS 60x40x4	0	45	275	430	210
b3	RHS 120x60x10	RHS 60x40x4	0	55	235	360	210
b4	RHS 120x60x10	RHS 60x40x4	0	55	275	430	210
b5	RHS 140x80x10	RHS 60x40x4	0	55	235	360	210
b6	RHS 140x80x10	RHS 60x40x4	0	55	275	430	210
b7	RHS 150x100x10	RHS 60x40x4	0	55	275	430	210
b8	RHS 150x100x10	RHS 60x40x4	0	55	355	490	210
b9	RHS 180x100x8	RHS 120x60x5	0	44	275	430	210
b10	RHS 180x100x8	RHS 120x60x5	0	44	355	490	210

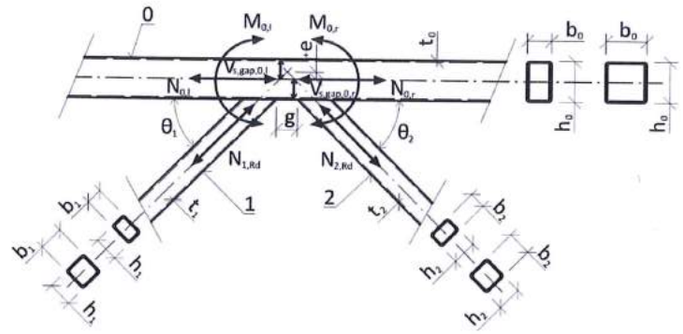

Fig. 7.1.2 Dimensions of gap K-joint

7.1.3 Verification of resistance

Results of the method based on failure modes (FM) is compared with the results of CBFEM. The comparison is focused on the resistance and determination of the critical component. Results are presented in Tab. 7.1.2. The study covers both two failure modes, thus chord plastification (cases a), and local yielding of brace (cases b) loaded by normal forces in the brace members.

Tab. 7.1.2 Comparison of results of prediction by CBFEM and FM

Example	Design resistance				
	FM	Mode of failure	CBFEM	Mode of failure	diff,
	[kN]		[kN]		[%]
a1	121	Chord plastification	118	Chord plastification	2,5
a2	141	Chord plastification	137	Chord plastification	2,8
a3	133	Chord plastification	127	Chord plastification	4,5
a4	172	Chord plastification	160	Chord plastification	7,0
a5	134	Chord plastification	122	Chord plastification	9,0
a6	173	Chord plastification	154	Chord plastification	11,0
a7	271	Chord plastification	271	Chord plastification	0,0
a8	350	Chord plastification	343	Chord plastification	2,0
a9	290	Chord plastification	316	Chord plastification	9,0
a10	375	Chord plastification	402	Chord plastification	7,2
b1	173	Local yielding of brace	166	Local yielding of brace	4,0
b2	202	Local yielding of brace	192	Local yielding of brace	5,0
b3	173	Local yielding of brace	164	Local yielding of brace	5,2
b4	202	Local yielding of brace	191	Local yielding of brace	5,4
b5	173	Local yielding of brace	164	Local yielding of brace	5,2
b6	202	Local yielding of brace	191	Local yielding of brace	5,4
b7	202	Local yielding of brace	192	Local yielding of brace	5,0
b8	261	Local yielding of brace	245	Local yielding of brace	6,1
b9	468	Local yielding of brace	435	Local yielding of brace	7,1
b10	604	Local yielding of brace	557	Local yielding of brace	7,8

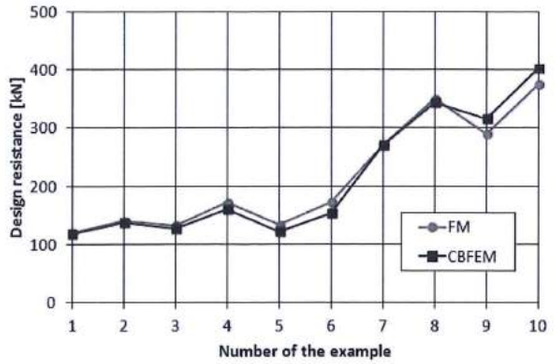

Fig. 7.1.3 Comparison of results of CBFEM to FM for failure mode chord plastification (cases a)

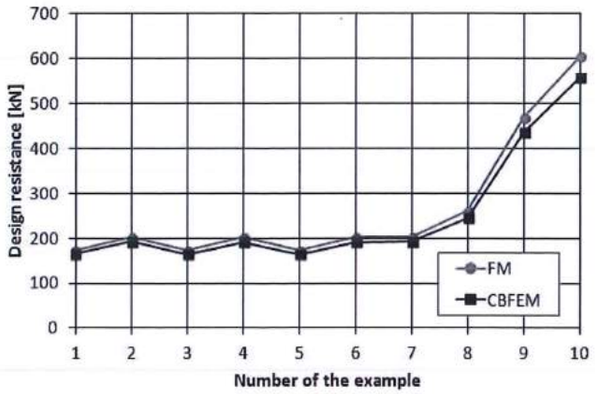

Fig. 7.1.4 Comparison of results of CBFEM to FM for failure mode local yielding of brace (cases b)

The sensitivity study shows good agreement for the applied load case, see Fig. 7.1.3 and Fig. 7.1.4. The results are summarized in a graph comparing CBFEM's and FM's design resistances, see Fig. 7.1.5. The results show that the difference of the two calculation methods is generally less than 11 %.

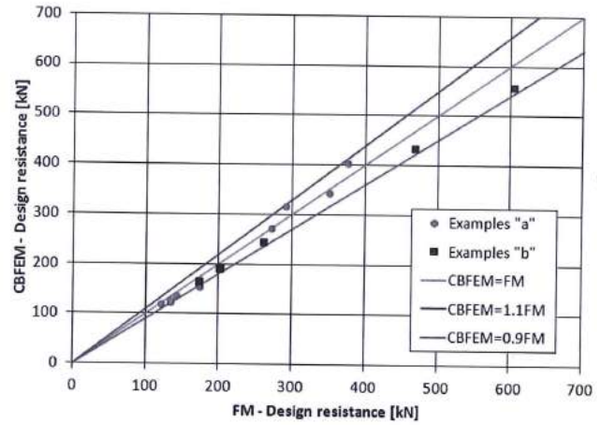

Fig. 7.1.5 Verification of CBFEM to FM
for the uniplanar gap K-joint between RHS braces and RHS chord

7.1.4 Range of validity

CBFEM was verified for usually used gap K-joints of welded rectangular hollow sections. Range of validity for these joints is defined in the Table 7.8 of EN 1993-1-8 or in the Table 6 of ISO/FDIS 14346, see Tab 7.1.6. The validation to experiments or verification to validated research model should be prepared in case of application of the CBFEM model outside the range of validity of FM.

Tab. 7.1.3 Range of validity for FM (Table 6 of ISO/FDIS 14346)

Range of validity			
		T-, Y- or X-joints	Gap K-joints
Brace –to-chord ratio	RHS braces	$b_i / b_0 \geq 0{,}1 + 0{,}01\ b_0 / t_0$ but $\geq 0{,}25$	
	CHS braces	$d_i / b_0 \geq 0{,}1 + 0{,}01\ b_0 / t_0$ and $0{,}25 \leq d_i / b_0 \leq 0{,}80$	
RHS chord	Compression	class 1 or 2 and $b_0 / t_0 \leq 40$ and $h_0 / t_0 \leq 40$	
	Tension	$b_0 / t_0 \leq 40$ and $h_0 / t_0 \leq 40$	
RHS braces	Compression	class 1 or 2 and $b_i / t_i \leq 40$ and $h_i / t_i \leq 40$	
	Tension	$b_i / t_i \leq 40$ and $h_i / t_i \leq 40$	
CHS braces	Compression	class 1 or 2 and $d_i / t_i \leq 50$	
	Tension	$d_i / t_i \leq 50$	
Gap		N/A	$0{,}5\ (1 - \beta) \leq g / b_0 \leq 1{,}5\ (1 - \beta)$ [a] and $g \geq t_1 + t_2$
Eccentricity		N/A	$e \leq 0{,}25\ h_0$
Aspect ratio		$0{,}5 \leq h_i / b_i \leq 2{,}0$	
Brace angle		$\theta_i \geq 30°$	
Yield stress		$\sigma_{yi} \leq \sigma_{y0}$ and $\sigma_y \leq 0{,}8\ \sigma_u$	

[a] For $g / b_0 > 1{,}5\ (1 - \beta)$, check the joint also as two separate T- or Y-joints.

7.1.5 Benchmark example

Inputs

Chord

- Steel S235
- Section RHS 120x80x5

Braces

- Steel S235
- Sections RHS 60x40x5
- Angle between the brace member and the chord 50°

Welds

- Fillet welds around the braces with throat thickness a_w = 5 mm

Outputs

- Design resistance in compression/tension is 118,2 kN
- Failure mode is chord plastification

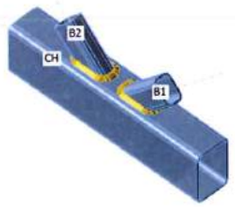

Fig. 7.1.5 Benchmark example for chord RHS 120x80x5 and braces RHS 60x40x5

7.2 Multiplanar TT joint between RHS braces and SHS chord

7.2.1 Description

The object of this study is a verification of component based finite element method (CBFEM) the multiplanar TT-joint of welded square hollow sections in which are RHS (SHS) braces welded directly onto the SHS chord without the use of reinforcing plates with the method of failure modes (FM). The TT-joint is considered to be only axially loaded in this study.

7.2.2 Method of failure modes

In the case of axially loaded TT-joint of welded rectangular (square) hollow sections four failure modes can occur. These are chord plastification (chord face failure), local yielding of brace (brace failure), chord punching shear and chord side wall failure. The chord plastification, local yielding of brace and chord side wall failure, see Fig. 7.2.1., are three failure modes examined in this study only. The welds are considered not to be the weakest components in the joint and they are designed according to EN1993-1-8:2006.

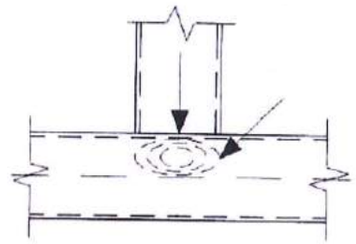

Fig. 7.2.1 The chord side wall failure as one examined failure mode

Chord plastification

The design resistance of the SHS chord face can be determined using the method given in section 7.5 of EN 1993-1-8. This method is also given in the International standard ISO/FDIS 14346 (CIDECT) and it is closely described in (Wardenier et al, 2010). The design resistance of the axially loaded TT-joint of welded rectangular (square) hollow sections is assumed as

$$N_{i,Rd} = Q_u Q_f \frac{f_{y0} t_0^2}{\sin \theta_i} \mu \qquad (7.2.1)$$

where Q_u is the function which depends on the joint geometry; Q_f is the chord stress function; f_{y0} is the yield stress of the chord; t_0 is the wall thickness of the SHS chord; θ_i is the included angle between the brace member i and the chord (i = 1, 2); and μ is the multiplanar factor.

Local yielding of brace

The design resistance of the RHS (SHS) brace in the joint can be determined using the method given in section 7.5 of EN 1993-1-8 and in the International standard ISO/FDIS 14346 (CIDECT). The design resistance of the axially loaded TT-joint of welded rectangular (square) hollow sections is:

$$N_{i,Rd} = f_{yi} t_i l_{b,eff} \mu \qquad (7.2.2)$$

where f_{yi} is the yield stress of the brace member i (i = 1, 2); t_i is the wall thickness of the RHS (SHS) brace member i; $l_{b,eff}$ is the effective perimeter for local yielding of the brace; and μ is the multiplanar factor.

Chord side wall failure

The design resistance of the SHS chord side walls can be determined using the method given in section 7.5 of EN 1993-1-8 and in the International standard ISO/FDIS 14346 (CIDECT).

Then the design resistance of the axially loaded TT-joint of welded rectangular (square) hollow sections is:

$$N_{i,Rd} = \frac{f_k t_0}{\sin\theta_i} b_w Q_f \mu \qquad (7.2.3)$$

where – f_k is the design stress for chord side wall failure; t_0 is the wall thickness of the SHS chord; θ_i is the included angle between the brace member i and the chord (i = 1, 2); b_w is the effective width for the SHS side wall; Q_f is the chord stress function; and μ is the multiplanar factor.

Examined examples

Overview of the considered examples are given in the Tab. 7.2.1. A geometry of the TT-joint with dimensions is shown in Fig. 7.2.2.

Tab. 7.2.1 Examples overview

Example	Chord	Braces	Angles		Material		
	Section	Section	ϕ	θ	f_y	f_u	E
			[°]	[°]	[MPa]	[MPa]	[GPa]
a1	SHS 100x100x4	RHS 60x40x4	90	90	235	360	210
a2	SHS 100x100x4	RHS 60x40x4	90	90	275	430	210
a3	SHS 100x100x5	RHS 60x40x5	90	90	275	430	210
a4	SHS 100x100x5	RHS 60x40x5	90	90	355	490	210
a5	SHS 50x50x5	RHS 60x40x5	90	90	275	430	210
a6	SHS 50x50x5	RHS 60x40x5	90	90	355	490	210
b1	SHS 80x80x12.5	RHS 60x40x5	90	90	235	360	210
b2	SHS 80x80x12.5	RHS 60x40x5	90	90	275	430	210
b3	SHS 100x100x12.5	RHS 60x40x5	90	90	235	360	210
b4	SHS 100x100x12.5	RHS 60x40x5	90	90	275	430	210

b5	SHS 140x140x12.5	RHS 60x40x5	90	90	275	430	210
b6	SHS 140x140x12.5	RHS 60x40x5	90	90	355	490	210
b7	SHS 120x120x16	RHS 80x40x4	90	90	275	430	210
b8	SHS 120x120x16	RHS 80x40x4	90	90	355	490	210
c1	SHS 120x120x8	SHS 120x120x8	90	90	235	360	210
c2	SHS 120x120x8	SHS 120x120x8	90	90	275	430	210
c3	SHS 140x140x8	SHS 140x140x8	90	90	235	360	210
c4	SHS 140x140x8	SHS 140x140x8	90	90	275	430	210
c5	SHS 160x160x8	SHS 160x160x8	90	90	275	430	210
c6	SHS 160x160x8	SHS 160x160x8	90	90	355	490	210

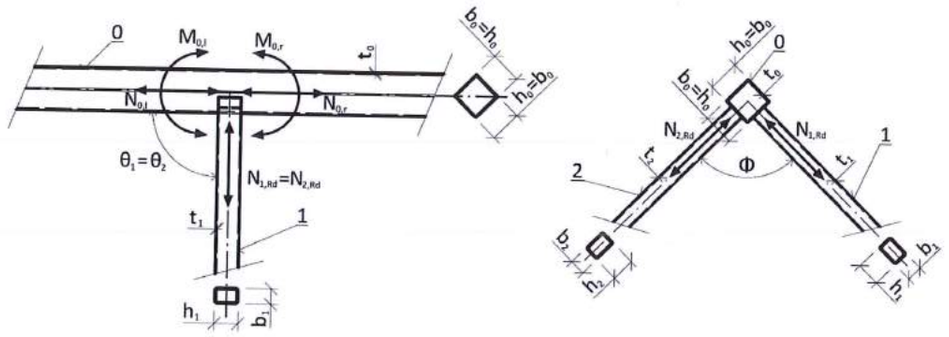

Fig. 7.2.2 Dimensions of TT-joint

7.2.3 Verification of resistance

Results of the method based on failure modes were compared with the results of CBFEM Idea RS software. The comparison was focused on the resistance and determination of the critical component. All results are presented in Tab. 7.2.2.

The study was performed so that three failure modes occurred: chord plastification (examples "a"), local yielding of brace (examples "b") and chord side wall failure (examples "c"); for one load case: tensile normal forces in the brace members.

Tab. 7.2.2 Comparison of results of prediction by CBFEM and FM

Example	Design resistance				
	FM	Mode of failure	CBFEM	Mode of failure	Diff.
	[kN]		[kN]		[%]
a1	27	Chord plastification	29	Chord plastification	7,4
a2	32	Chord plastification	33	Chord plastification	3,1
a3	49	Chord plastification	53	Chord plastification	8,2
a4	64	Chord plastification	67	Chord plastification	4,7
a5	144	Chord plastification	148	Chord plastification	2,8
a6	186	Chord plastification	188	Chord plastification	1,1

b1	212	Local yielding of brace	198	Local yielding of brace	6,6
b2	248	Local yielding of brace	230	Local yielding of brace	7,3
b3	212	Local yielding of brace	198	Local yielding of brace	6,6
b4	248	Local yielding of brace	229	Local yielding of brace	7,7
b5	248	Local yielding of brace	228	Local yielding of brace	8,1
b6	320	Local yielding of brace	290	Local yielding of brace	9,4
b7	246	Local yielding of brace	237	Local yielding of brace	3,7
b8	318	Local yielding of brace	304	Local yielding of brace	4,4
c1	602	Chord side wall failure	506	Chord side wall failure	15,9
c2	704	Chord side wall failure	588	Chord side wall failure	16,5
c3	677	Chord side wall failure	593	Chord side wall failure	12,4
c4	792	Chord side wall failure	689	Chord side wall failure	13,0
c5	880	Chord side wall failure	788	Chord side wall failure	10,5
c6	1136	Chord side wall failure	1001	Chord side wall failure	11,9

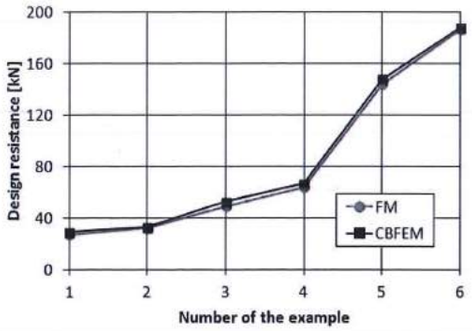

Fig. 7.2.3 Comparison of results of CBFEM to FM for failure mode chord plastification (a)

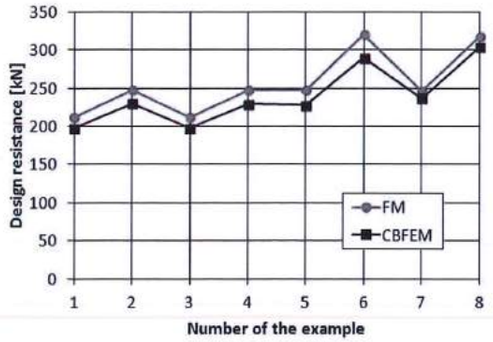

Fig. 7.2.4 Comparison of results of CBFEM to FM for failure mode local yielding of brace (b)

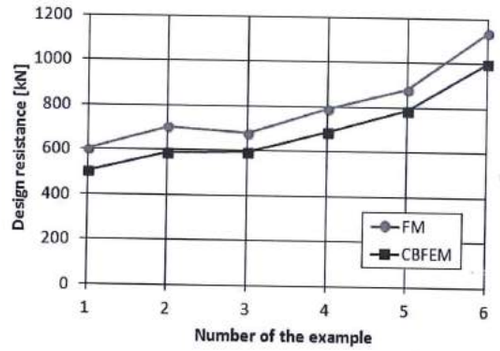

Fig. 7.2.5 Comparison of results of CBFEM to FM for failure mode chord side wall failure (c)

The parametric studies show good agreement for the applied load case, see Fig. 7.2.3, Fig. 7.2.4 and Fig. 7.2.5. Results of the parametric studies are summarized in a graph comparing CBFEM's and FM's design resistance, see Fig. 7.2.6. The results show that the difference of the two calculation methods is in most of cases less than 17 %.

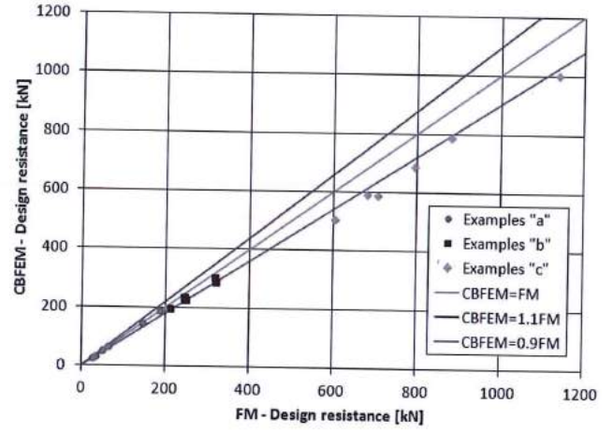

Fig. 7.2.6 Verification of CBFEM to CM
for multiplanar TT joint between RHS braces and SHS chord

7.2.4 Range of validity

CBFEM was verified for usually used TT-joints of welded rectangular (square) hollow sections. Range of validity for these joints is defined in tables 7.8 and 7.19 of EN1993-1-8:2006 or in tables 6 and 10 of ISO/FDIS 14346, see Tab. 7.2.3. The validation to experiments or verification to validated research model should be prepared in case of application of the CBFEM model outside of the range of validity of FM.

Tab. 7.2.3 Range of validity for FM (Tables 6 and 10 of ISO/FDIS 14346)

Range of validity			
		T-, Y- or X-joints	Gap K-joints
Brace –to-chord ratio	RHS braces	$b_i / b_0 \geq 0{,}1 + 0{,}01\ b_0 / t_0$ but $\geq 0{,}25$	
	CHS braces	$d_i / b_0 \geq 0{,}1 + 0{,}01\ b_0 / t_0$ and $0{,}25 \leq d_i / b_0 \leq 0{,}80$	
RHS chord	Compression	class 1 or 2 and $b_0 / t_0 \leq 40$ and $h_0 / t_0 \leq 40$	
	Tension	$b_0 / t_0 \leq 40$ and $h_0 / t_0 \leq 40$	
RHS braces	Compression	class 1 or 2 and $b_i / t_i \leq 40$ and $h_i / t_i \leq 40$	
	Tension	$b_i / t_i \leq 40$ and $h_i / t_i \leq 40$	
CHS braces	Compression	class 1 or 2 and $d_i / t_i \leq 50$	
	Tension	$d_i / t_i \leq 50$	
Gap		N/A	$0{,}5\ (1 - \beta) \leq g / b_0 \leq 1{,}5\ (1 - \beta)$ [a] and $g \geq t_1 + t_2$
Eccentricity		N/A	$e \leq 0{,}25\ h_0$
Aspect ratio		$0{,}5 \leq h_i / b_i \leq 2{,}0$	
Brace angle		$\theta_i \geq 30°$	
Yield stress		$\sigma_{yi} \leq \sigma_{y0}$ and $\sigma_y \leq 0{,}8\ \sigma_u$	
[a] For $g / b_0 > 1{,}5\ (1 - \beta)$, check the joint also as two separate T- or Y-joints.			

Range of validity	Same as in Table 7.2.3 $\theta = 90°$

7.2.5 Benchmark example

Inputs

Chord

- Steel S275
- Section SHS 140x140x12.5

Braces

- Steel S275
- Sections RHS 60x40x5
- Angle between the brace member and the chord 90°
- Angle between the braces 90°

Welds

- Fillet welds around the braces with throat thickness $a_w = 5$ mm

Outputs

- Design resistance in tension 228,0 kN
- Failure mode local yielding of brace

Fig. 7.2.7 Benchmark example for chord SHS 140x140x12.5 and braces RHS 60x40x5

7.3 Uniplanar T-joint between longitudinal gusset plate and RHS chord

7.3.1 Description

The object of this chapter is verification of component based finite element method (CBFEM) of the uniplanar welded T-joint of gusset plate to rectangular hollow sections with method of failure modes (FM). The gusset plate is welded directly onto the face of rectangular hollow sections in the lattice truss.

7.3.2 Method of failure modes

In these joints usually occurs only failure mode the chord face failure, see Fig. 7.3.1. Welds are designed according to EN 1993-1-8 not to be the weakest component in the joint. In the parts of lattice truss design continues load causes design internal forces in the form of normal forces and bending moments. Action of internal forces in location of T-joint is described as follows:

Axially-loaded RHS chord

The normal forces in the chord right and left of T-joint location act in location of chord longitudinal axis.

Diffraction-loaded RHS chord

For calculation only bending moments right and left of T-joint location in plane of T-joint are considered in the chord and these bending moments rotate around one of the axes in plane of chord cross-section for rotation in plane of T-joint.

Axially loaded gusset plate

The normal force in the brace of T-joint location acts in location of brace longitudinal axis.

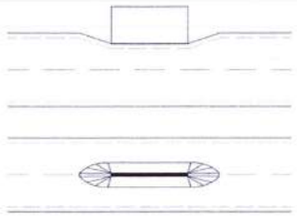

Fig. 7.3.1: Chord face failure

The design resistance of the chord web is determined using the method given in section 7.6 EN1993-1-8:2006, which background is described in (Wardenier et al, 2010). The load from the gusset plate has to be transferred through the face of the chord. The design resistance of the joint is predicted as

$$N_{i,Rd} = k_m \cdot f_{y0} \cdot {t_0}^2 \cdot \left(2 \cdot h_1/b_0 + 4 \cdot \sqrt{1 - t_1/b_0}\right)/\gamma_{M5} \qquad (7.3.1)$$

where

$$\text{For } n > 0\ (compression) \rightarrow\ k_m = 1{,}3 \cdot (1 - n) \leq 1{,}0 \qquad (7.3.2)$$

$$\text{For } n < 0\ (tensile) \rightarrow\ k_m = 1{,}0 \qquad (7.3.3)$$

Plates loaded by axial forces

Overview of the considered examples and the material are given in the Tab. 7.3.1. Geometries of joints with dimensions are shown in Fig. 7.3.2.

Tab. 7.3.1: Cases of plates loaded by axial forces

Example	Chord	Brace	Weld	Material		
	Section	Section	a	f_y	f_u	E
			[mm]	[MPa]	[MPa]	[GPa]
a1	SHS 100x5	P 8x100	12	355	490	210
a2	SHS 100x5	P 8x120	12	355	490	210
a3	SHS 100x5	P 10x150	15	355	490	210
a4	SHS 100x8	P 8x100	12	355	490	210
a5	SHS 100x8	P 8x120	12	355	490	210
a6	SHS 100x8	P 10x150	15	355	490	210
a7	SHS 150x6,3	P 8x100	12	355	490	210
a8	SHS 150x6,3	P 8x120	12	355	490	210
a9	SHS 150x6,3	P 10x150	15	355	490	210
a10	SHS 150x12,5	P 10x100	15	355	490	210
a11	SHS 150x12,5	P 12x120	18	355	490	210
a12	SHS 150x12,5	P 15x150	23	355	490	210
a13	SHS 200x12,5	P 15x150	23	355	490	210
a14	SHS 200x12,5	P 20x200	30	355	490	210
a15	SHS 300x10	P 15x200	23	355	490	210
a16	SHS 300x10	P 20x300	30	355	490	210
a17	SHS 300x16	P 15x200	23	355	490	210
a18	SHS 300x16	P 20x300	30	355	490	210

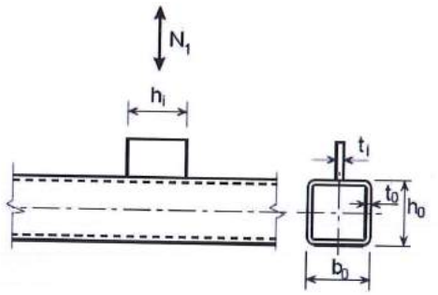

Fig. 7.3.2 Joint's geometry with dimensions

7.3.3 Verification of resistance

Results of the method based on failure modes (FM) are compared with the results of CBF. The comparison was focused on resistance and the critical component of the joint, see in Tab. 7.3.2.

Tab. 7.3.2 Comparison of CBFEM and FM for tensile force in plate

Tension in plate					
Example	Design resistance				
	FM [kN]	Mode of failure	CBFEM [kN]	Mode of failure	Diff. [%]
a1	52	Chord face failure	54	Chord face failure	3
a2	55	Chord face failure	60	Chord face failure	8
a3	60	Chord face failure	67	Chord face failure	10
a4	132	Chord face failure	139	Chord face failure	5
a5	141	Chord face failure	156	Chord face failure	10
a6	154	Chord face failure	180	Chord face failure	14
a7	74	Chord face failure	68	Plate failure	7
a8	77	Chord face failure	75	Chord face failure	2
a9	83	Chord face failure	83	Chord face failure	1
a10	288	Chord face failure	267	Chord face failure	7
a11	301	Chord face failure	305	Chord face failure	1
a12	321	Chord face failure	348	Chord face failure	8
a13	296	Chord face failure	298	Chord face failure	1
a14	321	Chord face failure	347	Chord face failure	7
a15	185	Chord face failure	171	Chord face failure	8
a16	208	Chord face failure	195	Chord face failure	6
a17	475	Chord face failure	431	Plate failure	9
a18	532	Chord face failure	551	Chord face failure	3

The parametric studies show good agreement for the applied load cases. To illustrate the accuracy of the CBFEM model, results of the parametric studies are summarized in a diagram comparing CBFEM's and FM's design resistance, see Fig. 7.3.3. The results show that the difference of the two calculation methods is in most of cases less than 14%.

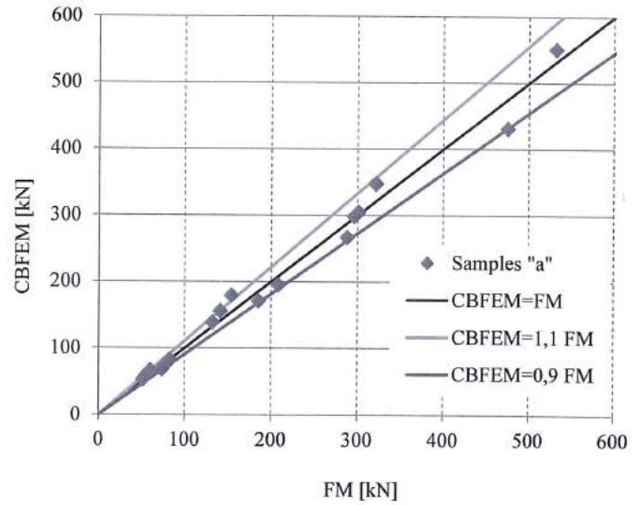

Fig. 7.3.3 Verification of CBFEM to CM for axial force in the brace of the uniplanar T-joint between longitudinal gusset plate and RHS chord

7.3.4 Range of validity

CBFEM is verified for T-joints between rectangular hollow section and open section. Range of validity is defined in Tab. 9 in ISO/FDIS 14346, see Tab. 7.3.3. The validation to experiments or verification to validated research model should be prepared in case of application of the CBFEM model outside the range of validity of FM.

Tab. 7.3.3 Range of validity of joints between longitudinal gusset plate and RHS chord (Table 9 in ISO/FDIS 14346)

Chord	Compression	class 1 or 2; $b_0/t_0 \leq 40$ and $h_0/t_0 \leq 40$
	Tensile	$b_0/t_0 \leq 40$ and $h_0/t_0 \leq 40$
	Aspect ratio	$0{,}5 \leq h_0/b_0 \leq 2$
Longitudinal plate	Compression	$1 \leq h_1/b_0 \leq 4$
Angle between chord and plate		$\theta_i = 90°$

7.3.5 Benchmark case

Inputs

Chord

- Steel S355
- SHS 200x12,5

Gusset plate

- Steel S355
- Plate P15x150

Weld

- Throat thickness a_w = 23 mm
- Fillet weld around the plate

Outputs

- Design resistance in tensile is $F_{c,Rd}$ = 298,4 kN
- Collapse mode is chord face failure

7.4 Uniplanar T-joint between RHS brace and H/I chord

7.4.1 Description

In this chapter the uniplanar T-joint of welded rectangular hollow sections to open sections which is located in the lattice truss, RHS brace is welded directly onto the H or I chord (open sections) without use of reinforcing plates is studied. The prediction by component based finite element method (CBFEM) with the experiments based method of failure modes (FM) implemented in EN1993-1-8:2006 is verified.

7.4.2 Analytical model

In the uniplanar T-joint of welded rectangular hollow sections to open sections occur only three failure modes, e.g. local yielding of brace (brace failure), chord web failure and chord shear, e.g. chord check in shear. The chord web failure and chord shear are two modes of failure examined in this study, see Fig. 7.4.1. The welds are designed not to be the weakest component in the joint according to EN 1993-1-8:2006. The elements of lattice trusses are loaded by the normal forces and the bending moments. Action of internal forces in location of T-joint is described as follows:

Axially loaded H/I chord

The normal forces in the chord right and left of T-joint location act in location of chord longitudinal axis.

Diffraction loaded H/I chord

For calculation only bending moments right and left of T-joint location in plane of T-joint are considered in the chord and these bending moments rotate around one of the axes in plane of chord cross-section for rotation in plane of T-joint.

Axially loaded RHS brace

The normal force in the brace of T-joint location acts in location of brace longitudinal axis.

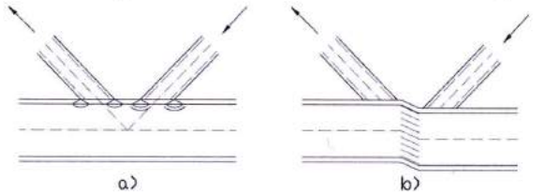

Fig. 7.4.1 Major failure modes a) chord web failure, b) chord shear (in case of gap)

The resistance of the chord web is determined using the method given in section 7.6 of the EN 1993-1-8:2005, which is described in (Wardenier et al, 2010). The stresses from the brace are transferred through the flange of the chord to an effective area of the chord web. This area is located in the chord web at the location, where the brace walls cross the chord web. The design resistance of the joint is:

$$N_{i,Rd} = \frac{f_{y0} \cdot t_w \cdot b_w}{\sin\theta_i \cdot \gamma_{M5}} \qquad (7.4.1)$$

$$N_{i,Rd} = \frac{f_{y0} \cdot A_v}{\sqrt{3} \cdot \sin\theta_i \cdot \gamma_{M5}} \quad (7.4.2)$$

$$M_{i,Rd} = 0{,}5 \cdot f_{y0} \cdot t_w \cdot b_w \cdot h_1 / \gamma_{M5} \quad (7.4.3)$$

where

$$b_w = \frac{h_1}{\sin\theta_i} + 5 \cdot (t_{f,0} + r) \leq 2 \cdot t_i + 10 \cdot (t_{f,0} + r) \quad (7.4.4)$$

where $N_{i,Rd}$ is design axial resistance of the joint chord web failure and chord shear; $M_{ip,1,Rd}$ is design axial resistance of the joint for chord web failure; b_w is the effective width of the chord web; A_v is the effective shear area. Overview of the considered examples and the material are given in the Tab. 7.4.1. Geometries of joints with dimensions are shown in Fig. 7.4.2.

Tab. 7.4.1 Samples overview

Sample	Chord	Brace	Weld	Material		
	Section	Section	a	f_y	f_u	E
			[mm]	[MPa]	[MPa]	[GPa]
a1	IPN 220	RHS 140x70x10	15	235	360	210
a2	IPN 240	RHS 140x70x10	15	235	360	210
a3	IPN 260	RHS 140x70x10	15	235	360	210
a4	IPN 280	RHS 140x70x10	15	235	360	210
a5	IPE 200	RHS 140x70x10	15	235	360	210
a6	IPE 220	RHS 140x70x10	15	235	360	210
a7	IPE 270	RHS 140x70x10	15	235	360	210
a8	IPE 330	RHS 140x70x10	15	235	360	210
a9	IPE 360	RHS 140x70x10	15	235	360	210
a10	HEA 240	RHS 140x70x10	15	235	360	210
a11	HEA 280	RHS 140x70x10	15	235	360	210
a12	HEA 300	RHS 140x70x10	15	235	360	210
a13	HEA 320	RHS 140x70x10	15	235	360	210
a14	HEA 340	RHS 140x70x10	15	235	360	210
a15	HEA 360	RHS 140x70x10	15	235	360	210
a16	HEB 220	RHS 140x70x10	15	235	360	210
a17	HEB 240	RHS 140x70x10	15	235	360	210
a18	HEB 260	RHS 140x70x10	15	235	360	210
c1	IPE 330	RHS 180x100x10,0	15	235	360	210
c2	IPE 330	RHS 180x100x11,0	17	235	360	210
c3	IPE 330	RHS 180x100x12,5	19	235	360	210
c4	IPE 330	RHS 180x100x14,2	21	235	360	210
c5	IPE 330	RHS 180x100x16,0	24	235	360	210
c6	IPE 330	RHS 180x100x17,5	26	235	360	210
d1	IPE 140	RHS 140x70x10	15	235	360	210
d2	IPE 160	RHS 140x70x10	15	235	360	210
d3	HEA 100	RHS 140x70x10	15	235	360	210
d4	HEA 120	RHS 140x70x10	15	235	360	210
d5	HEB 100	RHS 140x70x10	15	235	360	210
d6	HEB 120	RHS 140x70x10	15	235	360	210
d7	HEB 140	RHS 140x70x10	15	235	360	210
d8	HEB 160	RHS 140x70x10	15	235	360	210
e1	HEB 100	RHS 180x100x5,6	8	235	360	210
e2	HEB 100	RHS 180x100x8	12	235	360	210
e3	HEB 100	RHS 180x100x10	15	235	360	210
e4	HEB 100	RHS 180x100x12,5	19	235	360	210
e5	HEB 100	RHS 180x100x16,0	24	235	360	210

Braces loaded by in-plane moment

Overview of the considered cases and the material are given in the Tab. 7.4.2. Geometries of joints with dimensions are shown in Fig. 7.4.2.

Tab. 7.4.2 Cases for braces loaded by in-plane moment

Examples	Chord	Brace	Weld	Material		
	Section	Section	a	f_y	f_u	E
			[mm]	[MPa]	[MPa]	[GPa]
a1	IPN 160	RHS 140x70x10	15	235	360	210
a2	IPN 180	RHS 140x70x10	15	235	360	210
a3	IPE 140	RHS 140x70x10	15	235	360	210
a4	IPE 160	RHS 140x70x10	15	235	360	210
a5	IPE 180	RHS 140x70x10	15	235	360	210
a6	IPE 200	RHS 140x70x10	15	235	360	210
a7	IPE 220	RHS 140x70x10	15	235	360	210
a8	HEA 100	RHS 140x70x10	15	235	360	210
a9	HEA 120	RHS 140x70x10	15	235	360	210
a10	HEA 140	RHS 140x70x10	15	235	360	210
b1	HEB 220	RHS 220x120x16	24	235	360	210
b2	HEB 220	RHS 220x120x16	24	275	430	210
b3	HEB 220	RHS 220x120x16	24	355	490	210
c1	HEA 240	RHS 180x100x12,5	19	235	360	210
c2	HEA 240	RHS 180x100x14,2	21	235	360	210
c3	HEA 240	RHS 180x100x16,0	24	235	360	210
c4	IPE 330	RHS 180x100x12,5	19	235	360	210
c5	IPE 330	RHS 180x100x14,2	21	235	360	210
c6	IPE 330	RHS 180x100x16,0	24	235	360	210

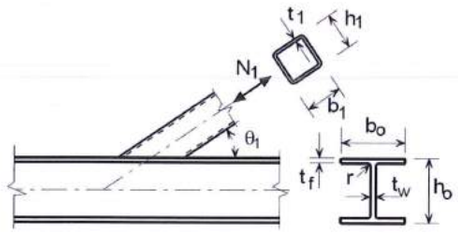

Fig. 7.4.2 Joint's geometry with dimensions

7.4.3 Verification of resistance

The study was focussed to distinguish of failure models and prediction of resistance. Results are presented in Tab. 7.4.3, 7.4.4 and 7.4.5. For failure of the chord web were studied parameters section of the H/I chord (marked a), material of members (b), and the thickness of the wall of RHS brace (c) and load cases axial force in brace and in-plane moment. Brace failure was not studied.

Tab. 7.4.3 Comparison of CBFEM and FM for axial force in brace

Sample	Design resistance				
	FM [kN]	Mode of failure	CBFEM [kN]	Mode of failure	Difference [%]
a1	425	Chord web	483	Chord web	12
a2	487	Chord web	556	Chord web	12
a3	563	Chord web	629	Chord web	10
a4	631	Chord web	692	Chord web	9
a5	296	Chord web	310	Chord shear	5
a6	322	Chord web	358	Chord shear	10
a7	413	Chord web	459	Chord web	10
a8	507	Chord web	554	Chord web	8
a9	552	Chord web	607	Chord web	9
a10	538	Chord web	494	Chord web	8
a11	611	Chord web	592	Chord web	3
a12	689	Chord web	657	Chord web	5
a13	746	Chord web	721	Chord web	3
a14	798	Chord web	772	Chord web	3
a15	852	Chord web	823	Chord web	3
a16	692	Chord web	614	Chord shear	11
a17	776	Chord web	689	Chord web	11
a18	817	Chord web	731	Chord web	11
c1	555	Chord web	625	Chord web	11
c2	559	Chord web	637	Chord web	12
c3	564	Chord web	645	Chord web	13
c4	570	Chord web	643	Chord web	11
c5	576	Chord web	643	Chord web	10
c6	577	Chord web	640	Chord web	10

Tab. 7.4.4 Comparison of CBFEM and FM for in-plane moment in brace

Sample	Design resistance				
	FM [kNm]	Mode of failure	CBFEM [kNm]	Mode of failure	Difference [%]
a1	17,1	Chord web	20,1	Chord web	15
a2	20,3	Chord web	23,7	Chord web	14
a3	11,4	Chord web	13,5	Chord web	16
a4	14,1	Chord web	15,6	Chord web	10
a5	15,4	Chord web	17,4	Chord web	11
a6	19,2	Chord web	20,8	Chord web	8
a7	20,9	Chord web	22,5	Chord web	7
a8	16,8	Chord web	14,5	Chord web	13
a9	16,8	Chord web	15,9	Chord web	6
a10	18,9	Chord web	19,0	Chord web	0
b1	84,7	Chord web	87,9	Chord web	4
b2	99,1	Chord web	101,8	Chord web	3
b3	128,0	Chord web	128,0	Chord web	0
c1	50,9	Chord web	51,0	Chord web	0
c2	50,4	Chord web	50,3	Chord web	0
c3	49,9	Chord web	50,1	Chord web	1
c4	47,2	Chord web	48,7	Chord web	3
c5	47,3	Chord web	47,9	Chord web	1
c6	47,3	Chord web	47,7	Chord web	1

The parametric studies show good agreement for all applied load cases, difference of the two calculation methods is in most of cases less than 15 %. To illustrate the accuracy of the CBFEM model, results of the parametric studies are summarized in a diagram comparing CBFEM's and FM's design resistance, see Fig. 7.4.3 and 7.4.4.

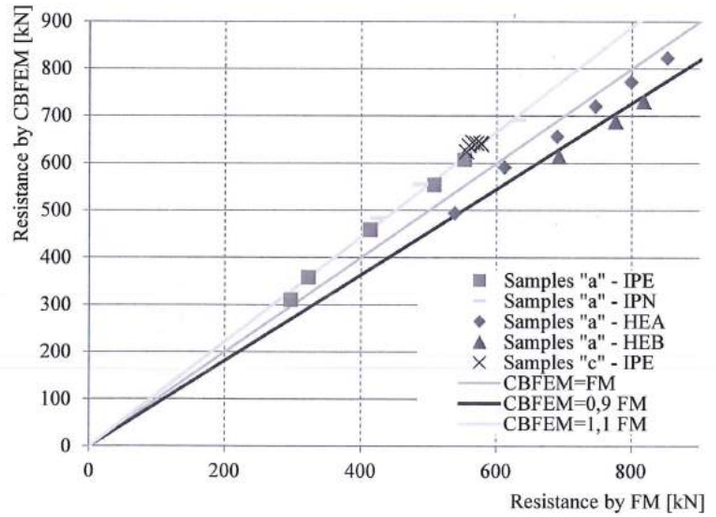

Fig. 7.4.3 Verification of CBFEM to CM for axial force in the brace

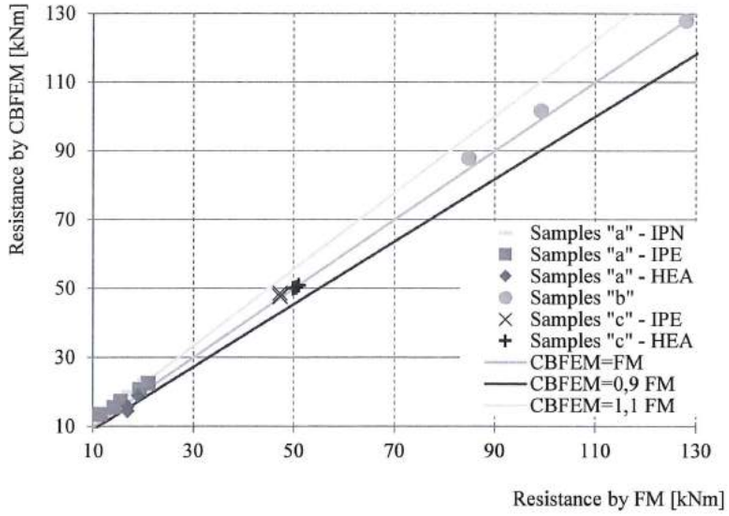

Fig. 7.4.4 Verification of CBFEM to CM for in-plane moment in the brace

The study for failure of the chord shear was performed for two parameters section of the H/I chord (samples "d") and the thickness of the wall of RHS brace (samples "e") and only one load case the axial force in brace.

Tab. 7.4.5 Comparison of CBFEM and FM for axial force in brace

Sample	Design resistance				
	FM [kN]	Mode of failure	CBFEM [kN]	Mode of failure	Difference [%]
d1	172	Chord shear	183	Chord shear	6
d2	213	Chord shear	223	Chord shear	4
d3	151	Chord shear	149	Chord shear	1
d4	173	Chord shear	174	Chord shear	1
d5	184	Chord shear	192	Chord shear	4
d6	229	Chord shear	247	Chord shear	7
d7	279	Chord shear	303	Chord shear	8
d8	368	Chord shear	391	Chord shear	6
e1	184	Chord shear	182	Chord web	1
e2	184	Chord shear	182	Chord web	1
e3	184	Chord shear	182	Chord web	1
e4	184	Chord shear	182	Chord web	1
e5	184	Chord shear	182	Chord web	1

The parametric studies show good agreement for all case, the difference less than 10 %. To illustrate the accuracy of the CBFEM model, results of the parametric studies are summarized in a diagram comparing CBFEM's and FM's design resistance, see Fig. 7.4.5.

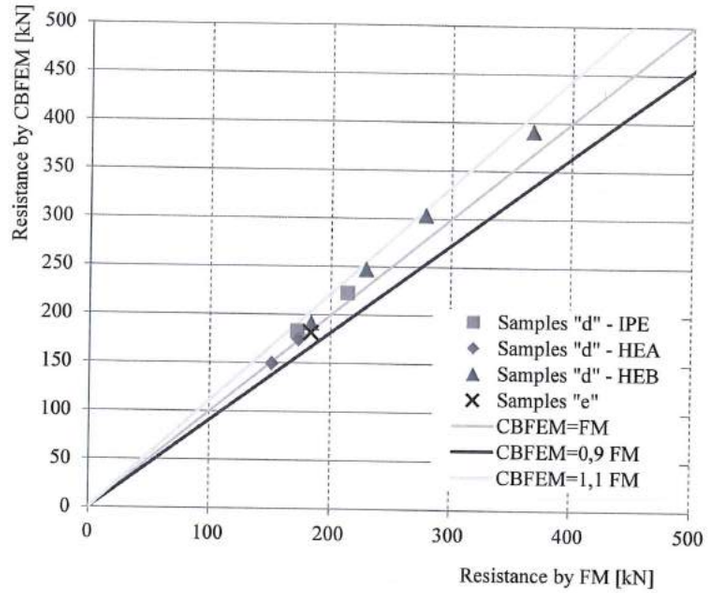

Fig. 7.4.5 Verification of CBFEM to CM for axial force in the brace

7.4.4 Range of validity

Range of validity, on which is verified CBFEM for T-joints between rectangular hollow section and open section, is defined in Table 7.20 of EN1993-1-8:2006, see Tab. 7.4.6. In case of application of the CBFEM model outside the range of validity of FM, the validation to experiments or verification to validated research model should be prepared to approve the quality of prediction.

Tab. 7.4.6 Range of validity of T-joints

Chord	Compression	Flange	class 1 or 2
		Web	class 1; $d_w \leq 400\ mm$
	Tensile		-
RHS Brace	Compression		class 1; $b_i/t_i \leq 40$ and $h_i/t_i \leq 40$
	Tensile		$b_i/t_i \leq 40$ and $h_i/t_i \leq 40$
	Other		$0{,}5 \leq h_i/b_i \leq 2$
Angle between chord and brace			$\theta_i \geq 30$

7.4.5 Benchmark example

Inputs

Chord

- Steel S235
- HEA340

Brace

- Steel S235
- RHS 140x70x10

Weld

- Throat thickness a_w = 15 mm
- Fillet weld around the brace

Outputs

- Design resistance in compression/tension $F_{c,Rd}$ = 772 kN
- Collapse mode is full yielding of the chord web

8 COLUMN BASE

8.1 Open section column in compression

8.1.1 Description

In this chapter, the component based finite element method (CBFEM) of the column base under the steel open section column loaded in pure compression on the component method (CM) is verified. The study is prepared for the column cross section, dimension of base plate, grade of concrete, and dimensions of concrete block.

8.1.2 Component method

Three components are taken into account: column flange and web in compression, concrete in compression including grout, welds. Component column flange and web in compression is described in EN1993-1-8:2006 Cl. 6.2.6.7. The concrete in compression including grout is modelled according to EN1993-1-8:2006 Cl. 6.2.6.9 and EN1992-1-1:2005 Cl. 6.7. Two iterations of effective area are used to determine the resistance.

The weld is designed around the column cross-section, see EN1993-1-8:2006 Cl. 4.5.3.2(6). The thickness of the weld on the flanges is selected the same as the thickness of the weld on the web. Shear force is transferred only by welds on the web and plastic stress distribution is considered.

8.1.3 Base plate under HEB 240

This study is focused on the component the concrete in compression including grout. An example of calculation is shown below for the concrete block $a' = 1000$ mm, $b' = 1500$ mm , $h = 800$ mm from concrete grade C20/25 with base plate $a = 330$ mm; $b = 440$ mm; $t = 20$ mm from steel grade S235, see Fig. 8.1.2.

The joint stength of the concrete is calculated under affective area of the cross section , see Fig. 8.1.1, iterating in two steps, For 1st step it is

$$f_{jd} = \frac{\beta_j \cdot k_j \cdot f_{ck}}{\gamma_c} = \frac{0{,}67 \cdot 2{,}908 \cdot 20}{1{,}5} = 26 \text{ MPa}$$

$$c = t \cdot \sqrt{\frac{f_y}{3 \cdot f_{jd} \cdot \gamma_{M0}}} = 20 \cdot \sqrt{\frac{235}{3 \cdot 26 \cdot 1{,}0}} = 35 \text{ mm}$$

$$l_{eff} = b + 2 \cdot c = 240 + 2 \cdot 35 = 310 \text{ mm}$$

$$b_{eff} = t_f + 2 \cdot c = 17 + 2 \cdot 35 = 87 \text{ mm}$$

and for 2nd step it is

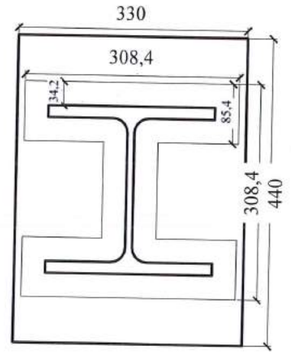

Fig. 8.1.1 Effective area under the base plate

$$f_{jd} = \frac{\beta_j \cdot k_j \cdot f_{ck}}{\gamma_c} = \frac{0{,}67 \cdot 3 \cdot 20}{1.5} = 27 \text{ MPa}$$

$$c = t \cdot \sqrt{\frac{f_y}{3 \cdot f_{jd} \cdot \gamma_{M0}}} = 20 \cdot \sqrt{\frac{235}{3 \cdot 27 \cdot 1{,}0}} = 34 \text{ mm}$$

$$l_{eff} = b + 2 \cdot c = 240 + 2 \cdot 34 = 308 \text{ mm}$$

$$b_{eff} = t_f + 2 \cdot c = 17 + 2 \cdot 34 = 85 \text{ mm}$$

$$A_{eff} = 63\,463 \text{ mm}^2$$

The normal force resistance of the base plate by CM is

$$N_{Rd} = A_{eff} \cdot f_{jd} = 63\,436 \cdot 27 = 1701 \text{ kN}$$

The stresses calculated by CBFEM are presented is Fig. 8.1.2. The normal force resistance of the base plate by CM is 1739 kN.

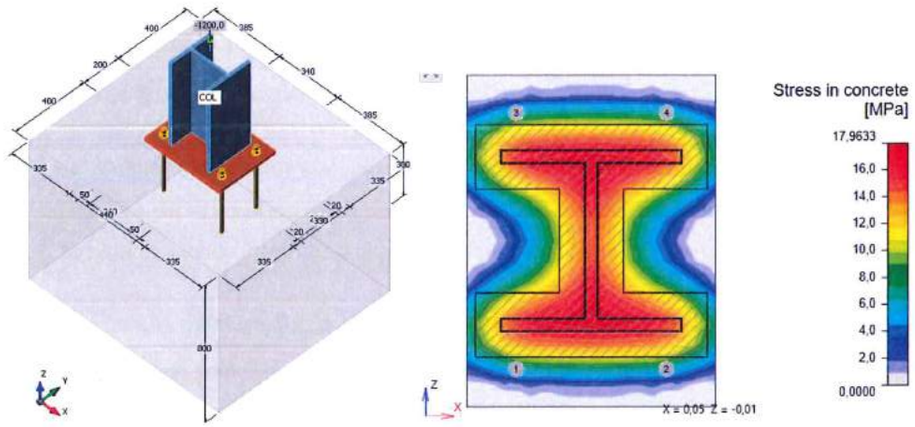

Fig. 8.1.2 Geometry of concrete block
and normal stresses under baseplate loaded by normal force only

8.1.4 Sensitivity study

Results of CBFEM software were compared with the results of the component method. The comparison was focused on the resistance and the critical component. Studied parameters are: size of the column, dimensions of the base plate, concrete grade, dimensions of the concrete pad. The column cross sections are HEB 200, HEB 300 and HEB 400. The base plate width and length are chosen as 100 mm, 150 mm and 200 mm larger than the column section, the base plate thickness 15 mm, 20 mm and 25 mm. The concrete block from grade C16/20, C25/30 and C35/45 of height 800 mm with width and length larger than the dimensions of the base plate by 200 mm, 300 mm and 400 mm. The input parameters are summarized in Tab. 8.1.1. The fillet welds around the column cross section have the throat thickness a = 8 mm.

Tab. 8.1.1 Selected parameters

Column section	HEB 200	HEB 300	HEB 400
Base plate offset	100 mm	150 mm	200 mm
Base plate thickness	15 mm	20 mm	25 mm
Concrete grade	C16/20	C25/30	C35/45
Concrete pad offset	200 mm	300 mm	400 mm

The resistances determined by CM are in Tab. 8.1.2. One parameter was changed and the others were held constant at the middle value. N_{Rd} is the resistance of component concrete in compression including grout" $F_{c,fc,Rd}$ is the resistance of component column flange and web in compression and $F_{c,weld}$ is the resistance of welds considering uniform distribution of stress. The joint coefficient $\beta_j = 0.67$ was used.

Table 8.1.2 Results of component method

Column	B.p. offset [mm]	B.p. thickness [mm]	Concrete	C.b. offset [mm]	N_{Rd} [kN]	$2.F_{c,fc,Rd}$ [kN]	$F_{c,weld}$ [kN]
HEB 200	150	20	C25/30	300	1753	1632	2454
HEB 300	150	20	C25/30	300	2352	3126	3466
HEB 400	150	20	C25/30	300	2579	4040	3822
HEB 300	100	20	C25/30	300	2296	3126	3466
HEB 300	200	20	C25/30	300	2408	3126	3466
HEB 300	150	15	C25/30	300	1909	3126	3466
HEB 300	150	25	C25/30	300	2795	3126	3466
HEB 300	150	20	C16/20	300	1789	3126	3466
HEB 300	150	20	C35/45	300	2908	3126	3466
HEB 300	150	20	C25/30	200	2064	3126	3466
HEB 300	150	20	C25/30	400	2517	3126	3466

The model in CBFEM was loaded by the compressive force equal to N_{Rd}, which was determined from the component method. The value of concrete block resistance was chosen as applied force divided by concrete block utilization obtained from the program. The same approach was used to get the resistance of welds $F_{c,weld}$: the applied force was divided by weld utilization of the most stressed weld.

Table 8.1.3 Results of CBFEM

Column	B.p. offset [mm]	B.p. thickness [mm]	Concrete grade	C.b. offset [mm]	Concrete block [kN]	$F_{c,weld}$ [kN]
HEB 200	150	20	C25/30	300	1626	2005
HEB 300	150	20	C25/30	300	2502	3115
HEB 400	150	20	C25/30	300	2767	3345
HEB 300	100	20	C25/30	300	2501	3111
HEB 300	200	20	C25/30	300	2524	3095
HEB 300	150	15	C25/30	300	1989	3155
HEB 300	150	25	C25/30	300	3051	3071
HEB 300	150	20	C16/20	300	1947	3090
HEB 300	150	20	C35/45	300	3120	3117
HEB 300	150	20	C25/30	200	2353	3108
HEB 300	150	20	C25/30	400	2502	3119

Summary

Verification of CBFEM to CM for base plate loaded in compression is shown in Fig. 8.1.3. The dashed lines correspond to the 110 % and 90 % value of resistance. The difference is up to 14 % due to more accurate evaluation of the design bearing strength of the joint f_{jd} and effective area A_{eff} in CBFEM.

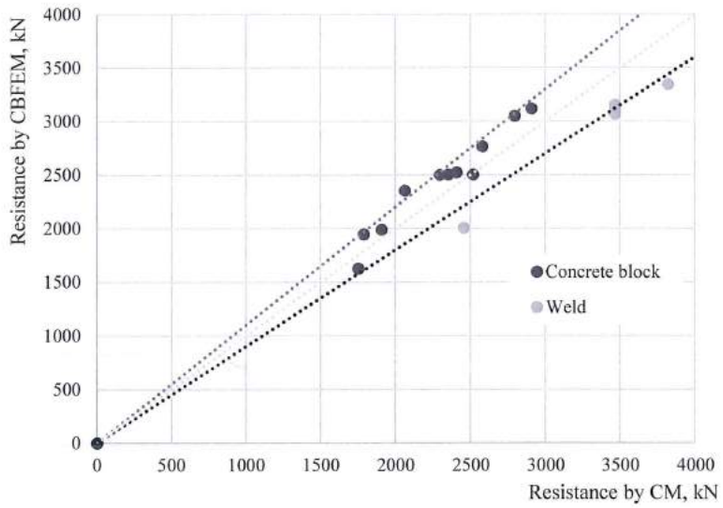

Fig. 8.1.3 Verification of CBFEM to CM for base plate loaded in compression

8.1.5 Benchmark case

Input

Column cross section

- HEB 240
- Steel S235

Base plate

- Thickness 20 mm
- Offsets top 100 mm, left 45 mm
- Steel S235

Foundation concrete block

- Concrete C20/25
- Offset 335 mm
- Depth 800 mm
- Grout thickness 30 mm

Anchor bolt

- M20 8.8

Output

- Axial force resistance $N_{j,Rd}$ = -1744,2 kN

8.2 Open section column in bending to strong axis

8.2.1 Description

The object of this chapter is verification of component based finite element method (CBFEM) of the column base of the steel open section column loaded in compression and bending to strong axis with the component method (CM). The study is prepared for size of the column, geometry and thickness of base plate. In the study, four components are examined: column flange and web in compression, concrete in compression including grout, base plate in bending and welds. All components are designed according to EN1993-1-8:2006, EN1992-1-1:2005 and ETAG 001 – Annex C.

8.2.2 Verification of resistance

An example of component method design is shown on the anchorage of column steel section HEB 240: Concrete block has dimensions $a' = 1000$ mm, $b' = 1500$ mm, $h = 900$ mm and grade C20/25. Base plate dimensions are $a = 330$ mm; $b = 440$ mm; $t = 20$ mm and steel grade S235. Anchor bolts are 4 x M20, $A_s = 245$ mm^2 with head diameter $a = 60$ mm and steel grade 8.8. Grout thickness is 30 mm.

Results of analytical solution may be presented on interaction diagram with distinctive significant points. Point 1 represents loading in pure tension and point 4 represents the compression bearing resistance. Detailed description of points 0, 1, 2 and 3 is shown in Fig. 8.2.1, see (Wald, 1995) and (Wald et al., 2008).

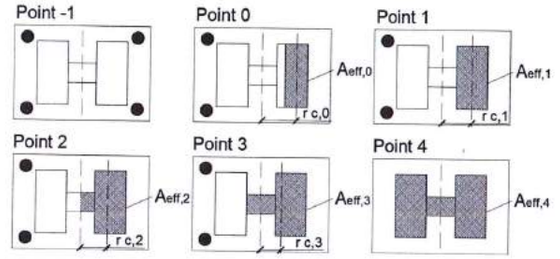

Fig. 8.2.1 Significant points on interaction diagram

The stress distribution for point 0 and 3 reached by CBFEM is displayed in Fig. 8.2.2 and 8.2.3.

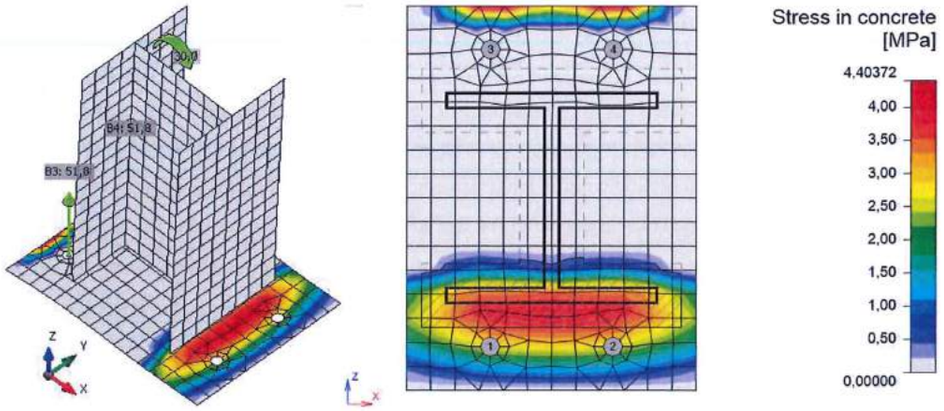

Fig. 8.2.1 Stress in concrete and forces in anchors for point 0 obtained by CBFEM (deform. scale 25)

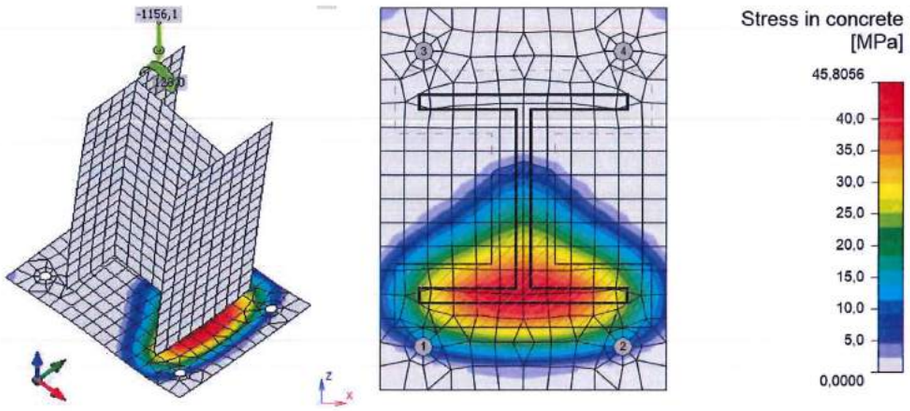

Fig. 8.2.2 Stress in concrete and forces in anchors for point 3 obtained by CBFEM (deform. scale 25)

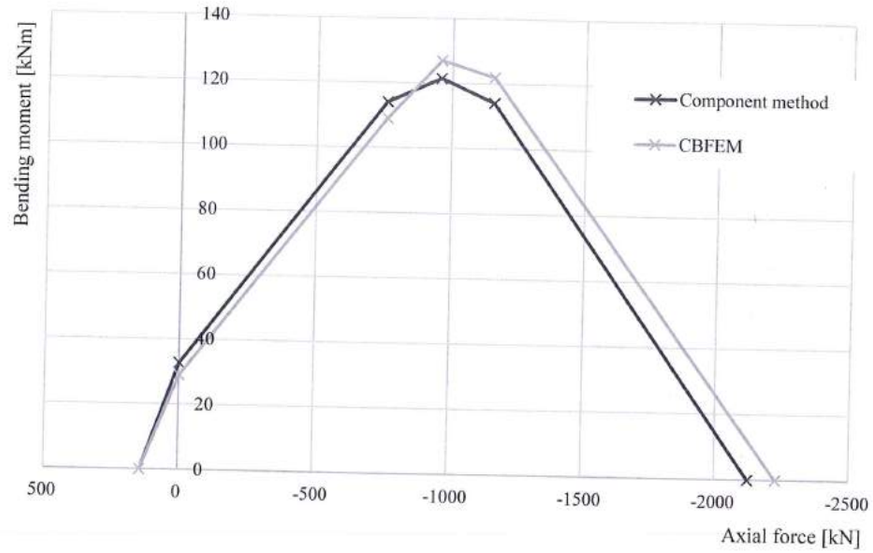

Fig. 8.2.4 Comparison of models on interaction diagram

Comparison of interaction diagram obtained by CBFEM to interaction diagram calculated according to CM is presented in Fig. 8.2.4 and Tab. 8.2.1.

Tab. 8.2.1 Comparison of results of interaction diagram for HEB 240 by analytic solution and by CBFEM

	Analytical solution		Results of CBFEM	
	Axial force [kN]	Bending resistance [kNm]	Axial force [kN]	Bending resistance [kNm]
Point -1	144	0	144	0
Point 0	0	33	0	29
Point 1	-760	114	-760	109
Point 2	-958	122	-958	127
Point 3	-1156	114	-1156	122
Point 4	-2125	0	-2229	0

8.2.3 Sensitivity study

Results of CBFEM were compared with the results of the component method. The comparison was made by bending moment resistance for the given level of normal force for each of the interaction diagram points.

In the sensitivity study, size of the column, dimensions of the base plate, grade of concrete, dimensions of concrete pad were changed. The selected column cross sections were HEB 200, HEB 300 and HEB 400. The base plate width and length was chosen 100 mm, 150 mm and 200 mm larger than the column section, the base plate thickness was 15 mm, 20 mm and 25 mm. The concrete pad was from

grade C16/20, C25/30 and C35/45. The concrete pad height was for all cases 900 mm and width and length was 200 mm, 300 mm and 400 mm larger than the dimensions of the base plate. The parameters are summarized in Tab. 8.2.2. Welds were the same around the whole column section with sufficient throat thickness in order not to be the critical component. One parameter was changed while the others were held constant at the middle value.

Tab. 8.2.2 Selected parameters

Column section	HEB 200	HEB 300	HEB 400
Base plate offset	100 mm	150 mm	200 mm
Base plate thickness	15 mm	20 mm	25 mm

In Fig. 8.2.5, results for changes in the column cross section are presented. In Fig. 8.2.6 and Fig. 8.2.7 the base plate offset and the base plate thickness are varied, respectively.

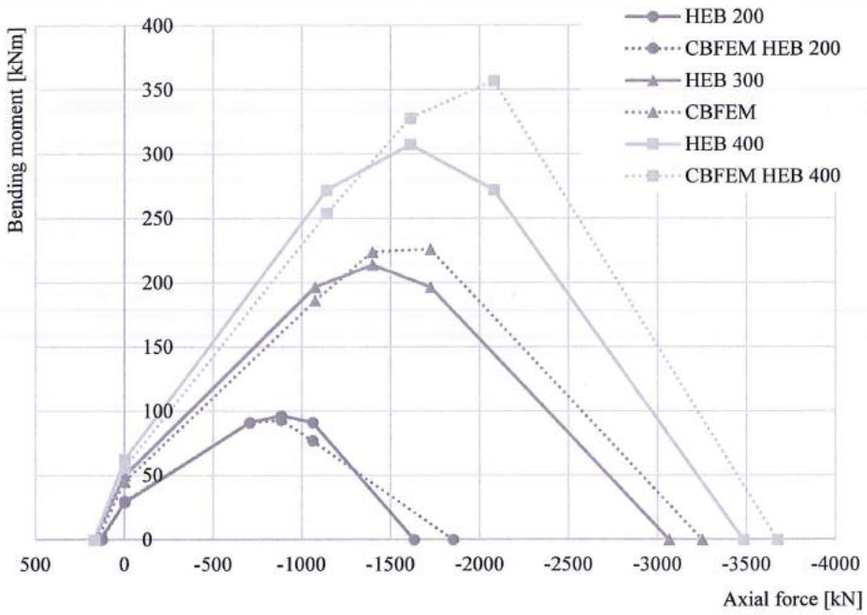

Fig. 8.2.5 Column section variation

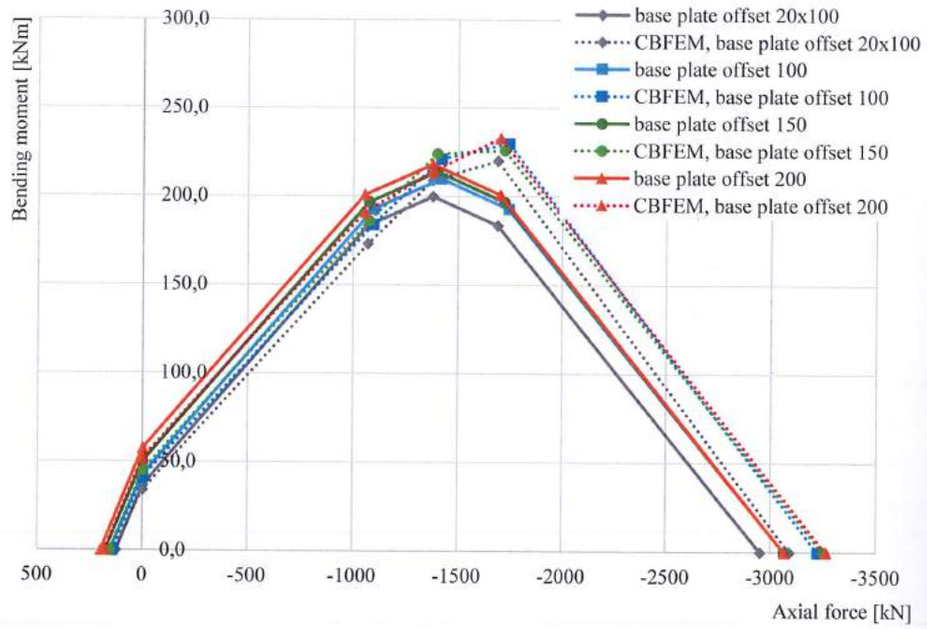

Fig. 8.2.6 Base plate offset variation

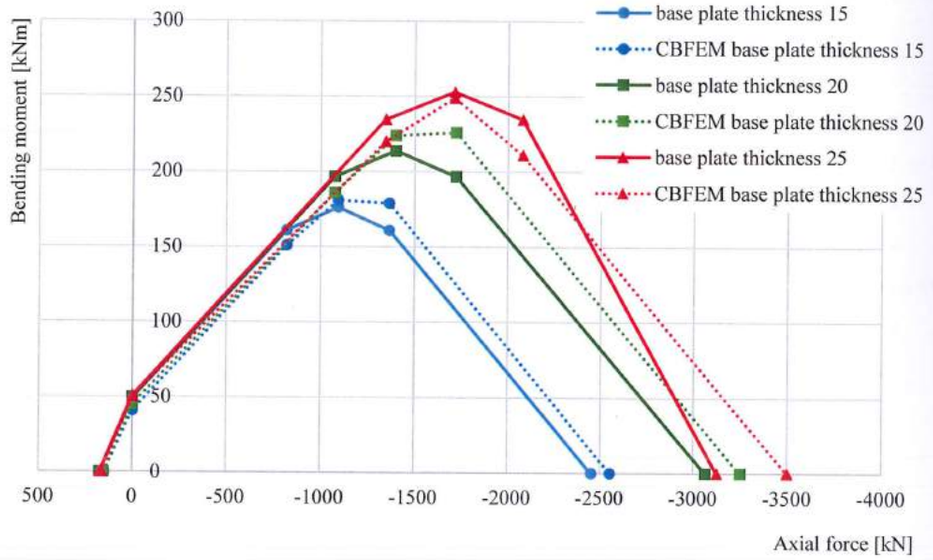

Fig. 8.2.7 Base plate thickness variation

(point 4 for base plate thickness 25 mm is reduced due to yielding of column

8.2.4 Benchmark case

Input

Column cross section

- HEB 240
- Steel S235

Base plate

- Thickness 20 mm
- Offsets top 100 mm, left 45 mm
- Steel S235

Anchor bolt

- M20 8.8
- Anchoring length 400 mm
- Offsets top layers 50 mm, left layers -50 mm
- Shear plane in thread
- Welds both 10 mm

Foundation block

- Concrete C20/25
- Offset 335 mm
- Depth 900 mm
- Shear force transfer friction
- Grout thickness 30 mm

Loading

- Axial force N = -1156 kN
- Bending moment M_y = 128 kNm

Output

- Anchor bolts 59,0 % (N_{Ed} = 30,6 kN ≤ N_{Rdc} = 51,8 kN - concrete core breakout)
- Concrete block 98,8 % (σ = 39,5 MPa ≤ f_{jd} = 40,0 MPa)

8.3 Open section column in bending to weak axis

8.3.1 Description

Open section steel column is anchored with anchor bolts to concrete pad; the column is loaded by moment around weaker axis and axial force. Compressed column is designed as maximal 3rd class to avoid stability problems. The study was performed for parameters: size of the column, dimensions of base plate and thickness of base plate. In the component method, components the column flange in bending and web in compression, the concrete including grout in compression and base plate in bending and welds are activated. All components are designed according to EN1993-1-8:2006, EN1992-1-1:2005 and ETAG 001 – Annex C.

8.3.2 Verification of resistance

An example of component method design is shown on the anchorage of the column steel cross section HEB 240. Concrete block has dimensions $a' = 1000$ mm , $b' = 1500$ mm , $h = 900$ mm and grade C20/25. Base plate is of $a = 330$ mm; $b = 440$ mm; $t = 20$ mm from steel S235. The anchor bolts are 4 x M20, A_s = 245 mm^2 with anchor head diameter a = 60 mm and steel grade 8.8. Grout has thickness 30 mm.

Results of analytical solution may be presented on interaction diagram with distinctive points. Point 1 represents loading in pure tension and point 4 represents the compression bearing resistance. Detailed description of points 0, 1, 2 and 3 is shown in Fig. 8.3.1, see (Wald, 1995) and (Wald et al., 2008).

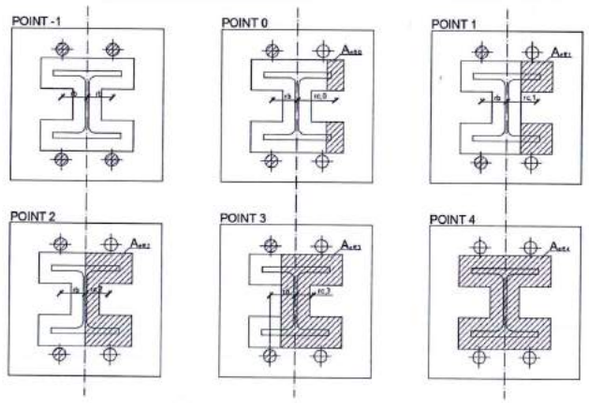

Fig. 8.3.1 Significant points on interaction diagram

Results by CBFEM are presented by the stress distribution for point 0 and 3, displayed in Fig. 8.3.2 and Fig. 8.3.3 and compared on interaction diagram in Fig. 8.3.4.

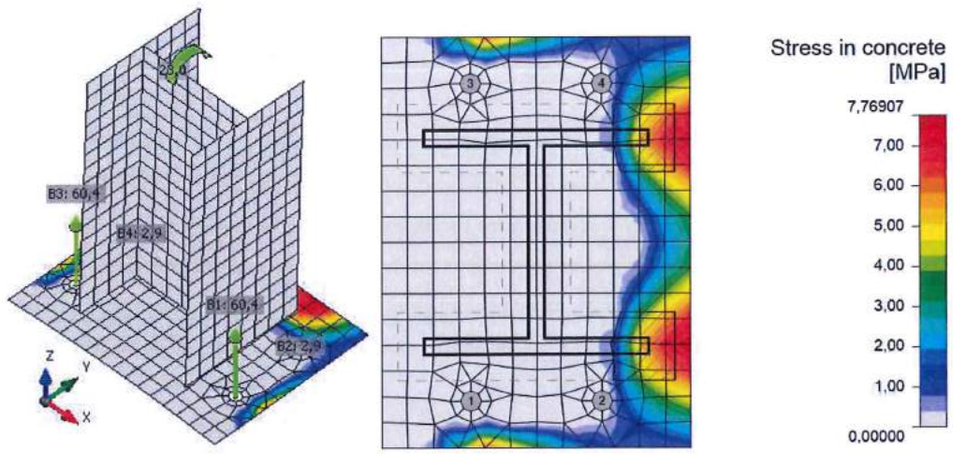

Fig 8.3.2 Stress distribution in concrete, effective area (hatched) and forces in anchors for point 0

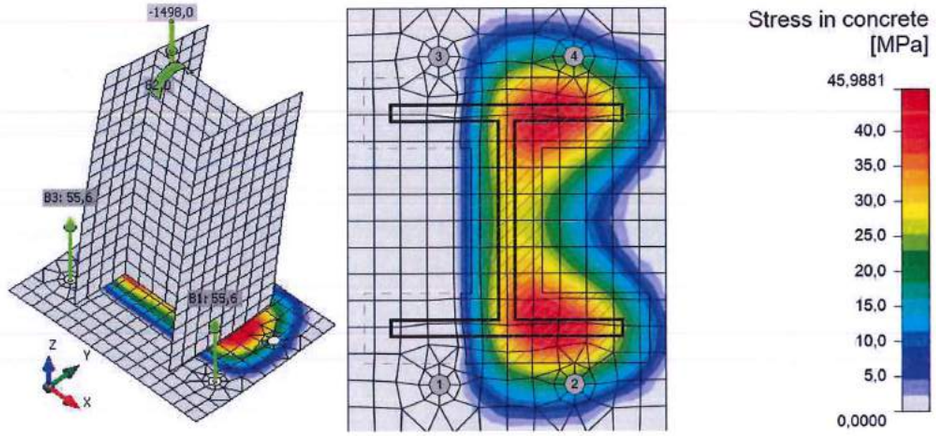

Fig. 8.3.3 Stress distribution in concrete, effective area (hatched) and forces in anchors for point 3

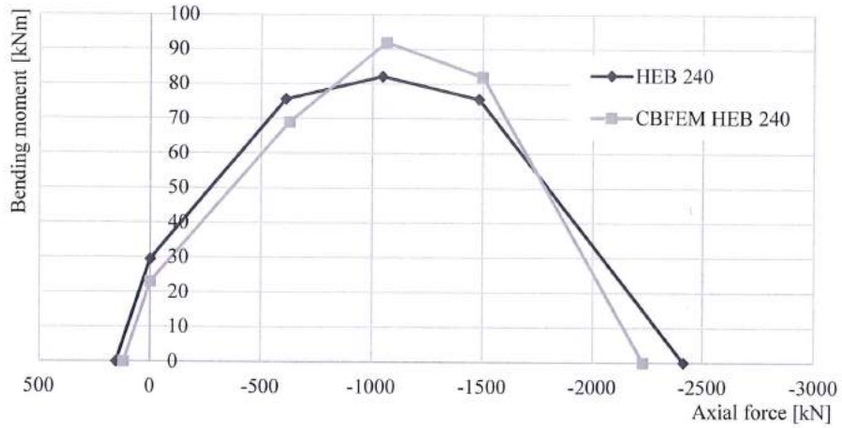

Fig. 8.3.4 Interaction diagram by CBFEM compared to CM

Tab. 8.3.1 Comparison of results of interaction diagram for HEB 240

	Analytic solution		Results of CBFEM	
	Axial force [kN]	Bending resistance [kNm]	Axial force [kN]	Bending resistance [kNm]
Point -1	153	0	119	0
Point 0	0,0	30	0	23
Point 1	-611	76	-627	69
Point 2	-1046	82	-1062	92
Point 3	-1482	76	-1498	82
Point 4	-2413	0	-2229	0

8.3.3 Sensitivity study

Results of CBFEM are compared with the results of the component method. The comparison is made for bending moment resistance for the given level of normal force for each of the interaction diagram points. The study is performed for size of the column, see Fig. 8.3.5, thickness of the base plate, see Fig. 8.3.6, and grade of concrete, see Fig. 8.3.7. The selected columns were HEB 200, HEB 300 and HEB 400. The base plate thickness is chosen to be 15 mm, 20 mm and 25 mm. The concrete pad is from grade C16/20, C25/30 and C35/45. The concrete pad height is for all cases 900 mm and width and length is 300 mm larger than the dimensions of the base plate. The parameters are summarized in Tab. 8.3.2 Welds are the same around the whole column section with sufficient throat thickness in order not to be the critical component. One parameter is changed while the others are held constant at the middle value.

Tab. 8.3.2 Selected parameters for sensitivity study

Column cross section	HEB 200	HEB 300	HEB 400
Base plate thickness	15 mm	20 mm	25 mm
Concrete grade	C16/20	C25/30	C35/45

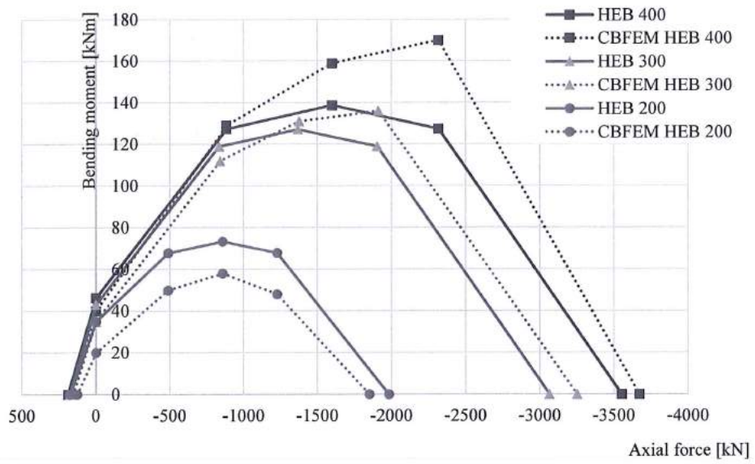

Fig. 8.3.5 Column section size variation

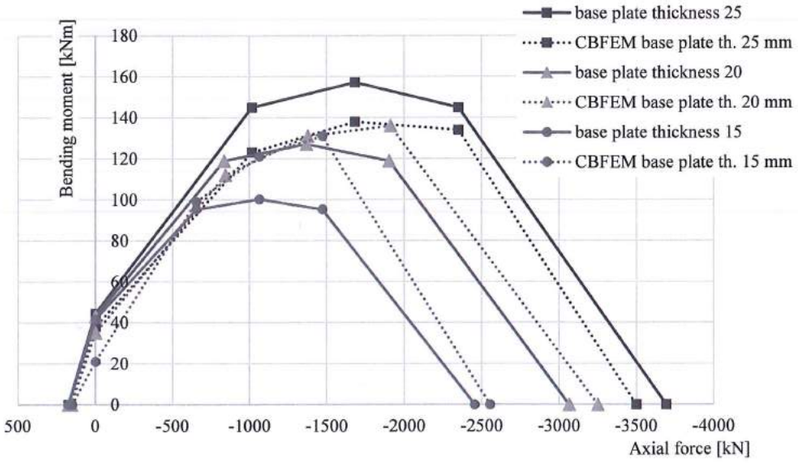

Fig. 8.3.6 Base plate thickness variation

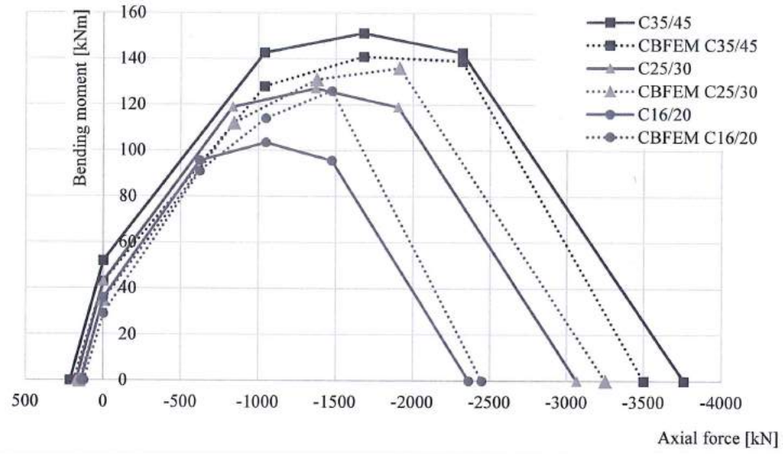

Fig. 8.3.7 Concrete grade variation

8.3.4 Benchmark case

Input

Column cross section

- HEB 240
- Steel S235

Base plate

- Thickness 20 mm
- Offsets top 100 mm, left 45 mm
- Welds both 10 mm
- Steel S235

Anchors

- Type M20 8.8
- Anchoring length 400 mm
- Offsets top layers 50 mm, left layers -50 mm
- Shear plane in thread

Foundation block

- Concrete C20/25
- Offset 335 mm
- Depth 900 mm
- Shear force transfer friction

- Grout thickness 30 mm

Loading

- Axial force N = -1498 kN,
- Bending moment M_z = 82 kNm

Output

- Anchor bolts 91,7 % (N_{Ed} = 55,6 kN ≤ N_{Rdc} = 60,7 kN - concrete core breakout)
- Concrete block 99,6 % (σ = 39,9 MPa ≤ f_{jd} = 40,0 MPa)
- Plates ε = 3,4 %
- Welds 78,4 % ($\sigma_{w,Ed}$ = 118,8 MPa ≤ $\sigma_{w,Rd}$ = 360 MPa)

8.4 Hollow section column

8.4.1 Description

The component based finite element method (CBFEM) for the hollow section column base verified to component method (CM) is described below. Compressed column is designed as class 3 cross section. The sensitivity study is prepared for the size of the column, dimension of base plate, grade of concrete, and dimension of concrete block. Four components are activated: the column flange and web in compression, the concrete in compression including grout, the anchor bolt in tension and welds. This study is mainly focused on two components: concrete in compression including grout and anchor bolt in tension.

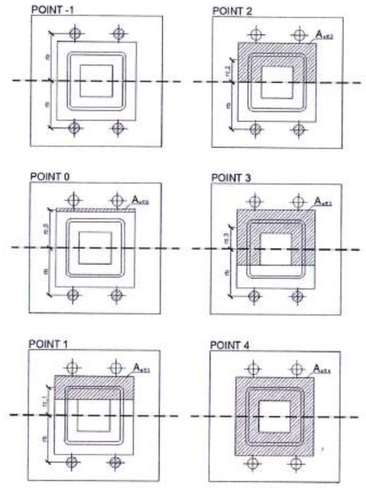

Fig. 8.4.1 Significant points of multilinear interaction diagram of square hollow section

8.4.2 Verification of resistance

In following example, the column from square hollow section SHS 150x16 is connected to concrete block with the area dimensions $a' = 750$ mm, $b' = 750$ mm and height $h = 800$ mm from concrete grade C20/25 by the base plate $a = 350$ mm; $b = 350$ mm; $t = 20$ mm from steel S420. Anchor bolts are designed 4 x M20, A_s = 245 mm^2 with head diameter a = 60 mm from steel 8.8 with offset at top 50 mm and left -20 mm. Grout has the thickness of 30 mm.

Results of analytical solution are presented as interaction diagram with distinctive points. Detailed description of points -1, 0, 1, 2 and 3 is shown in Fig. 8.4.1, see (Wald, 1995) and (Wald et al., 2008), where point -1 represents pure tensile force, point 0 pure bending moment, points 1 to 3 combined compressive force and bending moment, and point 4 pure compressive force.

In CBFEM, the prying forces occur in case of loading in pure tension loading; while in CM, no prying forces are developed by limiting the resistance to 1-2 failure mode only, see (Wald et al, 2008). Due to allowing the prying forces, the difference in resistance is about 10 %. The numerical model of column base is shown in Fig. 8.4.2. Results by CBFEM are presented by the stress distribution for point 0 and 3, displayed in Fig. 8.4.3 and Fig. 8.4.4 and compared on interaction diagram in Fig. 8.4.5.

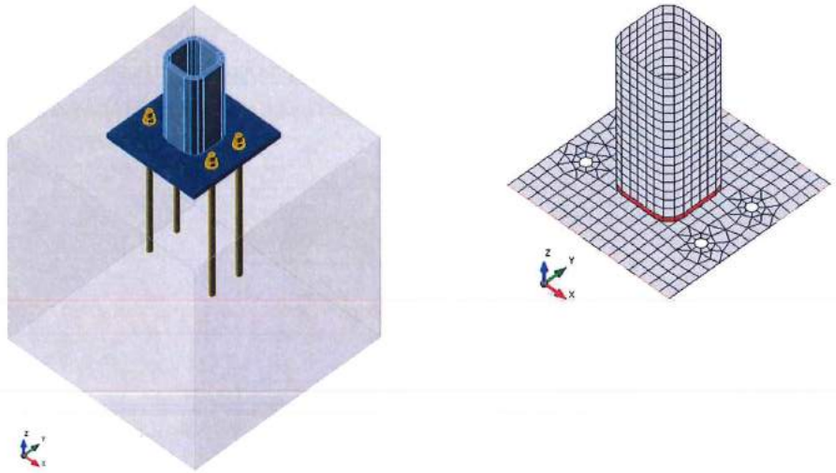

Fig.8.4.2 The column base for column SHS 150x16 and selected meshed of base plate

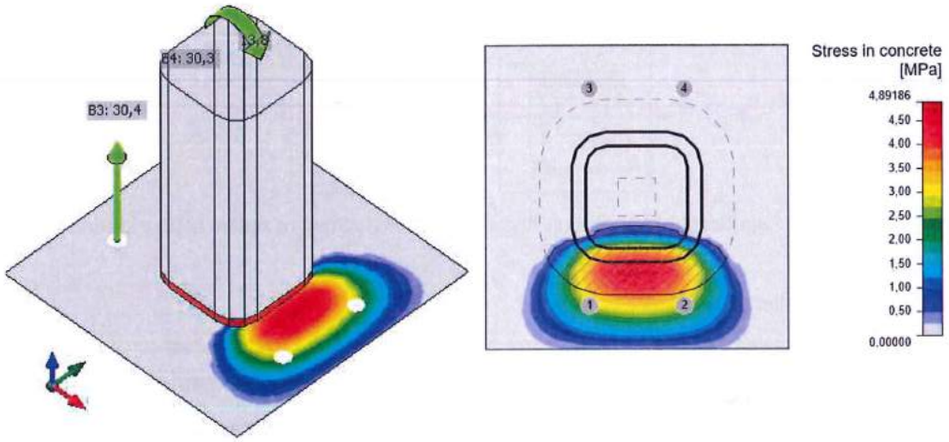

Fig. 8.4.3 CBFEM results for point 0, e.g. pure bending moment

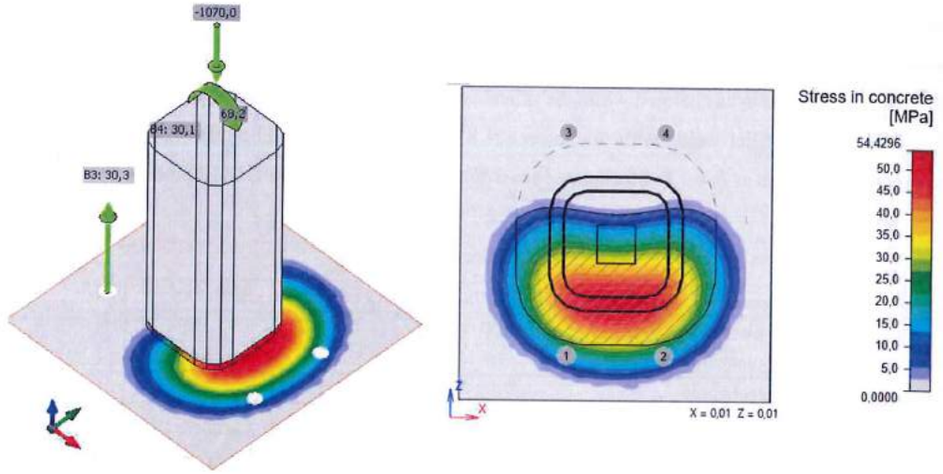

Fig. 8.4.4 CBFEM results for point 3, e.g. compressive force and bending moment

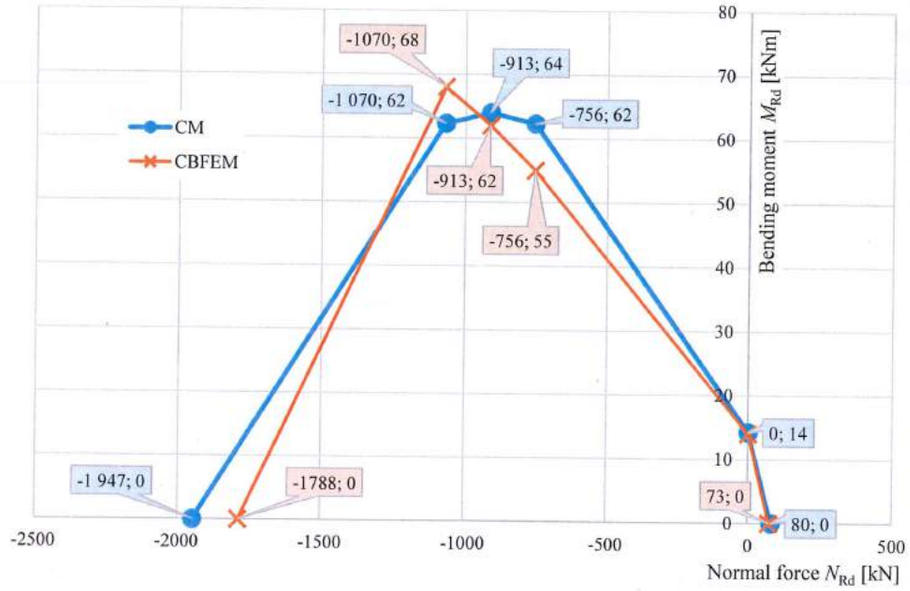

Fig. 8.4.5 Comparison of results of prediction of resistance by CBFEM and CM on interaction diagram for column base of column cross section SHS 150x16

8.4.3 Sensitivity study

The sensitivity study is prepared for the column cross section size, dimensions of the base plate, concrete grade, and dimensions of the concrete block. The columns are selected SHS 150x16, SHS 160x12.5 and SHS 200x16. The base plate is designed with area dimensions 100 mm, 150 mm and 200 mm larger than the column cross section. The base plate thickness is 10 mm, 20 mm and 30 mm. The foundation

block is from concrete grade C20/25, C25/30, C30/37 and C35/45 with height for all cases 800 mm and with area dimensions 100 mm, 200 mm, 300 mm and 500 mm larger than the dimensions of the base plate. One parameter was changed while the others were held constant. The parameters are summarized in Tab. 8.4.1. The fillet welds with thickness a = 8 mm were selected. The joint coefficient for high quality grout is taken as $\beta_j = 1{,}0$. Steel plates are from S420 with anchor bolts M20 grade 8.8 in all cases.

Table 8.4.1 Selected parameters

Column cross section	SHS 150x16	SHS 16x12,5	SHS 200x16
Base plate offset, mm	100	150	200
Base plate thickness, mm	10	20	30
Concrete grade	C20/25	C30/37	C35/45
Concrete pad offset, mm	100	300	500

For sensitivity study of column cross section, the concrete grade C20/25, the base plate thickness 20 mm, the base plate offset 100 mm and the concrete block offset 200 mm were used for varying parameter of column section. The comparison of CBFEM (marked IC) to analytical model by CM (marked An) is shown on the interaction diagrams in Fig. 8.4.6.

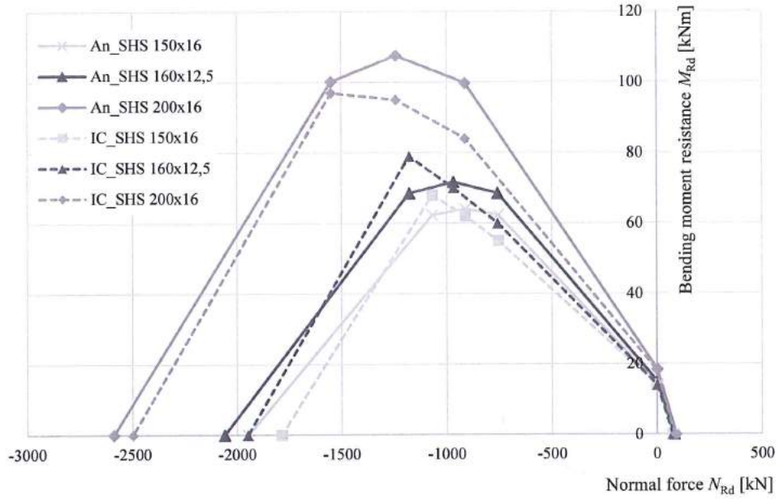

Fig. 8.4.6 Comparison of results of CBFEM (marked IC) to CM (marked An) for the different column cross sections

For sensitivity study of base plate offset, the column cross section SHS 200x16, concrete grade C25/30, base plate thickness 20 mm and concrete block offset 200 mm were selected. The comparison of interaction diagrams is in Fig. 8.4.7. The biggest difference is in the resistance in pure tension of large

base plate where significant prying forces were present in CBFEM analyses, which are limited by analytical design.

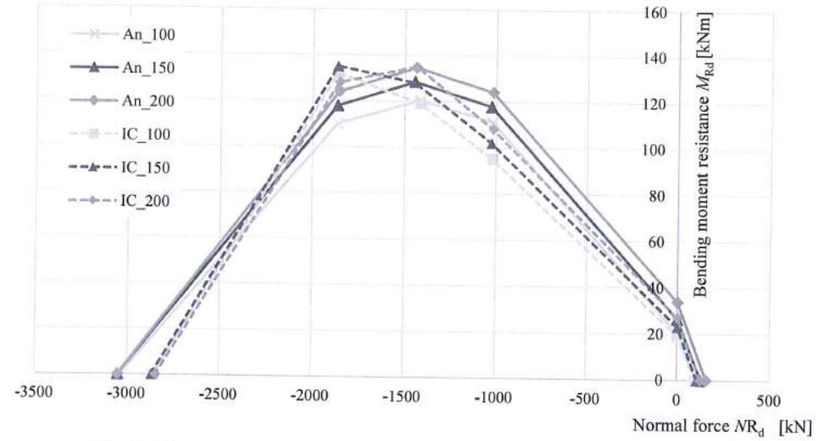

Fig. 8.4.7 Comparison of results of CBFEM (marked IC) to CM (marked An) for the different base plate offsets

For sensitivity study of base plate thickness, the column cross section SHS 200x16, concrete grade C25/30, base plate offset 100 mm and concrete block offset 200 mm were selected. 10 mm, 20 mm and 30 mm base plate thicknesses were used in this study. The comparison of interaction diagrams is in Fig. 8.4.8. The biggest difference is in the resistance in pure tension of thin base plate where significant prying forces were present in CBFEM analyses, which are limited in analytical design by CM.

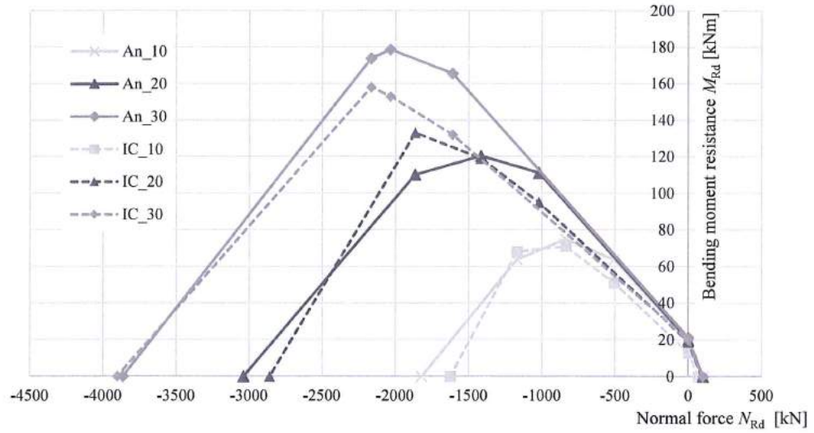

Fig. 8.4.8 Comparison of results of CBFEM (marked IC) to CM (marked An) for the different base plate thickness

For sensitivity study of concrete grade, the column cross section SHS 150x16, base plate thickness 20 mm, base plate offset 100 mm and concrete block offset 200 mm were selected. Concrete grades C20/25, C30/37 and C35/45 were used in this study. The comparison of interaction diagrams is in Fig. 8.4.9.

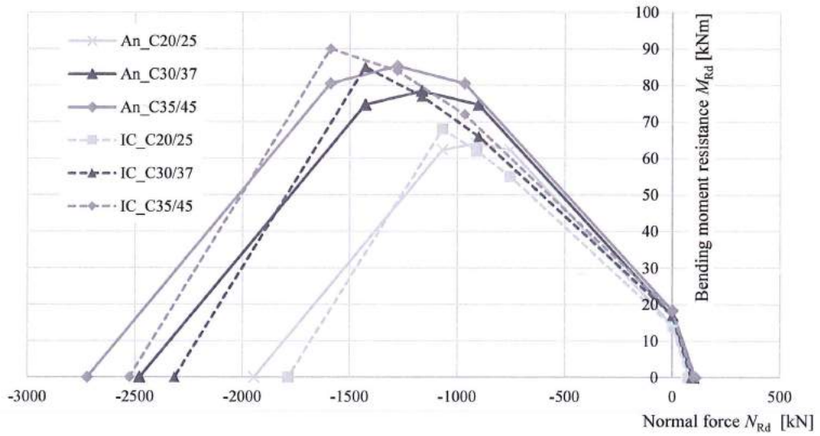

Fig. 8.4.9 Comparison of results of CBFEM (marked IC) to CM (marked An) for the different concrete grades

For sensitivity study of concrete block offset, the column cross section SHS 160x12.5, base plate thickness 20 mm, base plate offset 100 mm and concrete grade 25/30 were selected. 100 mm, 300 mm and 500 mm concrete block offsets were used in this study. The comparison of interaction diagrams is in Fig. 8.4.10.

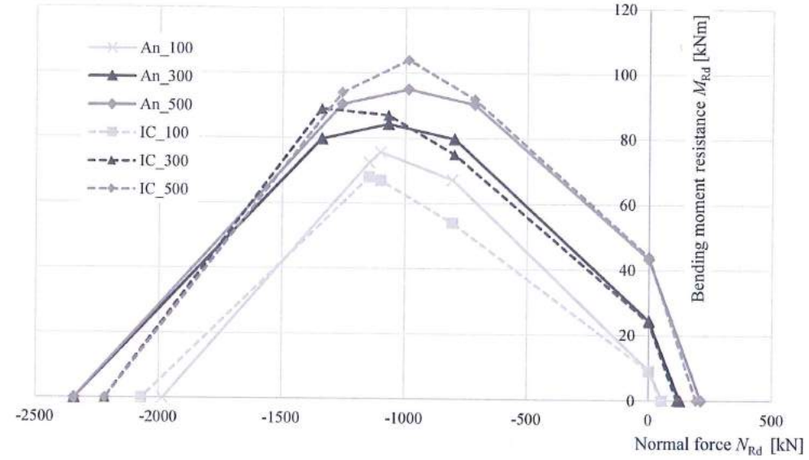

Fig. 8.4.10 Comparison of results of CBFEM (marked IC) to CM (marked An) for the different concrete block offsets

The differences in prediction of resistance of column base by CBFEM and CN are mainly in accepting the prying forces in CBFEM and avoiding it by CM according to EN1993-1-8:2006.

Tab. 8.4.2 Interaction diagram comparison of CBFEM and CM

Difference CBFEM/CM	Point -1	Point 0	Point 1	Point 2	Point 3	Point 4
Maximum %	99,3	101,6	101,8	109,5	120,9	104,4
Minimum %	70,2	69,4	79,8	85,6	90,9	89,3

8.4.4 Benchmark case

Input

Column cross section

- SHS 150/16
- Steel S460

Base plate

- Thickness 20 mm
- Offsets at top 100 mm, on left 100 mm

- Welds 8 mm
- Steel S460

Anchors

- M20 8.8.
- Anchoring length 400 mm
- Offsets top layers 50 mm, left layers -20 mm
- Shear plane in thread

Foundation block

- Concrete C20/25
- Offset 200 mm
- Depth 800 mm
- Shear force transfer friction
- Grout thickness 30 mm

Loading

- Axial force N = -913 kN
- Bending moment M_y = 62,1 kNm

Output

- Plates $\varepsilon = 0{,}3\ \%$
- Anchor bolts 99,7 % ($N_{Ed} = 30{,}3\ \text{kN} \leq N_{Rd,c} = 30{,}4\ \text{kN}$ (critical component concrete cone breakout)
- Welds 57,7 % ($\sigma_{Ed} = 239.9\ \text{MPa} \leq \sigma_{Rd} = 416\ \text{MPa}$)
- Concrete block 83,0 % ($\sigma = 33{,}4\ \text{MPa} \leq f_{jd} = 40\ \text{MPa}$)
- Secant rotational stiffness $S_{js} = 7{,}4 \frac{\text{MNm}}{\text{rad}}$

9 COLUMN WEB PANEL IN SHEAR

9.1 Welded portal frame eaves moment connection

9.1.1 Description

In this chapter the component based finite element method (CBFEM) for a welded portal frame eaves moment connection on component method (CM) is verified. An open section beam is welded to an open section column. The column is stiffened with two horizontal stiffeners opposite to beam flanges. Compressed plates, e.g. horizontal stiffeners of column, column web panel in shear, compressed beam flange, are limited to 3rd class to avoid stability problems. The rafter is loaded by shear force and bending moment.

9.1.2 Analytical model

Five components are examined in the study, namely the web panel in shear, the column web in transverse compression, the column web in transverse tension, the column flange in bending and the beam flange in compression. All components are designed according to EN1993-1-8:2006. Fillet welds are designed not to be the weakest component in the joint. The verification study of a fillet weld in a stiffened beam-to-column joint is in chapter 4.4.

Web panel in shear

The thickness of the column web is limited by slenderness to avoid stability problem, see EN1993-1-8:2006 cl 6.2.6.1(1). A class 4 column web panel in shear is studied in chapter 6.2. Two contributions to the load capacity are considered: resistance of the column panel in shear and the contribution from the frame mechanism of the column flanges and horizontal stiffeners, see EN1993-1-8:2006 cl. 6.2.6.1 (6.7 and 6.8).

Column web in transverse compression

Effect of the interaction of the shear load is considered see EN1993-1-8:2006 cl. 6.2.6.2, Tab. 6.3. Influence of longitudinal stress in the column panel is considered see EN1993-1-8:2006 cl. 6.2.6.2(2). The horizontal stiffeners are included in the load capacity of this component.

Column web in transverse tension

Effect of the interaction of the shear load is considered see EN1993-1-8:2006 cl. 6.2.6.2, Tab. 6.3. The horizontal stiffeners are included in the load capacity of this component.

Column flange in bending

Horizontal stiffeners brace column flange, this component is not considered.

Beam flange in compression

The horizontal beam is designed to be class 3 cross-section or better to avoid stability problem.

Overview of the considered examples and the material are given in the Tab. 9.1.1. A geometry of the joint with dimensions is shown in Fig. 9.1.1. The considered parameters in the study are beam cross-section, column cross-section and thickness of the column web panel.

Tab. 9.1.1 Examples overview

Example	Material					Beam	Column	Column stiffener	
	f_y	f_u	E	γ_{M0}	γ_{M2}	Section	Section	b_s	t_s
	[MPa]	[MPa]	[GPa]	[-]	[-]			[mm]	[mm]
IPE140	235	360	210	1	1,25	IPE140	HEB260	73	10
IPE160	235	360	210	1	1,25	IPE160	HEB260	82	10
IPE180	235	360	210	1	1,25	IPE180	HEB260	91	10
IPE200	235	360	210	1	1,25	IPE200	HEB260	100	10
IPE220	235	360	210	1	1,25	IPE220	HEB260	110	10
IPE240	235	360	210	1	1,25	IPE240	HEB260	120	10
IPE270	235	360	210	1	1,25	IPE270	HEB260	135	10
IPE300	235	360	210	1	1,25	IPE300	HEB260	150	10
IPE330	235	360	210	1	1,25	IPE330	HEB260	160	10
IPE360	235	360	210	1	1,25	IPE360	HEB260	170	10
IPE400	235	360	210	1	1,25	IPE400	HEB260	180	10
IPE450	235	360	210	1	1,25	IPE450	HEB260	190	10
IPE500	235	360	210	1	1,25	IPE500	HEB260	200	10

Example	Material					Beam	Column	Column stiffener	
	f_y	f_u	E	γ_{M0}	γ_{M2}	Section	Section	b_s	t_s
	[MPa]	[MPa]	[GPa]	[-]	[-]			[mm]	[mm]
HEB160	235	360	210	1	1,25	IPE330	HEB160	160	10
HEB180	235	360	210	1	1,25	IPE330	HEB180	160	10
HEB200	235	360	210	1	1,25	IPE330	HEB200	160	10
HEB220	235	360	210	1	1,25	IPE330	HEB220	160	10
HEB240	235	360	210	1	1,25	IPE330	HEB240	160	10
HEB260	235	360	210	1	1,25	IPE330	HEB260	160	10
HEB280	235	360	210	1	1,25	IPE330	HEB280	160	10
HEB300	235	360	210	1	1,25	IPE330	HEB300	160	10
HEB320	235	360	210	1	1,25	IPE330	HEB320	160	10
HEB340	235	360	210	1	1,25	IPE330	HEB340	160	10
HEB360	235	360	210	1	1,25	IPE330	HEB360	160	10
HEB400	235	360	210	1	1,25	IPE330	HEB400	160	10
HEB450	235	360	210	1	1,25	IPE330	HEB450	160	10
HEB500	235	360	210	1	1,25	IPE330	HEB500	160	10

Example	Material					Beam	Column	Column stiffener		
	f_y	f_u	E	γ_{M0}	γ_{M2}	Section	Section	t_w	b_s	t_s
	[MPa]	[MPa]	[GPa]	[-]	[-]			[mm]	[mm]	[mm]
tw4	235	360	210	1	1,25	IPE330	HEA320	4	160	10
tw5	235	360	210	1	1,25	IPE330	HEA320	5	160	10
tw6	235	360	210	1	1,25	IPE330	HEA320	6	160	10
tw7	235	360	210	1	1,25	IPE330	HEA320	7	160	10
tw8	235	360	210	1	1,25	IPE330	HEA320	8	160	10
tw9	235	360	210	1	1,25	IPE330	HEA320	9	160	10
tw10	235	360	210	1	1,25	IPE330	HEA320	10	160	10
tw11	235	360	210	1	1,25	IPE330	HEA320	11	160	10
tw12	235	360	210	1	1,25	IPE330	HEA320	12	160	10
tw13	235	360	210	1	1,25	IPE330	HEA320	13	160	10
tw14	235	360	210	1	1,25	IPE330	HEA320	14	160	10
tw15	235	360	210	1	1,25	IPE330	HEA320	15	160	10
tw16	235	360	210	1	1,25	IPE330	HEA320	16	160	10

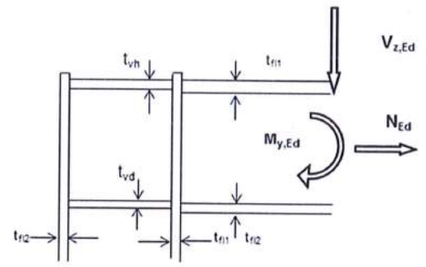

Fig. 9.1.1 Joint's geometry and dimensions

9.1.3 Numerical model

Nonlinear elastic-plastic material status is investigated in each layer of integration point. Assessment is based on the maximum strain given according to EN1993-1-5:2005 by value of 5%.

9.1.4 Global behaviour

Comparison of the global behaviour of a portal frame moment connection described by moment-rotation diagram is presented. Main characteristics of the moment-rotation diagram are initial stiffness, elastic resistance and design resistance. An open section beam IPE 330 is welded to a column HEB 260 in the example. A portal frame moment connection with horizontal stiffeners in column is considered according to component method as a rigid joint with $S_{j,ini} = \infty$. Therefore a joint without horizontal stiffeners in column is analysed. The moment-rotation diagram is shown in Fig. 9.1.2 and the results are summarised in Tab. 9.1.2. The results show very good agreement in initial stiffness and joint's global behaviour.

Tab. 9.1.2 Rotational stiffness of a portal frame moment connection in CBFEM and CM

		CM	CBFEM	CM/CBFEM
Initial stiffness $S_{j,ini}$	[kNm/rad]	48423,7	66889,6	0,72
Elastic resistance *2/3* $M_{j,Rd}$	[kNm]	93,3	90,0	1,04
Design resistance $M_{j,Rd}$	[kNm]	140,0	149,0	0,94

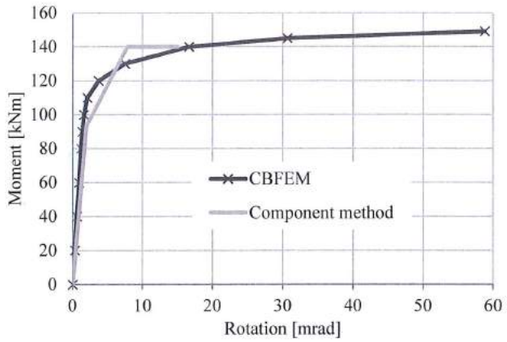

Fig. 9.1.2 Moment-rotation diagram for a joint without column stiffeners

9.1.5 Verification of resistance

The results calculated by CBFEM are compared with CM. The comparison is focused on the design resistance and the critical component. The study is performed for three different parameters: beam cross-section, column cross-section and thickness of the column web panel.

An open section column HEB260 is used in an example where the parameter is beam cross-section. The column is stiffened with two horizontal column stiffeners of thickness 10 mm opposite to the beam flanges. The stiffeners width is corresponding to the width of beam flange. The beam IPE sections are selected from IPE140 to IPE500. The results are shown in Tab. 9.1.3. The influence of beam cross-section on the design resistance of a welded portal frame moment connection is shown in Fig. 9.1.3.

Tab. 9.1.3 Design resistances and critical components in CBFEM and CM

Parameter	Component method		CBFEM	
	Resistance [kN/kNm]	Critical component	Resistance [kN/kNm]	Critical component
IPE140	24	Beam flange in compression	27	Beam flange in compression
IPE160	33	Beam flange in compression	34	Beam flange in compression
IPE180	44	Beam flange in compression	48	Beam flange in compression
IPE200	59	Beam flange in compression	67	Beam flange in compression
IPE220	77	Beam flange in compression	80	Beam flange in compression

IPE240	98	Beam flange in compression	103	Beam flange in compression
IPE270	113	Beam flange in compression	125	Beam flange in compression
IPE300	142	Web panel in shear	142	Beam flange in compression
IPE330	155	Web panel in shear	154	Beam flange in compression
IPE360	168	Web panel in shear	167	Web panel in shear
IPE400	186	Web panel in shear	183	Web panel in shear
IPE450	209	Web panel in shear	202	Web panel in shear
IPE500	231	Web panel in shear	223	Web panel in shear

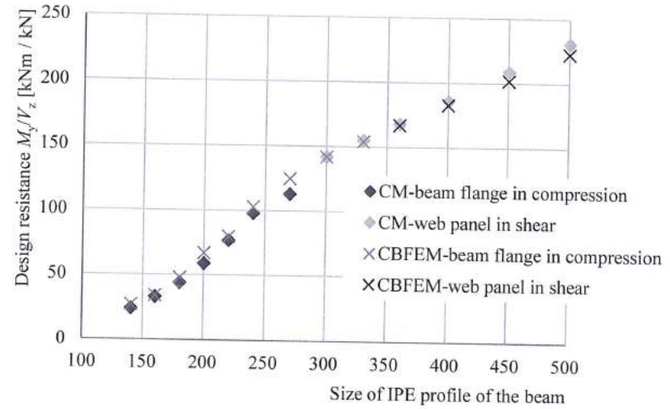

Fig. 9.1.3 A sensitivity study of beam size in a portal frame moment connection

An open section beam IPE330 is used in an example where the parameter is column cross-section. The column is stiffened with two horizontal column stiffeners of thickness 10 mm opposite to the beam flanges. The stiffeners width is 160 mm. The column sections are selected from HEB160 to HEB500. The results are shown in Tab. 9.1.4. The influence of column cross-section on the design resistance of a welded portal frame moment connection is shown in Fig. 9.1.4.

Tab. 9.1.4 Design resistances and critical components of a moment connection in CBFEM and CM

Parameter	Component method		CBFEM	
	Resistance [kN/kNm]	Critical component	Resistance [kN/kNm]	Critical component
HEB160	73	Web panel in shear	70	Web panel in shear
HEB180	84	Web panel in shear	88	Web panel in shear
HEB200	103	Web panel in shear	101	Web panel in shear
HEB220	116	Web panel in shear	124	Web panel in shear
HEB240	139	Web panel in shear	139	Web panel in shear
HEB260	155	Web panel in shear	154	Web panel in shear
HEB280	170	Web panel in shear	179	Beam flange in compression
HEB300	198	Web panel in shear	196	Beam flange in compression

HEB320	216	Web panel in shear	226	Beam flange in compression
HEB340	226	Beam flange in compression	240	Beam flange in compression
HEB360	228	Beam flange in compression	245	Beam flange in compression
HEB400	234	Beam flange in compression	251	Beam flange in compression
HEB450	241	Beam flange in compression	258	Beam flange in compression
HEB500	248	Beam flange in compression	266	Beam flange in compression

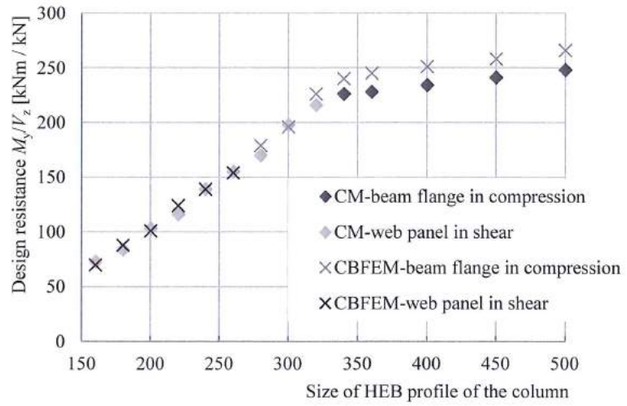

Fig. 9.1.4 A sensitivity study of column size in a portal frame moment connection

Third example presents a portal frame moment connection made out of an open section beam IPE330 and column HEA320. The parameter is the thickness of the column web. The column is stiffened with two horizontal column stiffeners of thickness 10 mm and width 160 mm. The column web thickness is chosen from 4 to 16 mm. The results are summarised in Tab. 9.1.5. The influence of column web thickness on the design resistance of a welded portal frame moment connection is shown in Fig. 9.1.5.

Tab. 9.1.5 Design resistances and critical components of a moment connection in CBFEM and CM

Parameter	Component method		CBFEM	
	Resistance [kN/kNm]	Critical component	Resistance [kN/kNm]	Resistance [kN/kNm]
tw4	82	Web panel in shear	99	Web panel in shear
tw5	94	Web panel in shear	115	Web panel in shear
tw6	106	Web panel in shear	131	Web panel in shear
tw7	118	Web panel in shear	147	Web panel in shear
tw8	130	Web panel in shear	162	Web panel in shear
tw9	142	Web panel in shear	177	Web panel in shear
tw10	155	Web panel in shear	190	Beam flange in compression
tw11	167	Web panel in shear	203	Beam flange in compression
tw12	179	Web panel in shear	216	Beam flange in compression

tw13	191	Web panel in shear	227	Beam flange in compression
tw14	203	Web panel in shear	236	Beam flange in compression
tw15	215	Beam flange in compression	240	Beam flange in compression
tw16	222	Beam flange in compression	241	Beam flange in compression

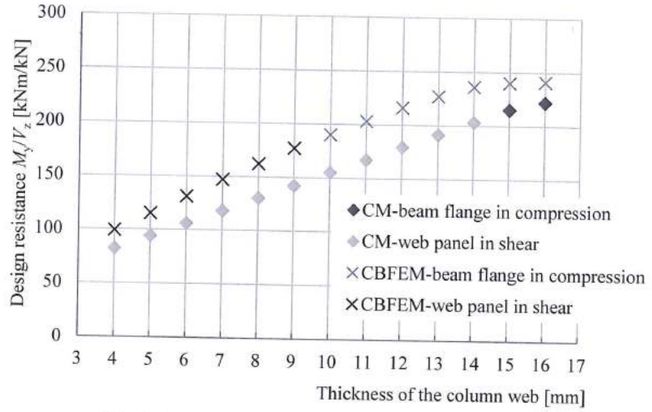

Fig. 9.1.5 A sensitivity study of column web thickness

To illustrate the accuracy of the CBFEM model, results of the parametric studies are summarized in a diagram comparing resistance of CBFEM and component method, see Fig. 9.1.6. The results show that the difference of the two calculation methods is less than 5%, which is a generally acceptable value. The study with parameter column web thickness gives higher resistance for CBFEM model compared to component method. This difference is caused by considering welded cross-sections. The transfer of shear load is in component method considered only in web and contribution of the flanges is neglected.

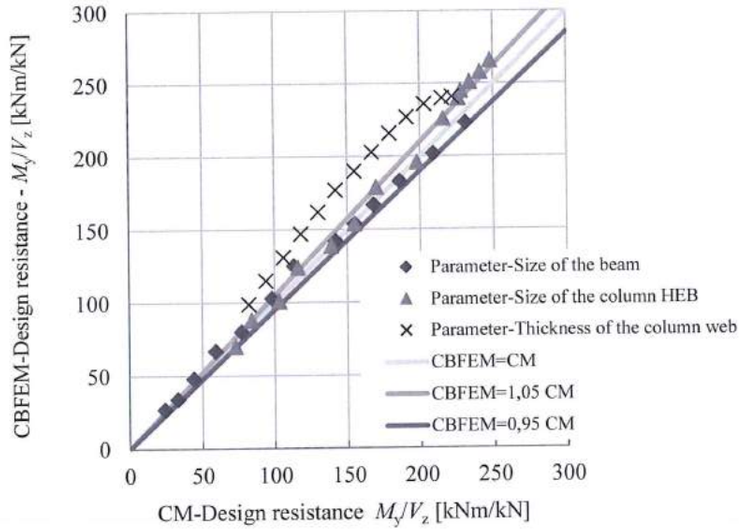

Fig. 9.1.6 Verification of CBFEM to CM

9.1.6 Benchmark example

Inputs

Column

- Steel S235
- HEB260

Beam

- Steel S235
- IPE330

Column stiffeners

- Thickness t_s = 10 mm
- Width b_s = 160 mm
- Opposite to beam flanges

Weld

- Throat thickness a_w = 5 mm
- Fillet weld

Outputs

- Design resistance in shear V_{Rd} = 154 kN
- Design resistance in bending M_{Rd} = 154 kNm

9.2 Bolted portal frame eaves moment connection

9.2.1. Description

The objective of this study is verification of bolted portal frame eaves connection as shown in Fig. 9.2.1. Rafter is bolted using end plate on the column flange. The column is stiffened with two horizontal stiffeners in levels of the beam flanges. Compressed plates, e.g. horizontal stiffeners of column, web panel in shear or compression and compressed beam flange, are designed as cross section class 3. Horizontal beam is considered of length 6 m loaded by continuous load over the entire length.

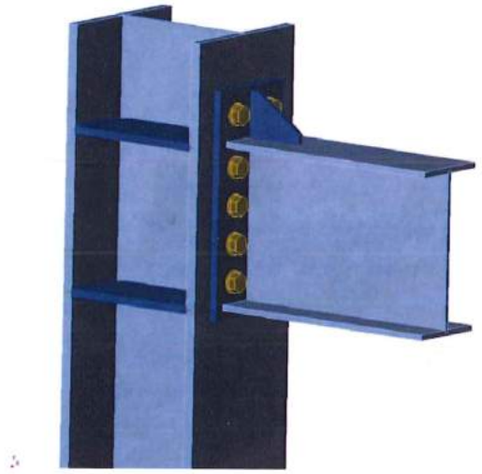

Fig. 9.2.1 Bolted portal frame eaves connection

9.2.2. Analytical model

Eight components are examined: fillet weld, web panel in shear, column web in transverse compression, column web in transverse tension, beam flange in compression and tension, column flange in bending, end plate in bending and bolts. All components are designed according to EN 1993-1-8:2006. Design loads of component depend on the position. The web panel in shear is loaded by design loads on the vertical axis of the column. Other components are loaded by reduced design loads in column flange to which horizontal beam is connected.

Fillet weld

The weld is closed around a cross-section of the beam. The thickness of the weld on the flanges can differ from the thickness of the weld on the web. Verticals hear force is transferred only by welds on the web and plastic stress distribution is considered. Bending moment is transferred by whole weld shape and elastic stress distribution is considered. Effective weld width depending on the horizontal stiffness of the column is considered (because of bending of the column flange). Design of the weld is done

according to EN1993-1-8:2006 cl. 4.5.3.2(6). The assessment is carried out in two major points: on the upper or lower edge of the flange (maximum bending stress) and in the crossing of the flange and the web (combination of shear force and bending moment stresses).

Web panel in shear

The thickness of the column web is designed to be maximally third class, see EN1993-1-8:2006 cl. 6.2.6.1(1). Two contributions to the load capacity yare considered: resistance of the column wall in shear and the contribution from the frame behaviour of the column flanges and horizontal stiffeners see EN1993-1-8:2006 cl. 6.2.6.1 (6.7 and 6.8).

Column web in transverse compression or tension

Effect of the interaction of the shear load is considered see EN1993-1-8:2006 cl. 6.2.6.2 and Tab. 6.3. Influence of longitudinal stress in the wall of the column is considered see EN1993-1-8:2006 cl. 6.2.6.2(2). Horizontal stiffeners prevent from stability problems. The horizontal stiffeners are included in the load capacity of this component with the effective area.

Beam flange in compression

The horizontal beam is designed to be maximally third class.

Column flange or end plate in bending

Effective lengths for circular and noncircular failures are considered according to EN 1993-1-8:2006 cl. 6.2.6. Three modes of collapse according to EN 1993-1-8:2006 cl. 6.2.4.1 are considered.

Bolts

Bolts are designed according to EN1993-1-8:2006 cl. 3.6.1. Design resistance considers punching shear resistance and rupture of the bolt.

9.2.3. Numerical design model

T-stub is modelled by 4-nodes shell elements as described in Chapter 3 and summarised further. Every node has 6 degrees of freedom. Deformations of the element consist of membrane and flexural contributions. Nonlinear elastic-plastic material status is investigated in each layer of integration point. Assessment is based on the maximum strain given according to EN1993-1-5:2005 by value of 5 %. Bolts are divided into three sub-components. The first is the bolt shank, which is modelled as a nonlinear spring and caries tension only. The second sub-component transmits tensile force into the flanges. The third sub-component solves shear transmission.

9.2.4. Global behaviour

Comparison of the global behaviour of the joint described by moment-rotation diagrams for both design procedures mentioned above was done. Attention was focused on the main characteristics of the moment-rotation diagram: initial stiffness, design resistance and deformation capacity. Beam IPE330 is connected to column HEB300 using extended end plate with 5 rows of the bolts M24 8.8. Results of

both design procedures are shown in the graph Fig. 9.2.2 and in the Tab. 9.2.1. CM generally gives higher initial stiffness compared to CBFEM. CBFEM gives slightly higher design resistance compared to CM in all cases as shown in Chapter 9.2.5. The difference is up to 10%. Deformation capacity is compared also. Deformation capacity was calculated according to (Beg et al, 2004) because EC3 provides limited background for deformation capacity of endplate joints.

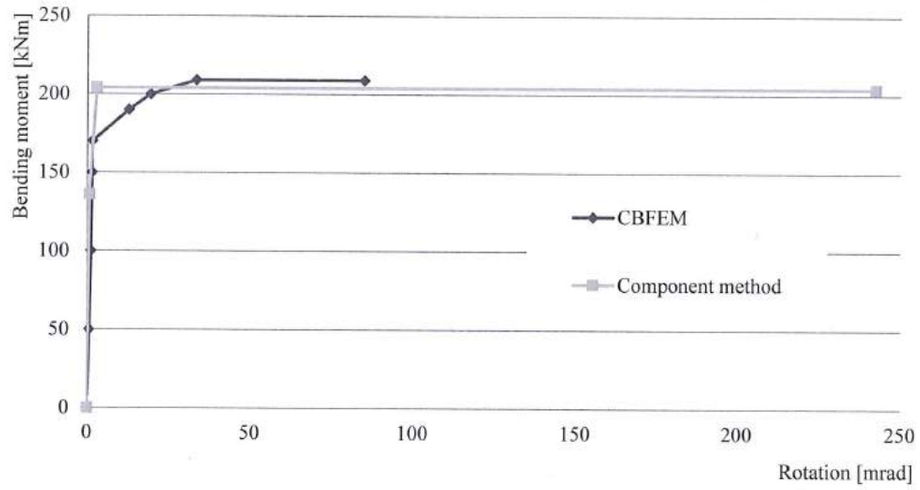

Fig. 9.2.2 Moment-rotation diagram

Tab. 9.2.1 Global behaviour overview

		CM	CBFEM	CM/CBFEM
Initial stiffness	[kNm/rad]	221394	138700	1,60
Design resistance	[kNm]	204	209	0,98
Deformation capacity	[mrad]	242	85	2,85

9.2.5. Verification of resistance

Design resistance calculated by CBFEM was compared with the results of the component method in the next step. The comparison was focused on the resistance and also to determine the critical component. The study was performed for the column cross section parameter. Beam IPE 330 is connected to column by extended endplate with 5 bolt rows. Bolts M24 8.8 are used. The dimensions of the end plate P15 with bolts' distances in millimetres are the height 450 (50-103-75-75-75-73) and the width 200 (50-100-50). The outer edge of upper flange is 91 mm from the edge of end plate. Beam flanges are connected to the end plate with welds throat thickness of 8 mm. The beam web is connected with weld throat thickness of 5 mm. The column is stiffened with horizontal stiffeners opposite to beam flanges. Stiffeners are 15 mm thick and their width corresponds to column width. The thickness of end plate stiffener is 10 mm and the width 90 mm. The results are shown in Tab. 9.2.2 and Fig. 9.2.3.

Tab. 9.2.2 Design resistance for parameter – column profile

Column cross section	CM		CBFEM		CM/ CBFEM
	Resistance kNm	Component	Resistance kNm	Component	
HEB 200	107	Column web in shear	116	Column web in shear	0,92
HEB 220	121	Column web in shear	135	Column web in shear	0,90
HEB 240	143	Column web in shear	155	Column web in shear	0,92
HEB 260	160	Column web in shear	169	Column web in shear	0,95
HEB 280	176	Column web in shear	188	Column web in shear	0,94
HEB 300	204	Column web in shear	209	Beam flange in tension/compression	0,98
HEB 320	222	Column web in shear	228	Beam flange in tension/compression	0,97
HEB 340	226	Beam flange in tension/compression	242	Beam flange in tension/compression	0,93
HEB 360	229	Beam flange in tension/compression	250	Beam flange in tension/compression	0,92
HEB 400	234	Beam flange in tension/compression	258	Beam flange in tension/compression	0,91
HEB 450	241	Beam flange in tension/compression	266	Beam flange in tension/compression	0,91
HEB 500	248	Beam flange in tension/compression	274	Beam flange in tension/compression	0,91

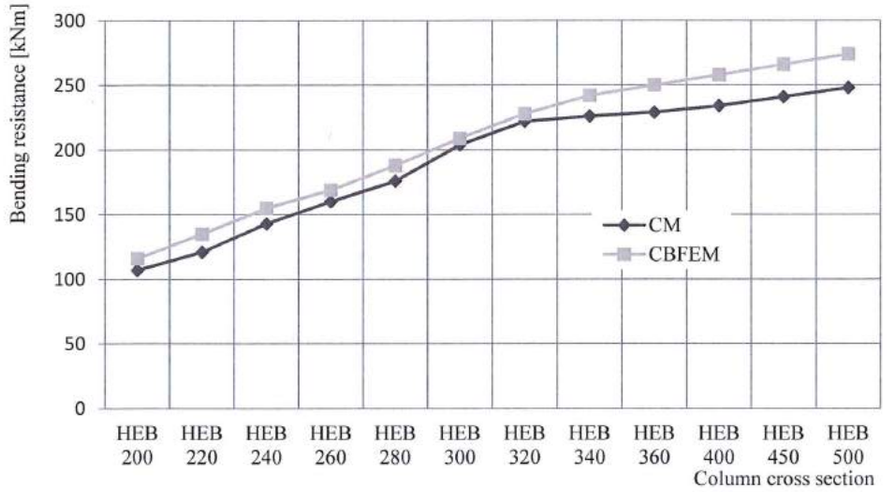

Fig. 9.2.3 Design resistance depending on column cross section

To illustrate the accuracy of the CBFEM model, results of the parametric studies are summarized in graph comparing resistance predicted by CBFEM and by CM, see Fig. 9.2.4. The results show that CBFEM gives higher design resistance compared to CM in all cases. The difference of both methods is up to 10%.

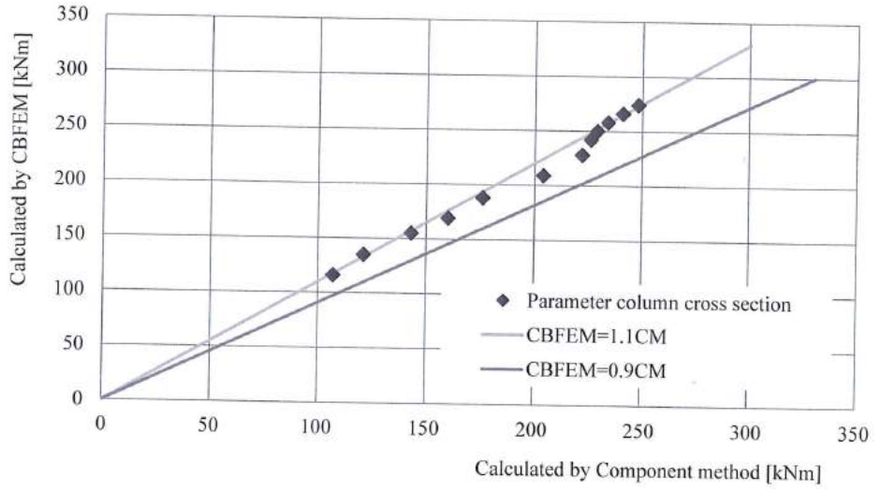

Fig. 9.2.4 Verification of CBFEM to CM

9.2.6. Benchmark example

Inputs

- Steel S235
- Beam IPE 330
- Column HEB 300
- End plate height h_p = 450 (50-103-75-75-75-73) mm
- End plate width b_p = 200 (50-100-50) mm
- End plate P15
- Column stiffeners 15 mm thick and 300 mm wide
- End plate stiffener 10 mm thick and 90 mm wide
- Flange weld throat thickness a_f = 8 mm
- Web weld throat thickness a_w = 5 mm
- Bolts M24 8.8

Outputs

- Design resistance in bending M_{Rd} = 209 kNm
- Corresponding vertical shear force V_{Ed}= 209 kN
- Collapse mode - yielding of the beam stiffener on upper flange
- Utilization of the bolts 89,5 %
- Utilization of the welds 87,2 %

10 PREDICTION OF STIFFNESS

10.1 Bending stiffness of welded joint of open sections

10.1.1 Description

The prediction of rotational stiffness is described on a welded eaves moment joint. A welded joint of open section column HEB and beam IPE is studied and the joint's behaviour is described on moment-rotation diagram. The results of analytical model by component method (CM) are compared with the numerical results obtained by component based finite element method (CBFEM) and a benchmark case is available.

10.1.2 Analytical model

The rotational stiffness of a joint should be determined from deformation of its basic components, which represented by the stiffness coefficient k_i. The rotational stiffness of the joint S_j is obtained from:

$$S_j = \frac{Ez^2}{\mu \sum_i \frac{1}{k_i}} \qquad (10.1.1)$$

where k_i is the stiffness coefficient for the joint component i;

z is the lever arm, see 6.2.7;

μ is the stiffness ratio, see 6.3.1.

The joint components that are taken into account in this example are column web panel in shear k_1, column web in compression k_2 and column web in tension k_3. The stiffness coefficients are defined in Table 6.11 in EN 1993-1-8:2006. The initial stiffness $S_{j,ini}$ is obtained for a moment $M_{j,Ed} \leq 2/3\ M_{j,Rd}$.

An open section beam IPE 400 is welded to a column HEB 300 in the example. Beam flanges are connected to the column flange with welds throat thickness of 9 mm. The beam web is connected with weld throat thickness of 5 mm. Plasticity is applied in welds. The material of the beam and column is S235. The design resistance is limited by the components column web in compression and column web in tension. The calculated stiffness coefficients of the basic components, initial stiffness, stiffness by design resistance and rotation of the beam are summarised in Tab. 10.1.1.

Tab. 10.1.1 Results of the analytical model

	k_1	k_2	k_3	2/3 $M_{j,Rd}$	$S_{j,ini}$	φ_{ini}	$M_{j,Rd}$	S_j	φ
CM	[-]	[-]	[-]	[kNm]	[MNm/rad]	[mrad]	[kNm]	[MNm/rad]	[mrad]
	4,7	9,6	9,6	123	74,3	1,7	185	26,0	7,1

10.1.3 Numerical model

Detailed information about the prediction of stiffness in CBFEM may be found in chapter 3.9. The same eaves moment joint is modelled and the results are in Tab. 10.1.2. The design resistance is reached by 5% plastic strain in a component column web in tension. The CBFEM analyses allows to calculate rotational stiffness in any stages of loading.

Tab. 10.1.2 Results of CBFEM

	$M_{j,Ed}$	S_j	φ
	[kNm]	[MNm/rad]	[mrad]
CBFEM	0	0	0,0
	60	80,5	0,7
	132	77,6	1,7
	150	60,0	2,5
	170	26,6	6,4
	180	15,8	11,4
	198	4,1	48,4

10.1.4 Global behaviour and verification

A comparison of the global behaviour of a welded eaves moment joint described by a moment-rotation diagram is prepared. The joint is analysed and the stiffness of the connected beam is calculated. The main characteristic is the initial stiffness calculated by $2/3M_{j,Rd}$, where $M_{j,Rd}$ is the design moment resistance of the joint. $M_{c,Rd}$ stands for a design moment resistance of the analysed beam. The moment-rotation diagram is shown in Fig. 10.1.1.

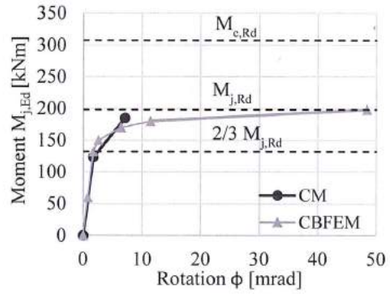

Fig. 10.1.1 Moment-rotation diagram for a welded eaves moment joint

10.1.5 Verification of stiffness

The rotational stiffness calculated by CBFEM compared with CM. The comparison shows good agreement in initial stiffness and correspondence of joint's behaviour. The calculated stiffness from CBFEM and CM are summarised in Tab. 10.1.3.

Tab. 10.1.3 Rotational stiffness of a eaves moment joint in CBFEM and CM

CM				CBFEM			
$M_{j,Ed}$		$S_{j,ini}$	S_j	$M_{j,Ed}$		$S_{j,ini}$	S_j
[kNm]		[MNm/rad]	[MNm/rad]	[kNm]		[MNm/rad]	[MNm/rad]
2/3 $M_{j,Rd}$	123	74,3	-	2/3 $M_{j,Rd}$	132	77,6	-
$M_{j,Rd}$	185	-	26,0	$M_{j,Rd}$	198	-	4,1

10.1.6 Benchmark case

Inputs

Beam and column

- Steel S235
- Column HEB300
- Beam IPE400
- Flange weld throat thickness a_f = 9 mm
- Web weld throat thickness a_w = 5 mm
- Column offset s = 150 mm
- Double fillet weld

Outputs

- Design resistance $M_{j,Rd}$= 198 kNm
- Load $M_{j,Ed}$ = 2/3 $M_{j,Rd}$ = 132 kNm
- Rotational deformation ϕ = 1,7 mrad
- Secant rotational stiffness S_{js} = 77,6 MNm/rad

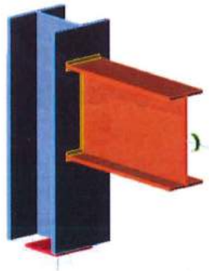

Fig. 10.1.2 Benchmark case for welded eaves moment joint (IPE400 to HEB300)

10.2 Bending stiffness of bolted joint of open sections

10.2.1 Description

The prediction of rotational stiffness is verified on a bolted eaves moment joint. A bolted joint of open section column HEB and beam IPE is studied and the joint's behaviour is described on moment-rotation diagram. The results of analytical model by the component based finite element method (CBFEM) are compared with the component method (CM). The numerical results in form of a benchmark case are available.

10.2.2 Analytical model

The rotational stiffness of a joint should be determined from deformation of its basic components, which represented by the stiffness coefficient k_i. The rotational stiffness of the joint S_j is obtained from:

$$S_j = \frac{Ez^2}{\mu \sum_i \frac{1}{k_i}} \qquad (10.2.1)$$

where k_i is the stiffness coefficient for the joint component i;

z is the lever arm, see 6.2.7;

μ is the stiffness ratio, see 6.3.1.

The joint components that are taken into account in this example are column web panel in shear k_1 and a single equivalent stiffness coefficient k_{eq} for end-plate joint with two or more bolt-rows in tension. The stiffness coefficients are defined in Table 6.11 in EN1993-1-8:2006. The equivalent stiffness coefficient may be obtained in chapter 6.3.3 in EN1993-1-8:2006. The initial stiffness $S_{j,ini}$ is obtained for a moment $M_{j,Ed} \leq 2/3\ M_{j,Rd}$.

An open section beam IPE 330 is connected with bolted end-plate to a column HEB 200 in the example. The end-plate thickness is 15 mm, the bolt type is M24 8.8 and the assembly is shown in Fig. 10.2.1. The stiffeners are inside column opposite to beam flanges with thickness of 15 mm. Beam flanges are connected to the end-plate with welds throat thickness of 8 mm. The beam web is connected with weld throat thickness of 5 mm. Plasticity is applied in welds. The material of the beam, column and end-plate is S235. The joint is loaded in bending. The design resistance is limited by the component column web panel in shear. The calculated stiffness coefficients of the basic components, initial stiffness, stiffness by design resistance and rotation of the beam are summarised in Tab. 10.2.1.

Tab. 10.2.1 Results of the analytical model

	k_1	k_{eq}	2/3 $M_{j,Rd}$	$S_{j,ini}$	φ_{ini}	$M_{j,Rd}$	S_j	φ
CM	[-]	[-]	[kNm]	[MNm/rad]	[mrad]	[kNm]	[MNm/rad]	[mrad]
	4,7	10,8	71	186,7	0,4	107	62,5	1,7

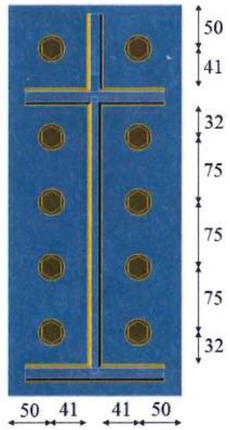

Fig. 10.2.1 Benchmark case for bolted eaves moment joint (IPE330 to HEB200)

10.2.3 Numerical model

Detailed information about the prediction of stiffness in CBFEM may be found in chapter 3.9. For this end-plate joint are results summarised in Tab. 10.2.2. The CBFEM analyses allows to calculate secant rotational stiffness in any stages of loading. The design resistance is reached by 5% plastic strain in a component column web panel in shear.

Tab. 10.2.2 Results of CBFEM

	$M_{j,Ed}$	S_j	φ
	[kNm]	[MNm/rad]	[mrad]
CBFEM	0	0	0,0
	40	40,0	1,0
	73	34,8	2,1
	80	22,9	3,5
	90	11,8	7,6
	100	6,0	16,7
	109	1,8	59,0

10.2.4 Global behaviour and verification

A comparison of the global behaviour of a bolted eaves moment joint described by the moment-rotation diagram is prepared. The joint is analysed and the stiffness of the connected beam is calculated. The main characteristic is the initial stiffness calculated by $2/3M_{j.Rd}$, where $M_{j.Rd}$ is the design moment

resistance of the joint. $M_{c.Rd}$ stands for a design moment resistance of the analysed beam. The moment-rotation diagram is shown in Fig. 10.2.2.

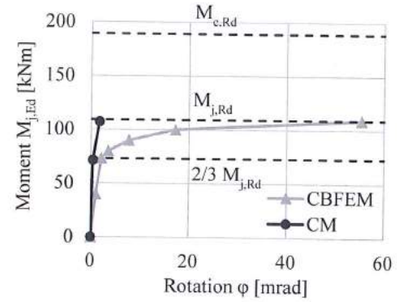

Fig. 10.2.2 Moment-rotation diagram for a bolted eaves moment joint

10.2.5 Verification of stiffness

The rotational stiffness calculated by CBFEM compared with CM. The comparison shows good agreement in initial stiffness and correspondence of joint's behaviour. The calculated stiffness from CBFEM and CM are summarised in Tab. 10.2.3.

Tab. 10.2.3 Rotational stiffness of an eaves moment joint in CBFEM and CM

CM				CBFEM			
$M_{j,Ed}$		$S_{j,ini}$	S_j	$M_{j,Ed}$		$S_{j,ini}$	S_j
[kNm]		[MNm/rad]	[MNm/rad]	[kNm]		[MNm/rad]	[MNm/rad]
2/3 $M_{j,Rd}$	71	186,7	-	2/3 $M_{j,Rd}$	73	34,8	-
$M_{j,Rd}$	107	-	62,5	$M_{j,Rd}$	109	-	1,8

10.2.6 Benchmark case

Inputs

Beam and column

- Steel S235
- Column HEB200
- Beam IPE330
- Column offset s = 200 mm

Weld

- Flange weld throat thickness a_f = 8 mm
- Web weld throat thickness a_w = 5 mm

End-plate

- Thickness t_p = 15 mm

- Height h_p = 450 mm
- Width b_p = 200 mm
- Bolts M24 8.8
- Bolts assembly in Fig. 10.2.3

Column stiffeners

- Thickness t_s = 15 mm
- Width b_s = 95 mm
- Related to beam flange, position upper and lower
- Weld throat thickness a_s = 6 mm

End-plate stiffener

- Thickness t_{st} = 10 mm
- Height h_{st} = 90 mm
- Weld throat thickness a_{st} = 5 mm

Outputs

- Design resistance $M_{j,Rd}$= 109 kNm
- Load $M_{j,Ed}$ = 2/3 $M_{j,Rd}$ = 73 kNm
- Rotational deformation ϕ = 2,1 mrad
- Secant rotational stiffness S_{js} = 34,8 MNm/rad

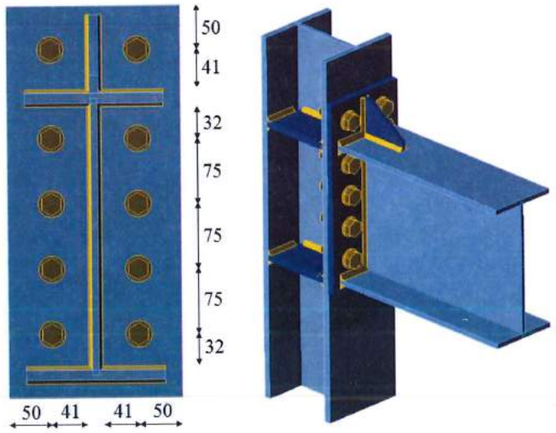

Fig. 10.2.3 Benchmark case for bolted eaves moment joint (IPE330 to HEB200)

10.3 Bending stiffness of column base

10.3.1 Description

The bending stiffness of the open and hollow section in case of loaded by combination of axial force and bending moment is studied. The design numerical model is validated to experiments presented at paper by Bajer et al (2014) and verified to the research numerical model in ATENA code and results of component method.

10.3.2 Validation

Under the project MERLION was tested the column base of column HEB 240, with concrete block of size $a' = 1000$ mm, $b' = 1500$ mm, $h = 900$ mm and concrete C20/25 with base plate $a = 330$ mm; $b = 440$ mm; $t = 20$ mm of steel S235, with the anchor bolts 4 x M20, A_s = 245 mm^2, head diameter a = 60 mm from 8.8, offset at top 50 mm and left - 20 mm and grout thickness 30 mm.

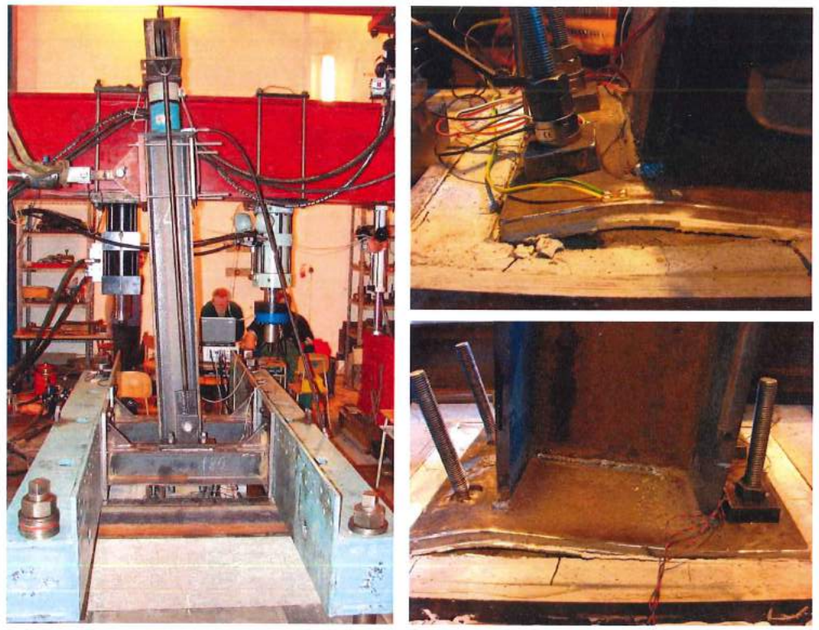

Fig. 10.3.1 Test set-up and deformed base plate and anchor bolts

Two specimens of this column base were tested at laboratory in Brno University of Technology, see (Bajer et al., 2014). The experimental initial stiffness was 10 MNm/rad. The specimens did not exhibit any significant damage until load combination with axial force -400 kN and bending moment 180 kNm,

which creates rotation 0,04 rad. Then concrete cracked with steel yielding of anchor bolts, base plate and column. At the end of loading was the joint still able to transfer bending moment 190 kNm up to rotation 0,15 rad.

ATENA software (Červenka et al., 2014) was used for research model of column base. The software includes for concrete a fracture-plastic material model; for the steel a material model with von Mises failure criterion and for the interfaces a Mohr-Coulomb criterion. Base plate is modelled by shell elements and anchors are presented as reinforcement elements without longitudinal bond. The anchors are fixed to the concrete at the location of the anchors heads. Supports by the concrete block are realized by springs. The model was validated using data from experiment. It well represents progress of cracking in the concrete block and deformation of steel parts. However, the idealisation of the model brings a higher initial stiffness compared to the measured one.

The same column base was examined by design oriented model using CBFEM. The initial stiffness is also lower 29 MNm/rad. The concrete cone breakout should occur at load combination of axial force −400 kN and bending moment 76.5 kNm. Another failure mode, steel rupture, occurs at −400 kN and 127 kNm. Steel plates yield by more than 5 %, which is a recommended value by EN 1993-1-5, at −400 kN and 131 kNm.

The comparison of bending moment normal force rotational diagram predicted by design oriented models CM and CBFEM and research oriented model by ATENA code to the experimental results is in Fig. 10.3.2.

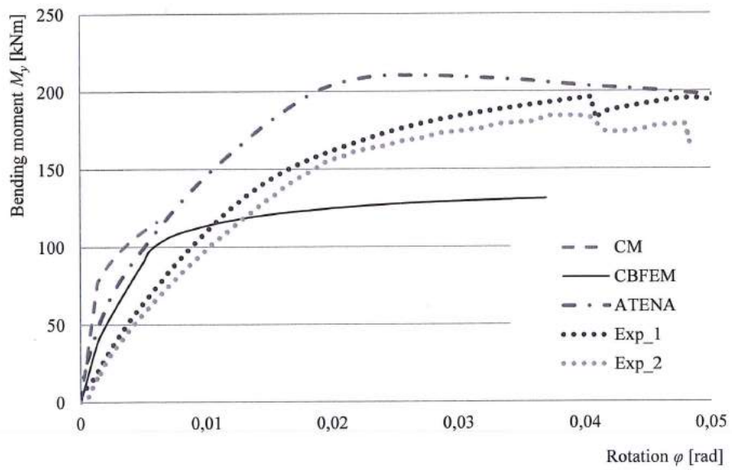

Fig. 10.3.1 Stiffness comparison of HEB 240 column base

10.3.3 Verification

The verification is prepared for a base plate with geometry $a = 350$ mm; $b = 350$ mm; $t = 20$ mm from steel S420 under column SHS 150x16 with anchor bolts 4 x M20, $A_s = 245$ mm^2, anchor head diameter $a = 60$ mm, steel grade 8.8, grout thickness 30 mm, concrete block dimension of $a' = 750$ mm , $b' = 750$ mm , $h = 800$ mm from concrete grade C20/25. The guiding component is mostly the concrete in compression including grout. An example of calculation of this component resistance is shown below. The interaction diagram of this column base example is shown in Chapter 8.4.3. For stiffness calculation, an example of load combination of compressive axial force -756 kN and bending moment 62 kNm is selected.

In CM is the weakest component concrete cone breakout for two anchor bolts in tension whose resistance is 61 kN. The stiffness coefficients of components are summarized in Tab. 10.3.1. The initial stiffness is 29 MNm/rad.

Tab. 10.3.1 Stiffness coefficients of components

Component	Stiffness coefficient
Concrete in compression (including grout)	$k_{13} = 15$ mm
Base plate in bending under tension	$k_{15} = 11$ mm
Anchor bolts in tension	$k_{16} = 2$ mm

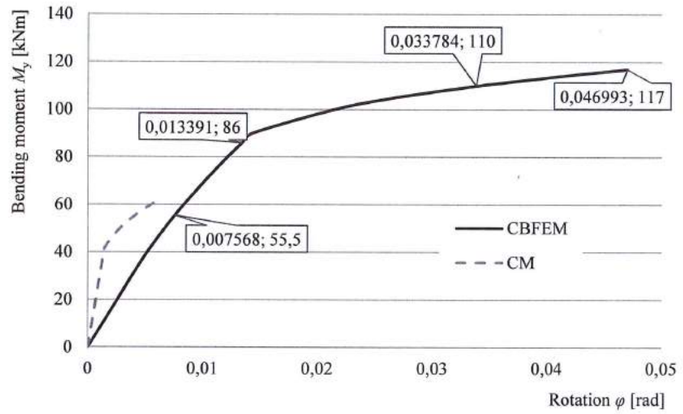

Fig. 10.3.2 Stiffness comparison of SHS 150x16 column base

In CBFEM is also the weakest component brittle component the concrete cone breakout, which gives the bending moment resistance 56 kNm. The program informs the user also about virtual next failure modes, which are concrete block failure at 86 kNm, then anchor bolts rupture at 111 kNm and excessive yielding of steel plates at 117 kNm. The initial stiffness is 8 MNm/rad. The results of prediction by CM and CBFEM is compared in Fig. 10.3.3.

10.3.4 Benchmark case

Input

Cross section

- SHS 150/16
- Steel S420

Base plate:

- Thickness 20 mm
- Offsets top 100 mm, left 100 mm
- Welds both 8 mm
- Steel S420

Anchors

- Type M20 8.8
- Anchoring length 400 mm
- Offsets is top layers 50 mm, left layers -20 mm
- Shear plane in thread

Foundation block

- Concrete C20/25
- Offset 200 mm
- Depth 800 mm
- Shear force transfer friction
- Mortar joint thickness 30 mm

Loading

- Axial force N = -756 kN
- Bending moment M_y = 55,4 kNm

Output

Utilization

- Plates $\varepsilon = 0{,}2$ %
- Bolts 99,8 % ($N_{Ed} = 30.3$ kN $\leq N_{Rd,c} = 30{,}4$ kN critical component is concrete cone breakout)
- Welds 53,7 % ($\sigma_{Ed} = 223{,}5$ MPa $\leq \sigma_{Rd} = 416$ MPa)
- Concrete block 72,6 % ($\sigma = 29$ MPa $\leq f_{jd} = 40$ MPa)

Stiffness

- Rotational deformation 7,568 mrad
- Secant rotational stiffness 7,333 MNm/rad

11 PREDICTION OF DEFORMATION CAPACITY

11.1 Deformation capacity of welded joint of open sections

11.1.1 Description

The prediction of deformation capacity is described on a welded eaves moment joint. An unstiffened welded joint of open section column HEB300 and beam HEB260 is studied and the joint's behaviour is described on moment-rotation diagram. The results of component method (CM) are compared with the component based finite element method (CBFEM) and a benchmark case is prepared.

11.1.2 Analytical model

According to EN1993-1-8:2006 cl. 6.4.3 may be assumed that an unstiffened welded eaves moment joint has a rotation capacity of at least 0,015 radians.

An example of a eaves moment joint is studied. An open section beam HEB260 is welded to a column HEB300 in the example. Welds with throat thickness of 11 mm are used to connect beam flanges to column flange and of 6 mm to connect the beam web. The material of the beam and column is S235. The design resistance is limited by the component column web in compression and column web in tension.

11.1.3 Numerical model

Detailed information about the prediction of deformation capacity in CBFEM may be found in chapter 3.10. The eaves moment joint is modelled and the limit plastic strain is set to 15% to obtain the deformation capacity of the joint. The results of the calculated rotations and stiffness are summarised in Tab. 11.1.1.

Tab. 11.1.1 Results of CBFEM

	$M_{j,Ed}$	S_j	φ
	[kNm]	[MNm/rad]	[mrad]
CBFEM	0	0	0,0
	84	31,1	2,7
	100	23,3	4,3
ε = 5%	126	4,4	28,8
ε = 15%	136	1,0	139,1

11.1.4 Verification

A comparison of the global behaviour of a welded eaves moment joint described by a moment-rotation diagram is prepared. The joint is analysed and the rotation of the connected beam is calculated. The

main characteristic is the rotation capacity calculated by limit plastic strain $\varepsilon = 15\%$. The joint's design resistance by $\varepsilon = 5\%$ is marked as $M_{j,Rd}$ while $M_{c,Rd}$ stands for a design moment resistance of the analysed beam. The moment-rotation diagram is shown in Fig. 11.1.1.

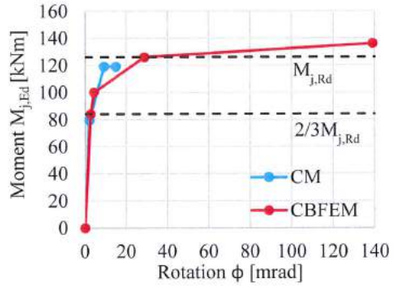

Fig. 11.1.1 Moment-rotation diagram for a welded eaves moment joint

The resistance of welds connecting the analysed beam to the column are verified to avoid brittle fracture. The plastic strain in welds is limited to 5% while the plastic strain of 15% in plates is allowed. The limit plastic strain 15% is reached in the component column web in compression as is shown in Fig. 11.1.2. The welds' design resistance is not reached. The equivalent design stress in the design throat verification plane $f_{w.Ed} = 355{,}5$ MPa $\leq f_u / \beta_w \gamma_{M2} = 360{,}0$ MPa.

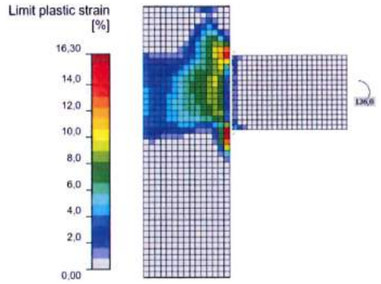

Fig. 11.1.2 Strains in eaves moment joint with yield strength $f_y = 235$ MPa

11.1.5 Capacity design check

In the capacity design checks the possibility that the actual yield strength of steel is higher than the nominal yield strength is taken into account by a material overstrength factor $\gamma_{ov} = 1{,}25$. The influence of not guaranteed values of yield strength on the ductility of connections is shown in Fig. 11.1.3. The rotation capacity is calculated for enlarged yield stress $f_{y,max} = \gamma_{ov} f_y$ and the welds' design resistance is checked. The equivalent design stress in the design throat verification plane $f_{w.Ed} = 357{,}0$ MPa $\leq f_u / \beta_w \gamma_{M2} = 360{,}0$ MPa confirms the adequate weld resistance.

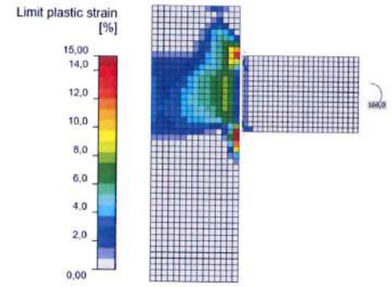

Fig. 11.1.3 Strains in the eaves moment joint with yield strength $f_y = 1{,}25 \cdot 235 = 293$ MPa

If the connection is located in a dissipative zone it's design should conform to the upper value of the yield strength of steel $f_{y,max} = 1{,}1\ \gamma_{ov} f_y$, see EN1998-1:2004. The rotation capacity is calculated and the welds' resistance is assessed as is shown in Fig. 11.1.4. The equivalent design stress in the design throat verification plane $f_{w.Ed} = 359{,}8$ MPa $\leq f_u / \beta_w \gamma_{M2} = 360{,}0$ MPa confirms in this case the adequate weld resistance. The influence of the increased yield strength of steel on the rotation capacity is shown in the Fig. 11.1.5.

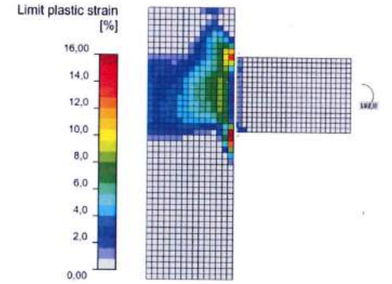

Fig. 11.1.4 Strains in the eaves moment joint with yield strength $f_y = 1{,}25 \cdot 1{,}1 \cdot 235 = 323$ MPa

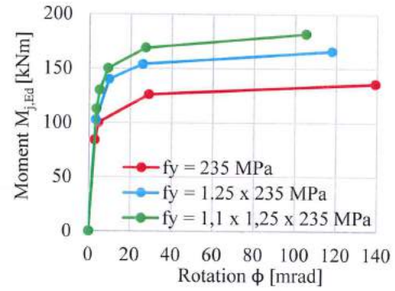

Fig. 11.1.5 Moment-rotational diagram for eaves moment joint for changed yield strengths of steel

11.1.6 Verification of deformation capacity

The rotational capacity φ_{Cd} = 139,1 mrad calculated by CBFEM is larger than the minimal guaranteed value φ_{Cd} = 15 mrad in EN1993-1-8:2006. The conservative prediction in standard is confirmed. It is expected that the deformation capacity in unstiffened eaves moment joint is larger than the prediction assumed in standard.

11.1.7 Benchmark example

Inputs

Beam and column

- Steel S235
- Column HEB300
- Beam HEB260
- Double fillet welds
- Flange weld throat thickness a_f = 11 mm
- Web weld throat thickness a_w = 6 mm

Outputs

- Design resistance by limit plastic strain ε = 15% is $M_{j,Rd}$ = 136 kNm
- Rotational capacity φ_{Cd} = 139,1 mrad

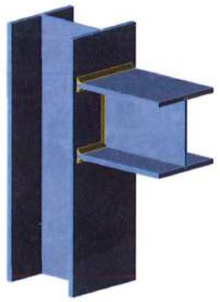

Fig. 11.1.6 Benchmark case for welded eaves moment joint (HEB260 to HEB300)

11.2 Deformation capacity of bolted joint of open sections

11.2.1 Description

The prediction of deformation capacity is verified on a bolted eaves moment joint. An unstiffened bolted joint of open section column HEB300 and beam HEB260 is studied and the joint's behaviour is presented on moment-rotation diagram. The results of the component based finite element method (CBFEM) are compared with component method (CM). A benchmark case is prepared.

11.2.2 Analytical model

According to EN1993-1-8:2006 cl. 6.4.2 may be assumed that the bolted eaves moment joint has adequate rotation capacity, if the design moment resistance of the joint is governed by the column web panel in shear with $d/t_w \leq 69\varepsilon$.

An open section beam IPE 330 is connected with bolted end-plate to a column HEB 200 in the example. The end-plate thickness is 15 mm, the bolt type is M27 10.9 and the assembly is shown in Fig. 11.2.1. The stiffeners are inside column opposite to beam flanges with thickness of 15 mm. Beam flanges are connected to the end-plate with welds throat thickness of 12 mm. The beam web is connected with weld throat thickness of 6 mm. Plasticity is applied in welds. The material of the beam, column and end-plate is S235. The design resistance is limited by the component column web panel in shear.

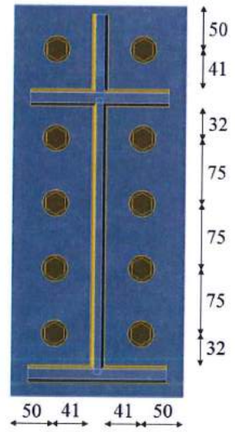

Fig. 11.2.1 Benchmark case for bolted eaves moment joint (IPE330 to HEB200)

11.2.3 Numerical model

Detailed information about the prediction of deformation capacity in CBFEM may be found in chapter 3.10. The eaves moment joint is modelled and the limit plastic strain is set to 15% to obtain the

deformation capacity of the joint. The results of the calculated rotations and stiffness are summarised in Tab. 11.2.1.

Tab. 11.2.1 Results of CBFEM

	$M_{j,Ed}$	S_j	φ
	[kNm]	[MNm/rad]	[mrad]
CBFEM	0	0	0,0
	73	24,2	2,0
	90	12,5	7,2
$\varepsilon = 5\%$	109	2,3	47,6
$\varepsilon = 15\%$	120	0,5	233,4

11.2.4 Verification

A comparison of the global behaviour of a bolted eaves moment joint described by a moment-rotation diagram is prepared. The joint is analysed and the rotation of the connected beam is calculated. The main characteristic is the rotation capacity calculated by limit plastic strain $\varepsilon = 15\%$. The joint's design resistance by $\varepsilon = 5\%$ is marked as $M_{j,Rd}$ while $M_{c,Rd}$ stands for a design moment resistance of the analysed beam. The moment-rotation diagram is shown in Fig. 11.2.2.

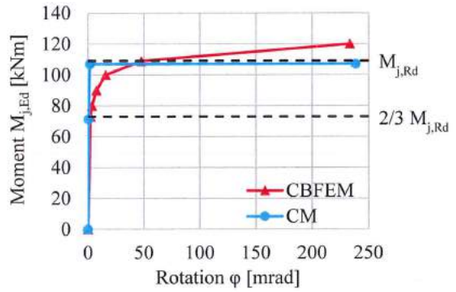

Fig. 11.2.2 Moment-rotation diagram for a bolted eaves moment joint

The resistance of bolts connecting the analysed beam to the column are verified to avoid brittle fracture. The plastic strain in bolts is limited to 5% while the plastic strain of 15% in plates is allowed. The limit plastic strain 15% is reached in the component column web panel in shear as is shown in Fig. 11.2.3. The bolts' tension resistance is not reached. The tension force in first bolt row $F_{t,1} = 316{,}0$ kN $\leq F_{t,Rd} = 330{,}5$ kN.

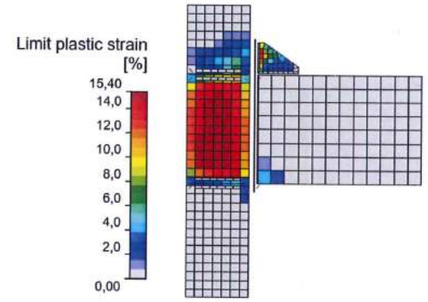

Fig. 11.2.3 Strains in eaves moment joint with yield strength $f_y = 235$ MPa

11.2.5 Capacity design check

In the capacity design checks the possibility that the actual yield strength of steel is higher than the nominal yield strength is taken into account by a material overstrength factor $\gamma_{ov} = 1{,}25$. The influence of not guaranteed values of yield strength on the ductility of connections is shown in Fig. 11.2.4. The rotation capacity is calculated for enlarged yield stress $f_{y,max} = \gamma_{ov} f_y$ and the bolts' tension resistance is checked. The tension force in first bolt row $F_{t,1} = 322{,}7$ kN $\leq F_{t,Rd} = 330{,}5$ kN confirms the adequate bolt resistance.

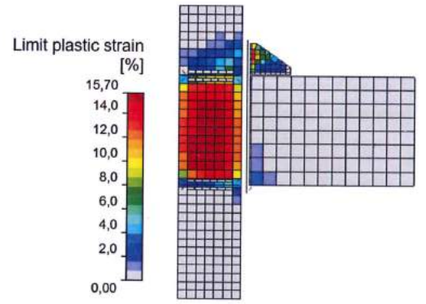

Fig. 11.2.4 Strains in the eaves moment joint with yield strength $f_y = 1{,}25 \cdot 235 = 293$ MPa

If the connection is located in a dissipative zone it's design should conform to the upper value of the yield strength of steel $f_{y,max} = 1{,}1\ \gamma_{ov} f_y$, see EN 1998-1:2004. The rotation capacity is calculated and the bolts' resistance is assessed. The limit plastic strain 15% is reached in the component column web panel in shear as is shown in Fig. 11.2.5. The tension force in first bolt row $F_{t,1} = 325{,}5$ kN $\leq F_{t,Rd} = 330{,}5$ kN confirms in this case the adequate tension bolt resistance. The influence of the increased yield strength of steel on the rotation capacity is shown in the Fig. 11.2.6.

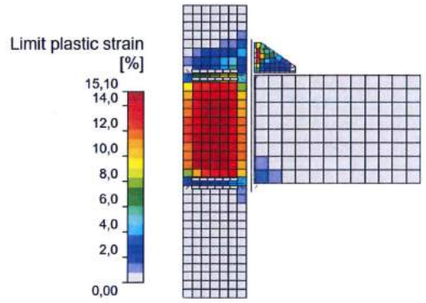

Fig. 11.2.5 Strains in the eaves moment joint with yield strength $f_y = 1{,}25 \cdot 1{,}1 \cdot 235 = 323$ MPa

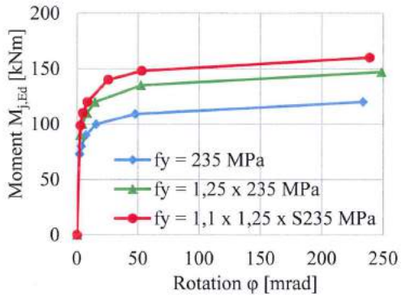

Fig. 11.2.6 Moment-rotational diagram for eaves moment joint for changed yield strengths of steel

11.2.6 Verification of deformation capacity

The rotational capacity φ_{Cd} = 233,4 mrad is calculated by CBFEM. The prediction in standard is confirmed and the joint has adequate rotational capacity. The design resistance is limited by column web panel in shear while the tension resistance of bolts connecting the analysed beam to the column are verified to avoid brittle fracture.

11.2.7 Benchmark example

Inputs

Beam and column

- Steel S235
- Column HEB200
- Beam IPE330
- Column offset s = 200 mm

Weld

- Flange weld throat thickness a_f = 12 mm

- Web weld throat thickness a_w = 6 mm

End-plate

- Thickness t_p = 15 mm
- Height h_p = 450 mm
- Width b_p = 200 mm
- Bolts M27 10.9
- Bolts assembly in Fig. 11.2.7

Column stiffeners

- Thickness t_s = 15 mm
- Width b_s = 95 mm
- Related to beam flange, position upper and lower
- Weld throat thickness a_s = 12 mm

End-plate stiffener

- Thickness t_{st} = 10 mm
- Height h_{st} = 90 mm
- Weld throat thickness a_{st} = 7 mm

Outputs

- Design resistance by limit plastic strain ε = 15% is $M_{j,Rd}$ = 120 kNm
- Rotational capacity φ_{Cd} = 233,4 mrad

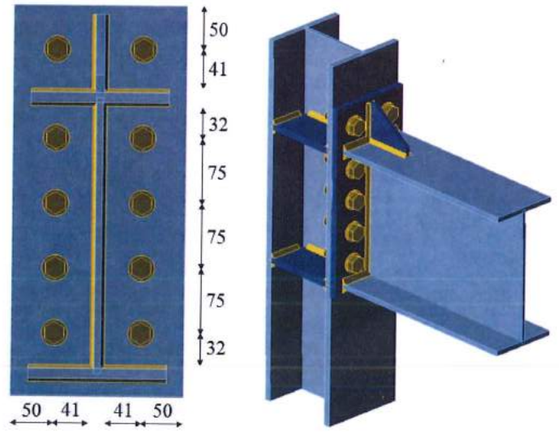

Fig. 11.2.7 Benchmark case for bolted eaves moment joint (IPE330 to HEB200)

REFERENCES

Agerskov H., High-strength bolted connections subject to prying, *Journal of Structural Division*, ASCE, 102 (1), 1976, 161-175.

AIAA, *Guide for the Verification and Validation of Computational Fluid Dynamics Simulations*, American Institute of Aeronautics and Astronautics, AIAA-G-077-1998, Reston, VA, 1998.

ASME, *Guide for Verification and Validation in Computational Solid Mechanics*, The American Society of Mechanical Engineers, 2006, ISBN 079183042X.

Babuska, I., Oden, J.T., Verification and validation in computational engineering and science: Basic concepts, *Computer Methods in Applied Mechanics and Engineering,* 193 (36-38), 2004, 4057-4066.

Bajer M., Vild M., Barnat J., Holomek J., Influence of Selected Parameters on Design Optimisation of Anchor Joint, in *Steel, Space and Composite Structures,* Singapore, 2014,149–158.

Beg D., Zupančič E., Vayas I., On the rotation capacity of moment connections, *Journal of Constructional Steel Research*, 60 (3–5), 2004, 601–620.

Block F.M., Davison J.B., Burgess I.W., Plank R.J., Deformation-reversal in component-based connection elements for analysis of steel frames in fire, *Journal of Constructional Steel Research*, 86, 2013, 54-65.

Braun B., *Stability of steel plates under combined loading*, Institut für Konstruktion und Entwurf, Stuttgart, 2010.

Brito P. H., Rocha C.R., Filho F.C., Martins E., Rubira C.M.F., *A Method for Modeling and Testing Exceptions in Component-Based Software Development*, Dependable Computing, Lecture Notes in Computer Science, 3747, 2005, 61-79.

Bursi O. S .and Jaspart J. P. Calibration of a Finite Element Model for Isolated Bolted End-Plate Steel Connections, *Journal of Constructional Steel Research,* 44, 3, 1997, 225-262.

Bursi O. S., Jaspart J. P., Benchmarks for finite element modelling of bolted steel connections, *Journal of Constructional Steel Research*, 43, 1-3, 1997, 17-42.

Červenka V., Jendele L., Červenka J., *ATENA Program Documentation Part 1: Theory*, Červenka Consulting s.r.o., http://www.cervenka.cz/downloads.

Chen, W.F., Abdalla K.M., Expanded database of semi-rigid steel connections, *Computers and Structures*, 56, (4), 1995, 553-564.

Da Silva L., Lima L., Vellasco P., Andrade S., *Experimental behaviour of end-plate beam-to-column joints under bending and axial force*, Database reporting and discussion of results, Report on ECCS-TC10 Meeting in Ljubljana, 2002.

Da Silva Simoes L., Towards a consistent design approach for steel joints under generalized loading, *Journal of Constructional Steel Research*, 64, 2008, 1059-1075.

Dlubal RFEM 5.0 - FEM Structural Analysis Software, Prague, https://www.dlubal.com/en

Dvorkin E. N., Bathe K. J., Continue A., Mechanics Based Four Node Shell Element for General Nonlinear Analysis, *Engineering Computations*, 1, 1984.

EN1992-1-1, Eurocode 2, Design of concrete structures, Part 1-1, *General rules and rules for buildings,* CEN, Brussels, 2005.

EN1993-1-5, Eurocode 3, Design of steel structures, Part 1-5, *Plated Structural Elements*, CEN, Brussels, 2005.

EN1993-1-8, Eurocode 3, Design of steel structures, Part 1-8, *Design of joints*, CEN, Brussels, 2006.

EN1994-1-1, Eurocode 4, Design of composite steel and concrete structures, Part 1-1, *General rules and rules for buildings*, CEN, 2010.

EN1998-1, Eurocode 8, Design of structures for earthquake resistance – Part 1: General rules, *Seismic actions and rules for buildings*, CEN, Brussels, 2004.

ETAG 001, *Guideline for European Technical Approval of Metal Anchors for Use in Concrete – Annex C: Design Methods for Anchorages,* Brussels, EOTA, 2010.

Faella C, Piluso V, Rizzano G., Plastic deformation capacity of bolted T-stubs: theoretical analysis and testing, in *Moment resistant connections of steel frames in seismic area, design and reliability*, E&FN Spoon. 2000.

Foley C.M., Vinnakota S., Toward design office moment–rotation curves for end-plate beam-to-column connections, *Journal of Constructional Steel Research*, 35, 1995, 217–53.

Gioncu V., Mazzolani F., *Ductility of seismic resistant steel structures*, Spon Press; 2002.

Girao A.M.C., Bijlaard F.S.K., da Silva L.S., Experimental assessment of the ductility of extended end plate connections, *Journal of Engineering Structures,* 26, 2004, 1185–1206.

Gödrich L., Wald F., Sokol Z., To Advanced modelling of end plate joints, *Connection and Joints in Steel and Composite Structures*, Rzeszow, 2013.

Gödrich L., Kurejková M., Wald F., Sokol, Z., The bolts and compressed plates modelling, in *Steel, Space and Composite Structures*, Singapore, 2014, 215-224.

Gödrich L., Wald F., Sokol Z., Advanced modelling of end plate, in *Eurosteel 2014*, Brussels, ECCS, 2014, 287-288.

Grecea D., Stratan A., Ciutina A., Dubina D., Rotation capacity of the beam-to-column joints under cyclic loading, in *Connections in Steel Structures V*, Amsterdam, 2004.

Gresnight N., Romeijn A., Wald F., Steenhuis M., Column Bases in Shear and Normal Force, *HERON,* 53, 1/2, 2008, 87-108, ISSN 0046-7316.

Holdren J. P., *Increasing Access to the Results of Federally Funded Scientific Research, Memorandum for the Heads of Executive Departments and Agencies*, Office of Science and Technology Policy, Washington, D.C, 2013.

Ibrahimbegovic A., Taylor R.L., Wilson E. L., A robust quadrilateral membrane element with drilling degrees of freedom, *International Journal for Numerical Methods in Engineering*, 30/3, 1990, 445-457.

IDEA RS: *Product documentation*, www.idea-rs.com, 2016.

IIW XV-1439-13 ISO/FDIS 14346, *Static Design Procedure for Welded Hollow Section Joints – Recommendations*, ISO, 2012.

ISO 898-1, Mechanical properties of fasteners made of carbon steel and alloy steel, Part 1, *Bolts, screws and studs with specified, property classes*, Coarse thread and fine pitch thread, Geneva, 2009.

ISO, Guide to the Expression of Uncertainty in Measurement, ISO Geneva, 1993.

Jaspart J.P., Design of structural joints in building frames, *Prog. Struct. Engng Mater.*, 4, 2002, 18–34.

Jaspart J.P., Wald F., Weynand K., Gresnight N., Steel Column Base Classification, *Heron*, 2015, 53, 1/2, 69-86.

Jaspart J.P., Weynand K., Design of hollow section joints using the component method, *Tubular Structures XV,* 2015, 403-410.

Jetteur P., Cescotto S., A mixed finite element for the analysis of large inelastic strains, *International Journal for Numerical Methods in Engineering*, 31, 1991, 229-239.

Krishnamurthy N., *Analytical investigation of bolted stiffened tee stubs*, Report No. CE-MBMA-1902, Van-derbilt University, Nashville, 1978.

Krishnamurthy N., Fresh Look at Bolted End-Plate Behavior and Design, *Engineering Journal*, 15 (2), 1978, 39-49.

Kuhlmann U., Kuhnemund F., Rotation capacity of steel joints, *Verification Procedure and Component Tests*, 2000.

Kurejková M., Wald F., Compressed Stiffeners in Structural Connections, in *Eurosteel 2014*, Brussels, ECCS, 2014, 317-318.

Kurejková M., Wald F., Kabeláč J., Šabatka L., Slender Compressed Plate in Component Based Finite Element Model, in *2nd International Conference on Innovative Materials, Structures and Technologies*, Riga, Latvia, 2015.

Kwaśniewski L., Nonlinear dynamic simulations of progressive collapse for a multistorey building, *Engineering Structures*, 32 (5), 2010, 1223-1235.

Kwaśniewski L., Numerical verification of post-critical Beck's column behavior, *International Journal of Non-Linear Mechanics,* 45 (3), 2010, 242-255.

Kwaśniewski, L., Bojanowski, C., Principles of verification and validation, *Journal of Structural Fire Engineering*, 6, 1, 2015, 29-40.

Kwaśniewski, L., On practical problems with verification and validation of computational models, *Archives of Civil Engineering*, 55, 3, 2009, 323-346

Lima L. R. O., F. Freire J. L., S. Vellasco P. C. G., Andrade S. A. L., Silva J. G. S., Structural assessment of minor axis steel joints using photoelasticity and finite elements, *Journal of Constructional Steel Research*, 65, 2009, 466-478.

NAFEMS, National Agency for Finite Element Methods, http://www.nafems.org/, 2013.

Neumann, N. Design model for combined in-plane and out-of-plane bending of steel joints connecting H or I sections, in *Eurosteel 2014*, Naples, 2014, 2050-2056.

Oberkampf W.L., Trucano T.G., Verification and validation benchmarks, *Nuclear Engineering and Design*, 238, 2008, 716–743.

prEN1992-1-4, Eurocode 2: Design of concrete structures, Part 1-4, *Design of fastenings for use in concrete*, Brussels, 2015.

Roache P.J., Verification and validation in computational science and engineering, *Computing in Science Engineering*, Hermosa publishers, 1998, 8-9.

Šabatka L., Wald F., Kabeláč J., Kolaja D., Pospíšil M., Structural Analysis and Design of Steel Connections Using Component Based Finite Element Model, *Journal of Civil Engineering and Architecture*, 9 (9), 2015, 1-7. ,

Sherbourne A.N, Bahaari M.R. 3D simulation of bolted connections to unstiffened columns—II. Extended endplate connections, *Journal of Constructional Steel Research,* 40, 1996, 189–223.

Sherbourne A.N, Bahaari M.R., 3D simulation of end-plate bolted connections, *Journal of Structural Engineering,* 120, 1994, 3122–3136.

Sherbourne A.N., Bahaari M.R., Simulation of bolted connections to unstiffened columns T-stub connections, *Journal of Constructional Steel Research,* 40, 1996, 169–87.

SIMULIA, Abaqus 6.11, *Benchmarks Manual*, Dassault Systèmes, 2011.

Steenhuis M., Gresnigt N., Weynand K., Pre-Design of Semi-Rigid Joints in Steel Frames, in *Second state of the art workshop on semi-rigid behaviour of civil engineering structural connections*, COST C1, Prague, 1994, 131-140.

Steenhuis M., Jaspart J. P., Gomes F., Leino T., Application of the component method to steel joints, in *Control of the Semi-rigid Behaviour of Civil Engineering Structural Connections Conference*, COST C1, Liege, Belgium, 1998, 125-143.

Steenhuis M., Wald F., Sokol Z., Stark J.W.B., Concrete in Compression and Base Plate in Bending, *Heron*, 2008, 53, 1/2, 51-68.

VDI2230 *Systematic calculation of high duty bolted joints – Joints with one cylindrical bolt*, Association of German Engineers, Berlin, 2003.

Virdi K. S. et al, *Numerical Simulation of Semi Rigid Connections by the Finite Element Method*, Report of Working Group 6 Numerical, Simulation COST C1, Brussels Luxembourg, 1999.

Wald F., Burgess I., Kwasniewski L., Horová K, Caldová E., *Benchmark studies*, Experimental validation of numerical models in fire engineering, CTU Publishing House, 198 p., Prague, 2014.

Wald F., Burgess I., Kwasniewski L., Horová K., Caldová, E., *Benchmark studies*, Verification of numerical models in fire engineering. CTU Publishing House, 328 p., Prague, 2014.

Wald F., *Column Bases*, CTU Publishing House, Prague, 1995.

Wald F., Gödrich L., Šabatka L., Kabeláč J., Navrátil J., Component Based Finite Element Model of Structural Connections, *in Steel, Space and Composite Structures*, Singapore, 2014, 337-344.

Wald F., Sokol Z., Steenhuis M., Jaspart, J.P., Component Method for Steel Column Bases, *Heron*, 53, 2008, 3-20.

Wald F., Sokol, Z., Jaspart J.P., Base Plate in Bending and Anchor Bolts in Tension, *Heron*, 2008, 53, 1/2, 21-50.

Wald F., Kurejková M., Gödrich L., Kočka M., Martínek K., Simple and Advanced Models for Connection Design in Steel Structures, in *International Conference on Advances in Civil and Environmental Engineering*, Universiti Teknologi Mara, 14-23, Pulau Pinang, 2015.

Wald F., Kwasniewski L. Gödrich L., Kurejková M., Validation and verification procedures for connection design in steel structures, in *Steel, Space and Composite Structures,* Singapore, 2014, 111-120.

Wald F., Šabatka L., Kabeláč J., Kolaja D., Pospíšil M., Structural Analysis and Design of Steel Connections Using Component Based Finite Element Model (CBFEM), *Journal of Civil Engineering and Architecture*, 10, 2015.

Wald F., Šabatka L., Kabeláč J., Gödrich L., Kurejková M., Future Design Procedure for Structural Connections is Component Based Finite Element Model, in *13th Nordic Steel Construction Conference (NSCC-2015)*, Tampere University of Technology, Tampere, 2015.

Wald F., Sokol Z., Moal M., Mazura V., Muzeau J. P., Stiffness of cover plate connections with slotted holes, in *Eurosteel 2002*, Coimbra, 2002, 1007-1016

Wald F., Gödrich L., Kurejková M., et al, Generally loaded connections by component based finite element method, in *Connections VIII*, Boston, May 24-26, 2016, in printing.

Wang Z., Wang T. Experiment and finite element analysis for the end plate minor axis connection of semi-rigid steel frames, *Tumu Gongcheng Xuebao/China Civil Engineering Journal*, 45 (8), 2012, 83-89.

Wardenier J., *Hollow Sections Joints*, Delft University press, Delft, 1982.

Wardenier J., Packer J. A., Zhao X.-L., van der Vegte G. J., *Hollow Sections in Structural Applications*, CIDECT, Geneve, 2010.

Wu Z., Zhang S., Jiang S., Simulation of tensile bolts in finite element modelling of semi-rigid beam-to-column connections, *International Journal of Steel Structures* 12 (3), 2012, 339-350.

Zoetemeijer P., *Summary of the Researches on Bolted Beam-to-Column Connections*, Report 6-85-7, University of Technology, Delft 1985.

IDEA StatiCa®

Calculate yesterday's estimates

WHAT WE DO

We develop software for structural engineers, fabricators, consultants and all others who perform or use structural analysis. Our development team researches, tests and applies new methods of analyzing behavior of structures and their members. Based on this, we create IDEA StatiCa – software that enables engineers to work faster, evaluate requirements of the national code thoroughly and use optimal amount of material. For us, creating software is a way to contribute to making every new construction around the world safer and cheaper.

IDEA StatiCa Steel

IDEA StatiCa Concrete and Prestressing

Calculate yesterday's estimates

PARTNERS

We build partnerships with key companies in the field and link IDEA StatiCa with their software. IDEA StatiCa is a part of a global workflow which improves productivity of structural engineers and fabricators.
We are AEC Solution Associate of Autodesk, a recommended 3rd party solution for Autodesk users.
IDEA StatiCa works with Robot Structural Analysis and Advance Steel. Revit link is coming.
IDEA StatiCa has a strong synergy with Tekla Structures. We partnered up with Trimble to create a seamless link between these two programs. The largest distributor of Tekla Structures worldwide, company Construsoft, resells IDEA StatiCa in several EU countries and Latin America.

AUTODESK. Trimble.

Other partners include Dlubal Software, MIDAS IT and InterCAD.

www.ideastatica.com www.idea-rs.com